COMPARATIVE ASSESSMENT OF CONVENTIONAL VERSUS REMOTE SENSING BASED APPROACH FOR LAKE EVAPORATION ESTIMATION: THE CASE OF LAKE HAWASSA

GIRUM FIKADE WOLDE SENBET

ADVISOR: SIRAK TEKLEAB GEBREKRISTOS (PhD)

CO-ADVISOR: TESHALE TADESSE (MSc)

THE THESIS SUBMITED TO FACULTY OF CIVIL ENGINEERING AND BUILT ENVIRONMENT, DEPARTMENT OF CIVIL ENGINEERING, INSTITUTE OF TECHNOLOGY, SCHOOL OF GRADUATE STUDIES

HAWASSA UNIVERSITY, HAWASSA, ETHIOPIA

OCTOBER, 2018

COMPARATIVE ASSESSMENT OF CONVENTIONAL VERSUS REMOTE SENSING BASED APPROACH FOR LAKE EVAPORATION ESTIMATION: THE CASE OF LAKE HAWASSA, ETHIOPIA

GIRUM FIKADE WOLDESENBET

A THESIS SUBMITTED TO THE

FACULTY OF CIVIL ENGINEERING AND BUILT ENVIRONMENT,

INSTITUTE OF TECHNOLOGY, SCHOOL OF

GRADUATE STUDIES

HAWASSA UNIVERSITY

HAWASSA, ETHIOPIA

IN PARTIAL FULFILLMENT OF THE

REQUIREMENTS FOR THE

DEGREE OF

MASTER OF SCIENCE IN HYDRAULICS ENGINEERING

MAIN ADVISOR: - Dr. SIRAK TEKLEAB GEBREKRISTOS

CO-ADVISOR: - TESHALE TADESSE

HAWASSA UNIVERSITY

SCHOOL OF GRADUATE STUDIES

ADVISORS' APPROVAL SHEET

(Submission Sheet-1)

This is to certify that the thesis entitled "**Comparative Assessment of Conventional Versus Remote Sensing Based Approach Lake Evaporation Estimation: The Case of Lake Hawassa"** submitted in the partial fulfillment of the requirement for the degree of Master's with specialization in **Hydraulics Engineering**, the Graduate program Faculty of Civil Engineering and Built Environment, and has been carried out by **Girum Fikade** Id. No **PGHYD/045/07**, under our supervision. Therefore, we recommend that the student has fulfilled the requirement and hence hereby can submit the thesis to the department.

Sirak Tekleab (PhD)	________________	____________________
Major Advisor	signature	Date
Teshale Tadesse (MSc)	________________	____________________
Co-advisor	signature	Date

Declaration

I hereby declare that this MSc thesis is my original work and has not been presented for a degree in any other university, and all sources of material used for this thesis have been duly acknowledged.

Name: Girum Fikade WoldeSenbet

Signature: ____

Place and Date of Submission: Hawassa University, (Oct, 2018)

Acknowledgement

First of all I want to thank Ethiopian Road Authority and Hawassa University for the education chance. In completion of this thesis, I am indebted to many people without whose help and expertise it would have been difficult to carry this study.

My sincere gratitude goes to my main advisor Dr Sirak Tekleab for the guidance and kind support in the development of the topic idea and writing of this thesis, thank you very much I have learned much from you. Co-advisor Mr. Teshale you helped me to acquire some relevant GIS software and closely monitored my progress, I thank you so much.

I am also grateful to Hawassa Meteorological Services Department, for the meteorological data, Mr. Ashenafi in particular for letting me access to the Pan data and other meteorological data. Thanks to my colleagues and friends for your kind support in providing useful data and ideas.

I am humbled by the love and inspiration that I received from my family specially my brother Birhanu and his family throughout this study. You were so patient with me and I promise to be a success story beyond all boundaries. My youngest brother Yared without your technical support this could have been impossible, thank you so much.

Finally and above all, to my Lord Holly Trinity, who has never failed the love He has for me, I feel unworthy in your love and grace. You are molding me into great man in the world of science and I long for Your Eternal Kingdom.

Dedication

I dedicate every work of mine to my mother Belyanesh Meka who thought me the struggle of life by being a great example.

Table of Contents

List of Tables

List of Figures

Acronyms and Abbreviations

AVHRR	Advanced Very High Resolution Radiometer
AATSR	Advanced Along-Track Scanning Radiometer
ASL	Atmospheric Surface Layer
ASTER	Advanced Thermal Emission and Reflection Radiometer
AOT	Aerosol Optical Thickness
BREB	Bowen Ratio Energy Balance
CWSI	Crop Water Stress Index
DN	Digital Number
EOS	Earth Observation System
ETM+	Enhanced Thematic Mapper Plus
ETCOLD	Ethiopian Committee on Large Dams
FAO	Food and Agriculture Organization
FVC	Fractional vegetation coverage
GDAL	Geospatial Data Abstraction Library
GIS	Geographic Information System
HDF	Hierarchical Data Format
ILWIS	Integrated Land and Water Information System
ITCZ	Inter-tropical convergence zone
LAI	Leaf area index
LAADS	Level 1 and Atmospheric Archive and Distribution System
LWIR	Long Wave Infrared
METRIC	Mapping Evapo-Transpiration at High Resolution with Internalized Calibration

MODIS	Moderate Resolution Imaging Spectro-radiometer
MOST	Monin-Obukhov Similarity Theory
MRT	MODIS Reprojection Tool
MoWR	Ministry of Water Resources
NASA	National Aeronautics and Space Agency
NDVI	Normalized Difference Vegetation Index
NIR	Near Infrared
RS	Remote Sensing
SEBAL	Surface Energy Balance Algorithm for Land
SEBI	Surface Energy Balance Index
SEBS	Surface Energy Balance System
S-SEBI	Simplified Surface Energy Balance Index
SMAC	Simplified Method for Atmospheric Correction
SNNPR	Southern Nations Nationalities and Peoples Region
SWIR	Short Wave Infrared
SWT	Split Window Technique
TIFF	Tagged Image Format
TM	Thematic Mapper
TIR	Thermal Infrared Region
VITT	Vegetation Index Temperature Trapezoid
VPD	Vapor pressure or saturation deficit
WWDSE	Water Works Design and Supervision Enterprise

List of Symbols

<T> pbl = Average planetary boundary layer temperature (K)

h_{pbl} = Height of the PBL (m)

V = Wind speed (m/s)

T_s = Surface temperature (w/m^2)

Tc = Vegetation canopy temperature (K)

R_n = Surface net radiation (w/m^2)

G = Water heat flux density (w/m^2)

ha = Measurement height of wind speed and air temperature (m)

VI = Vegetation Index

LAI = Leaf Area Index

F_r = Fractional vegetation cover

αs = Surface shortwave albedo

Tair = Air temperature measured at a reference height (K)

Abstract

Evaporation is the major component of the water and energy budget of the water bodies. The Evaporation process needs special attention for a better allocation and management of water resources. The main objective of this study was to compare evaporation estimates based on conventional and Remote Sensing approach. Different methods have been developed and implemented to estimate total evaporation, including meteorological ground-based point data, field measurements and spatially explicit remotely sensed data. Surface Energy Balance System (SEBS) was employed to estimate the Lake Hawassa evaporation and other energy balance components. The SEBS results were compared with meteorological methods results (Debruine-Keigeman, BREB method, and Penman), using Pan Evaporation as a reference. Nash-Sutcliffe, efficiency coefficient (E), Wilmott's index (dr) for evaporation estimates, and Root Mean Square Deviation (RMSD) were used as a statistical performance measures for energy balance component estimates. The SEBS results indicate that the Lake Hawassa average evaporation estimate is 1.16 mm/day in September and 5.2 mm/day in February. Using Pan Evaporation measurements as a tool; evaporation estimates of SEBS perform better than any other metrological method, with Nash-Sutcliffe, efficiency coefficient (E) = 0.48 and Wilmott's index (dr) = 0.48 as well. Penman and BREB methods perform poor in evaporation estimation from Lake Hawassa. SEBS heat fluxes RMSD from the meteorological based estimation were 15.01W/m^2 for Net Radiation (R_n), 13.7 W/m^2 for Stored Heat Flux (G_0), and 11.54 W/m^2 for Sensible Heat Flux (H). Generally it was concluded that the SEBS remote sensing algorithm is applicable for evaporation and other energy balance components estimation on Lake Hawassa.

Key Words; Evaporation, Lake Hawassa, Remote Sensing, Pan Evaporation, Heat Fluxes

1 Introduction

1.1 Background

Our planet earth comprises over 70% of water bodies of its capacity, but only small amount is considered to be fresh. It has been suggested by scholars that, managing such a scarce resource is the key for survival of human being. Surface water bodies include oceans, lakes, dam, and large rivers and in developing countries lakes contain the most accessible water available for human consumption and ecosystems. These water bodies attribute to 0.27 % of global fresh water and 0.008% of the earth water budget (Chow, et.al, 1988). Lakes and dams are the main sources for urban water supply, irrigated agriculture and hydropower but evaporation loss from these surface waters is not properly accounted for.

Ethiopia ‘the water tower of East Africa’ has been ranked among the first ones in fresh water resources worldwide. The country’s annual renewable fresh water resources amount to some 122 BCM/yr in the twelve river basins, and Ethiopian Rift Valley Basin is among these basins (ETCOLD, 2014). Lake Hawassa, which situated in southern part of the country, is among fresh water resources (Belete, 2013; Gebreegziabher, 2004). The lake is a part of Ethiopian rift valley basin and it is considered the livelihood of millions of people, directly and indirectly. Many studies have been carried out on the lake regarding, its water level, amount, pollution status, sedimentation, water balance, etc. Lake evaporation, which is considered to be the main lose from water bodies, has been studied under different kinds of researches (e.g. Yibeltal et.al, 2015; Brook and Deganovsky, 2008; Belete, 2013; Gebreegziabher, 2004).

Evaporation is one of the major components of the water budget of open water bodies and also one of the main components of energy budget of open water bodies. Because of the variability of region and seasons, water resources managers who are responsible for planning and adjudicating the distribution of water resources need to have a thorough understanding of the Water loses and knowledge about the spatial and temporal rates of evapotranspiration or evaporation Process Duan, (2014).

The advancement of evaporation estimation techniques, now a days is unquestionably appreciable at a global scale. Application of remote sensing in hydrology is playing the key role in evaporation estimation process. Many studies have been carried out regarding finding out the best estimation method for a certain area. The best estimation method is the one which correlated reasonably with the direct field measurement data. However, many study areas in the world have only the traditional evaporation estimation tool as a direct measurement device (e.g. Pan Evaporation). Application of more advanced evaporation estimation system (e.g. Eddy Covariance and Bowen Ratio), require strong finance and more sophisticated technical ability to install, operate and maintain the overall instrumentation (Duan, and Bastiaanssen, 2015). Even though the cost and technical aspect remain a constraint for the advanced direct measurements, they have been used as a validating tool for application of remote sensing for evapotranspiration and open water evaporation. As the validation results reveal, application of remote sensing for open water evaporation estimation is promising. In Ethiopia Abraham (2009) makes use of satellite images to determine evaporation and driving variables from Lake Tana, and validated the results with the advanced ground based estimates. This study is aiming at comparing the conventional versus remote sensing based evaporation estimation of Lake Hawassa.

1.2 Statement of the Problem

Attaining improved management of planet's fresh water can't be realized without monitoring the Earth's water vapor cycle. Evaporation is an important component of the water and energy balance of lakes and reservoirs. Duan, (2014) also pointed out that this component is considered as a consumptive use of water for the services (i.e. domestic, industrial, irrigation, hydropower, wetlands, recreational, and environmental water use sectors, among others,) that this water provides. Brutsaert, (1982), indicated that the annual evaporation from entire Earth's land surfaces accounts approximately 65% of annual precipitation. It is clear that this percent of value would increase on open water sources. Even though determining evaporation from open water sources is crucial, it is costly and difficult to install or implement direct measurements. To compensate the gap, lake evaporation needs to be computed using indirect methods, such as the water balance methods, mass transfer methods and energy balance methods (Finch and Hall, 2001). Most of previous studies on the lake regarding evaporation estimation were conducted on the basis of pan-evaporation time series data and meteorological data based model (e.g. Lemlem, 2007; Gebreegziabher, 2004). Only few studies were used Remote Sensing as a tool (e.g.

Yibeltal et.al, 2015). The previous application of remote sensing on Lake Hawassa is based on SEBAL algorithm, which is considered to be poor in application for homogeneous areas.

Assefa et.al, (2009) used Land sat imageries of the 1986 and 2000 to estimate monthly Lake ET and comparing the estimate with the Simple Abtew Method (i.e. which is developed and named by Wossenu Abetew) and Penman Methods. In the analysis it has been proved that, Remote Sensing and surface energy balance approach was promising on large scale applications to understand the spatial variation of the latent heat flux. After all, it is clear that, Remote Sensing and Surface Energy Balance approach has the power to assess the reliability of the ground based data if any exists. Ground based estimates have uncertainties and do not have a capability to be used in large scale area of interest (Evans, 2009). The uncertainties are resulted on the cause that, the estimates are based on extrapolation of point measurements. Additionally, evaporation estimation is crucial due to the fact that lake evaporation facilitates disappearance of lakes after in-lake sedimentation, therefore more emphasis should be given to lake evaporation.

1.3 Objective

Main objective of this study is to compare the remote sensing approach with conventional method for the estimation of evaporation on Lake Hawassa.

Specific objectives of the study are:

- To compute the rate of evaporation from Lake Hawassa with the surface energy balance application.
- To estimate the other energy balance components, net radiation flux (Rn), heat storage flux (G), and sensible heat flux (H) with the aid of remote sensing application.
- To generate maps showing spatial and temporal variation of evaporation and the other energy balance components on Lake Hawassa.
- To compare the remote sensing application results with conventional methods (i.e. Penman, De bruin-Keijman, Pan Evaporation, Bowen Ratio Energy Balance (BREB) and other empirical methods.

1.4 Research Questions

1. How does remote sensing approach perform to estimate evaporation from Lake Hawassa compared with conventional methods?
2. Can remote sensing approach estimate evaporation from Lake Hawassa reasonably?
3. Can remote sensing approach give reasonable estimates of other energy balance components on Lake Hawassa?
4. How does look like the spatial and temporal maps of the evaporation and other energy balance components on Lake Hawassa?

2 Literature Review

2.1 Evaporation Process from Open Water Bodies

Total evaporation is defined as a summation of evaporation from different surfaces, including interception (I), transpiration (T), surface evaporation (Es) and open water bodies (Eo) (Savenije ,2004). Evaporation is the slow transformation from the liquid to the gaseous phase below the boiling point. Boiling differs from evaporation in that; during boiling, vapor is formed on the surface and inside the liquid, then vapor bubbles go upward. Evaporation come about at different temperature at different rates, but boiling takes place only at the temperature at which the pressure of the saturated vapor in the liquid and atmospheric pressure attain the same value (Vuglinsky, 2002).

Evaporation forms a major segment of the hydrologic cycle combined with precipitation; it links the earth's major water bodies (ocean-atmosphere-mainland). Evaporation occurs during each stage of the hydrologic cycle. It even occurs during precipitation, before the rain reaches the earth. A portion of the rain is intercepted by vegetation (predominantly by leaves) and evaporated directly back into the atmosphere (Interception). A portion of the water infiltrated into the ground is absorbed by plant roots and eventually discharged back into the atmosphere (transpiration). Another share of water evaporates from soil and open water bodies (evaporation). The combined total loss from the drainage basin is termed evapotranspiration. The term free water evaporation (ETo), is used for evaporation from open/free water surface (lakes, reservoirs, river channels) (Xu et.al, 2006).

Evaporation is characterized by three interconnected phases: evaporation of molecules from the evaporating surface; migration of some molecules to the evaporating surface; diffusion of the remaining molecules into the surrounding space. Molecules in the inner water layers move irregularly in any direction, because they are affected by the attraction of the surrounding molecules, which is similar on average. Meanwhile molecules in the surface water layer are affected by less attraction of the air molecules than the molecular attraction in the inner water layers due to the lower concentration of the air molecules. The rates of molecular motion are different; those molecules which reach the evaporating surface at high speeds and at big angles, overcome the attraction of other water molecules and, when separating from the evaporating surface, they escape into vapor (Vuglinsky, 2002).

2.2 Factors Affecting Evaporation Rates from Fresh Water Bodies

There are a number of factors that can affect the evaporation rates, notably the climate (Solar Radiation, Temperature, Wind Velocity, Relative Humidity, and Atmospheric Pressure) and physiography (mainly Heat Storage Capacity and Albedo)of the water body and its surroundings (Harbeck, 1962). The rate of evaporation is, however, fundamentally controlled by the available energy and the ease with which water vapor diffuses into the atmosphere. In addition, the water has the potential to transport stored heat within the water body itself and into and out of it (Brutsaert, 1982).

For sustainability of the evaporation process from open water bodies, there are three main influencing factors; supply of energy to provide latent heat of vaporization, ability to transport the vapor away from the water surface, and continuous supply of moisture at water surface (Brutsaert, 1982). Sources of heat include solar (short-wave) radiation, thermal (long-wave) radiation and inflows of water into the body of water (advection). Thus, evaporation is the difference between two rates, a vaporization rate determined by the temperature of the water, and a condensation rate determined by vapor pressure (Finch and Hall, 2001).

Turbulence and convection facilitates evaporation process, by combining the air near the water surface with the air above the water surface. Higher magnitude of wind resulted in vigorous and effective turbulent mixing. The difference between the temperatures of the surface and overlaying air is directly proportional to convective mixing process (Finch and Hall, 2001).

2.2.1 Solar Radiation

Incoming solar radiation is the dominant source of heat and affects evaporation amounts over the surface of the earth based on latitude and season. This source of energy for evaporation at the Earth's surface is solar radiation and is governed by the following laws and factors:

Three basic laws govern radiation and complete descriptions of these laws are beyond the scope of this study but are summarized as follows (Bras, 1990):

• Kirchoff's Law which states that at thermal equilibrium the amount of radiation absorbed by the atmosphere at a particular wavelength is equal to the amount of radiation emitted at the same wavelength.

• Planck's Law which states that the intensity emitted from a black body changes at 14 different wavelengths and temperatures.

• The Stefan-Boltzmann Law which states that the radiation of a black body is proportional to the fourth power of the absolute temperature (degrees Kelvin) of the body.

Atmospheric Effects on Solar Radiation

Radiation comes directly from the Sun or indirectly from the surrounding atmosphere. The rate at which solar radiation reaches the upper limits of the earth's atmosphere on a surface normal to the incident radiation at the earth's mean distance from the sun is known as the solar constant and is 1353 W/m^2 (Iqbal, 1983). The solar constant, sun's altitude, latitude, season, time of day and atmospheric conditions determine the amount of solar radiation reaching the earth's surface. The sun transmits light and other radiation at different wavelengths, but only a fraction of this energy reaches the Earth's surface. Approximately half of the total energy emitted by the sun is in the visible light range, with wavelengths ranging from 0.4 to 0.7μm and the rest reaches the earth as ultraviolet or infrared wavelengths from 0.15 to 4.0μm. The maximum rate of the sun's emission occurs at 0.5μm wavelength in the visible light range and is 10,500 KW/m^2 (Bras, 1990).

As solar radiation passes through the atmosphere there is a loss of energy known as attenuation and is a function of three (3) main components: scattering, absorption and reflection. About 9% of incoming radiation is scattered back into space through collisions with molecules of air or water vapor. Another 16%is also scattered, but reaches the Earth as diffuse radiation giving the sky a blue appearance. Approximately 15%of solar radiation is absorbed by the gases of the atmosphere, particularly by the ozone, water vapor and carbon dioxide. On average, 33%of solar radiation is reflected from clouds and the ground back into space. The amount depends on the albedo or reflectivity of the surfaces.

Thus, as a result of the various atmospheric losses, approximately 43% of solar radiation reaches and heats the earth's surface (Iqbal, 1983). However, the earth itself radiates energy in the long-wave range and this long-wave radiation is readily absorbed by the atmosphere. The net radiation may then be determined from the incoming and reflected short-wave radiation plus the incoming, reflected and radiated long-wave radiation.

2.2.2 Latent Heat of Vaporization

The energy required to convert liquid water into gaseous water vapor at the same temperature is known as the latent heat of vaporization (Bedient et.al, 1992). This latent heat is the amount of heat absorbed by a unit mass of a substance, with no change in temperature, while passing from the liquid to the vapor state. For continuous occurrence of evaporation, a latent heat of vaporization must be available and a vapor pressure deficit between the air and surface water must exist. The difference between the vapor pressure of the liquid and the pressure of the atmosphere decides how much water evaporated.

2.2.3 Temperature

Evaporation from lakes can be enhanced when cold air overlays a warm water surface. As a result, temperature of both air and the evaporating water surface is important in determining the amount of surface water evaporation. Temperature is dependent on the sun, latitude, and season, time of day, cloud cover and wind speed and is a measure of the thermal energy that a body possesses. As air temperature increases, the amount of water vapor it can hold increases and the surface water temperature also increases. This increase in surface water temperature causes the kinetic energy of water molecules to become more active and more readily transformed into the vaporized state. For this reason, the warmer the water, the greater the evaporation rate be (kettle et. al 2004).

2.2.4 Vapor Pressure Deficit and Relative Humidity

The rate of evaporation is also affected by the vapor pressure of the water vapor in the air which indicates the amount of additional water vapor the air can absorb if the vapor pressure is less than the maximum or saturated value. This additional amount of water vapor that the air can hold at the temperature before becoming saturated is known as the vapor pressure or saturation deficit

(VPD) and, according to Dalton's Law, the greater this deficit the greater the rate of evaporation and vice-versa. This deficit varies with height above the water surface and is the difference between the saturation vapor pressure at air temperature, Ta, and the vapor pressure represented by the saturation vapor pressure at the dew point temperature, Td. Dew point temperature, Td' is the temperature at which a mass of unsaturated air becomes saturated when cooled, with constant pressure. Corresponding saturation vapor pressure, es' represents the amount of water vapor or moisture in the air. Therefore, the higher the dew point temperature, the higher the moisture content is for air at a given temperature. Relative humidity is a useful tool in determining the vapor pressure of the air and can be expressed as the ratio of the vapor pressure to the saturated vapor pressure (Bedient et.al, 1992).

2.2.5 Wind Speed

Wind speed at the water surface is another important factor in evaporation because; the wind above the water body determines the movement of water molecules from the water surface into the air. As water evaporates, the air above the evaporating surface gradually becomes more humid until it become saturated and is unable to hold more vapors. However, when the air is moving, the amount of evaporation increases as air with lower moisture content replaces the saturated air mass. For low wind speeds, less water will evaporate because of the relatively higher vapor content of the overlying air mass while strong wind speeds cause waves and turbulence at the water surface which causes an increase in surface area and an increase in evaporation. Wind speed varies with the height above the water surface is the wind speed (meters/sec) at the height (meters) of the anemometer (McCuen, 1989).

2.2.6 Atmospheric Pressure

Atmospheric pressure can be defined as the downward force on a unit horizontal area resulting from the action of gravity on the mass of air vertically above (Singh, 1992). Evaporation is higher at lower atmospheric pressures than at higher atmospheric pressures because there are fewer air molecules for escaping water molecules to collide with even though air temperature is decreased. Thus, evaporation is higher at higher altitudes as atmospheric pressure decreases with altitude.

2.2.7 Albedo

'Albedo' is Latin, meaning whiteness. The albedo of a surface is the fraction of the incident sunlight that the surface reflects. Radiation that is not reflected is absorbed by the surface. The absorbed energy raises the surface temperature, evaporates water, melts and sublimates snow and ice, and energizes the turbulent heat exchange between the surface and the lowest layer of the atmosphere. The surface albedo is a key ingredient in the remote sensing of surface and atmospheric properties from space. The spectral and angular dependence of reflected sunlight is used to infer surface properties such as the extent and nature of vegetation cover. It must also be allowed for when determining atmospheric composition such as the amount, size, and optical properties of haze particles (McCormick and Meadows, 1988).

Over continents, the largest component of the reflected sunlight under cloud-free conditions is due to reflection by the surface. Consequently, the determination of atmospheric composition from reflected sunlight requires accurate knowledge of the contribution made by the reflecting surface. Different surfaces have different albedo values. Oceans, lakes, and forests reflect relatively small fractions of the incident sunlight and have low albedo values. Snow, sea ice, and deserts reflect relatively large fractions of the incident sunlight and have large albedo values. An albedo is not an intrinsic property of a surface. Instead, for any surface, the albedo depends on the spectral and angular distributions of the incident light, which in turn are governed by atmospheric composition and the direction of the beam of light from the sun (Cogley, 1979).

There are a number of factors which affect the albedo, the solar angle, with water turbidity, wave height and the ratio of diffuse to total solar radiation. The proportion of direct to diffuse solar radiation matters because the albedo is a function of the elevation angle of the incoming solar radiation: the values of albedo are relatively constant, at a low value, at elevation angles greater than 37˚. However as the elevation angle decreases below this value, the albedo of water increases exponentially. Thus, on a cloudy day when the downward solar radiation is entirely diffuse, the albedo of the lake, averaged over a day, will have a higher albedo than on a sunny day when the direct downward solar radiation will be dominant (Finch and Calver, 2008).

2.2.8 Heat Storage Change

The water heat storage change is often termed as water heat flux density at water-atmosphere interface. It is not only controlled by conduction and solar radiation, but is also governed by all heat convective flows inside the water body (Duan, and Bastiaanssen, 2015).

Seasonal variations in the evaporation rate can be significantly affected by the heat storage capacity of the water body which is, to a large extent, determined by its depth. In higher latitudes, where there is a strong seasonal variation in the sun's elevation at noon, the increasing incoming solar radiation serves to warm the water body during the colder seasons. During the colder seasons, as the incoming solar radiation decreases, the water body cools as the stored energy is released. The result is that the evaporation rate can be de-coupled in time from the net radiation. It is generally considered that the effect can be ignored for water bodies with a depth less than 0.5 m. and that the effect reaches a maximum (i.e. the seasonal evaporation ceases to change) once the depth increases beyond 4.5 m (because little of the incoming solar radiation penetrates below this depth). The situation becomes more complex if a water body becomes thermally stratified. Stratification occurs in large, deep water bodies (at mid and high latitudes) and may accentuate the time lag between the net radiation and the evaporation rate. The temperature dependence of the density of water is a key factor (the maximum density occurs at a temperature of 4o C) (Finch and Calver, 2008).

A survey of water temperature profile is the common procedure to estimate the change in heat storage in lakes. Although this procedure is considered the most accurate method to estimate the change in heat stored in lakes, it is very costly and time and labor consuming. Moreover, the accuracy of this method decreases rapidly for short periods. In the Lake Hefner, Oklahoma studies, Anderson (1954) showed that with all the components measured with great care and when the measurements periods were weeks or longer, accuracy of evaporation estimates approached ±5%. In another study, the accuracy of evaporation estimates was determined to approach ±10% at Lake Mead, Nevada for biweekly measurement periods (Koberg, 1958).

Many researchers tried to evaluate the impact of using fewer measurement sites in the accuracy of lake heat storage estimation. Rosenberry et.al, (2007) reported only a 2% deviation from evaporation best estimates, when using one location rather than 16 locations to estimate lake heat storage, from William Lake (maximum depth is 9.8 m), Minnesota. Similar results were concluded during the Lake Hefner (average depth is about 10m) studies (Anderson, 1954; Crow and Hottman, 1973).

2.3 Open Water Evaporation Estimation Methods

Different methods have been developed and put into practice to estimate total evaporation, including meteorological ground-based point data, field measurements and spatially explicit remotely sensed data. Total evaporation is estimated either directly, when it is measured by an instrument, or indirectly, when it is derived by means of its relationship with other parameters, as well as using reference total evaporation (Rana and Katerji, 2000). Depending on data availability and the purpose of estimating total evaporation, different methods can be used. Nevertheless, some methods are more appropriate than others in terms of accuracy, availability and cost, while others are suitable for a particular given space and time-scale. Direct measurements of total evaporation are rarely available and estimates are often derived from reference evaporation estimates (Chen et.al, 2005; Sumner and Jacobs, 2005).

2.3.1 Meteorological Methods

Meteorological methods are based on a point measurement of meteorological conditions to estimate reference evaporation, which can be used to derive total evaporation (Sumner and Jacobs, 2005). Reference evaporation is defined by Chen et.al, (2005) as the atmospheric demand for water from vegetation and soil, without the influence of vegetation characteristics or soil management. McMahon et.al, (2012) define reference evaporation as the loss of water from a prescribed reference surface, where water is abundantly available and soil factors have no effect. It includes evaporation from vegetated surfaces, such as grass or alfalfa, and measurements from free water, such as an evaporation pan or the British standard tank (S- tank). Therefore, the potential evaporation from a grassed surface, pan or tank provides a reference for the estimation of total evaporation for other surfaces.

Table 2.1:Summary of the Data Requirements by Different Meteorological-based Methods

Method	**Reference**	**Meteorological variables required**
Empirical Group		
Blaney- Criddle (1962)	(Fooladmand, 2011 ; Lee et.al, 2004)	Daily temperature, wind speed, relative humidity, sunshine hours
Hargreaves (1956)	(Lu et.al, 2005)	Daily temperature, radiation. Latitude, day of the year
Thornthwaite (1948)	(Maeda et.al, 2011; Pereira and Pruitt, 2004)	Mean daily temperature Daytime length, latitude
Makkink (1957)	(Lu et.al, 2005)	Mean daily temperature, radiation
Dalton/Mass Transfer Group		
Mayer (1942)	(Safavi, 2009)	Mean monthly wind speed, relative humidity
Rohver (1931)	(Dingman, 2008)	Mean monthly wind speed, relative humidity, air pressure
Energy Balance Group		
Priestley–Taylor (1972)	(Mosner and Aulenbach, 2003; Rasmussen et.al, 1995)	Mean daily temperature, radiation, calibration constant
Debruin-Keijman (1979)	(Winter, et.al, 1995; Mosner and Aulenbach, 2003)	Mean daily temperature, radiation, calibration constant
Combination (Mass Transfer and Energy Balance) Group		
Penman (1948)	(Penman, 1948; Mosner and Aulenbach, 2003; Rosenberry et. al, 2007)	Daily temperature, radiation, wind speed, atmospheric pressure, relative humidity

Winter et.al, (1995) compared eleven well-known methods with the energy budget method over Williams Lake, and proposed a ranking based on performance from best to worst. They ranked these methods as Penman, DeBruin-Keijman, Makkink, first to third. Rosenberry et.al, (2007) evaluated 15 methods in comparison with the energy budget method. Rasmussen et.al, (1995) compared seven methods used in lake temperature modeling. Four methods of Priestley-Taylor, deBruin-Keijman, Papadakis and Penman were compared with energy budget method by Mosner and Aulenbach (2003) and, the Priestley-Taylor method results performed the best among the four methods.

Several studies were carried out in order to compare and assess evapotranspiration methods for land surfaces or estimate of required parameters in limited data conditions around the world. On the contrary, a few studies have been conducted to find the most appropriate methods to estimate lake evaporation in the conditions that long term data required are not available. Therefore, there is no clear consensus on which methods are better to employ when lacking important long term measured data such as temperature profile, radiation and heat fluxes as is the case in Lake Hawassa.

Although meteorological-based methods have been used, literature shows that they have limitations in mapping the spatial variations of total evaporation. It has been noted that these methods are based on meteorological stations, which are unevenly distributed spatially (Lee et.al, 2004; Maeda et.al, 2011) and reference evaporation is derived from the interpolation of point-based estimates. Interpolation introduces errors, especially in areas characterized by varying climatic conditions and land cover types (Gibson et. al, 2013).

Total evaporation can also be estimated using micro-meteorological techniques (see Table 2.2). All the methods are used to derive total evaporation directly, except for the A-pan or British Standard tank (S-tank), which estimate reference evaporation and use coefficients to derive total evaporation (Chen et.al, 2005). Brutsaert (2013) highlights that total evaporation from the surrounding area is proportional to the measured pan evaporation, using pan coefficients which vary, due to spatial variations of vegetation characteristics, as well as the environmental conditions (Brutsaert, 2013; Chen et.al, 2005). Micro-meteorological methods have been applied across the globe for various land cover types, including agricultural fields and natural ecosystems (Water Bodies, Forests, mountains etc), with useful estimates.

Table 2.2: Summary of micro-meteorological methods to estimate total evaporation

Method	**Application**	**Reference**
A-pan / S-tank	Estimates reference evaporation and then total evaporation is estimated using pan coefficients	(Brutsaert ,2013;McMahon et.al, ,2012)
Bowen ratio	Estimates total evaporation at a point	(Elsawwaf and Willems, 2012; Hicks and Hess, 1977)
Eddy covariance	Estimates total evaporation at a point	(Mengistu and Savage ,2010; Abraham 2009)
Scintillometer	Estimates total evaporation along a transect	(McJannet et.al, 2011; Hemakumara et.al, 2003)
Surface renewal	Estimates total evaporation at a point	(Spano et.al, 2000; Mengistu and Savage , 2010)

Micro-meteorological techniques have limitations in estimating total evaporation (Jarmain et.al, 2009). With the exception of scintillometry, micro-meteorological methods are not representative of the spatial variability of total evaporation within the landscape, because their estimates are based on point measurements (Gibson et.al, 2013; Jarmain et.al, 2009). On the other hand, scintillometry estimates total evaporation as the average of the fluxes along a defined transect (Meijninger and de Bruin, 2000), which allows the detection of ground-based areal total evaporation variations for a defined path, usually not more than ten kilometers (Hoedjes et.al, 2007). According to Meijninger and de Bruin (2000), scintillometry is a reliable method and an intermediate scale of measurement between ground-based point measurements and the spatial estimates from remotely-sensed data. It has a better spatial representation of total evaporation, when compared to point-based methods. Scintillometry has been successfully applied in open water bodies and landscapes with mixed land cover types (McJannet et.al, 2011; Hemkumara et.al, 2003). The method has also been used to validate remote sensing-based total evaporation estimates (Bastiaanssen, 2000). Although scintillometry has been widely-used, Hoedjes et.al, (2007) highlighted that it is more applicable in homogenous areas, such as agricultural fields and large open water bodies.

In conclusion, the use of point-based and micro-meteorological methods in estimating the spatial variations of total evaporation remains a challenge. Remote sensing is gaining acceptability in the spatial mapping and monitoring of natural resources at different spatial scales.

2.3.2 Remote Sensing Algorithms

Remotely sensed data has been used as an input for different field of studies, and it has been widely applied in estimation of evapotranspiration and evaporation for open water bodies, wet lands and lands. The advent and advancement in remote sensing enables the spatial monitoring of total evaporation over large areas. The increased availability and advancement of satellite data products provides an opportunity to monitor variations of total evaporation at different spatial and temporal scales (Ruhoff et.al, 2012) and allows the monitoring of inaccessible areas (Li et.al, 2009). In addition, Gibson et.al, (2013) highlight that remote sensing technology holds great promise for the long-term monitoring of water resources on a relatively large scale and in a cost effective manner.

Methods based on the use of remote sensing data are therefore well-suited for the spatial variations of total evaporation over time. The methods include the use of vegetation indices and the energy balance models, such as the Surface Energy Balance Index (SEBI), the Simplified Surface Energy Balance Index (S-SEBI), the Surface Energy Balance System (SEBS), the Surface Energy Balance Algorithm for Land (SEBAL) and Mapping Evapo-Transpiration at High Resolution with Internalized Calibration (METRIC). Energy balance models are based on the energy balance approach, since total evaporation requires energy in order to occur.

Table 2.3: Different Remote Sensing Evapotranspiration Algorithms

Algorithms	Input Parameters	Merits	Demerits
SEBI	<T>pbl, hpbl, v, Ts, Rn, G	Relating the effects of Ts and ra directly on LE	Requires ground based Measurement
SEBS	T_{air}, h_a, v, Ts, Rn, G	Uncertainty in SEBS from Ts and meteorological parameters can partially be solved; Roughness height for heat transfer is computed explicitly instead of using fixed values	Requires too many parameters; Relatively complex derivation of turbulent heat fluxes
S-SEBI	Ts, αs, Rn, G	Ground based measurements are not required	Extreme temperatures are location specific
SEBAL	v, ha,Ts, VI, Rn, G	Requires minimum Ground based measurements; Equipped with automatic internal calibration; Exact atmospheric corrections are not required	Applied over plain surfaces; Possesses uncertainties in the determination of anchor pixels
METRIC	v, h_a, T_s, VI, R_n, G	Similar to SEBAL, but surface slope and aspect can be considered	Possesses uncertainties in the determination of anchor pixels
TSM	v, ha, Ts, VI, Rn, G	(1) Includes the view geometry; (2) Eliminates the need of empirical corrections for the “excess resistance”	(1) Many ground measurements and components are needed

2.3.2.1 Surface Energy Balance Index

According to van den Hurk (2001), SEBI is a modified Crop Water Stress Index (CWSI). The SEBI model computes total evaporation by combining remotely sensed inputs and meteorological data. SEBI derives total evaporation and the evaporative fraction, based on land surface dry and wet limits, which are characterized by maximum surface temperature, with low or no evaporation, and minimum surface temperature, with high or maximum evaporation, respectively (Li et.al, 2009). In the SEBI model, the evaporative fraction is estimated from minimum and maximum surface temperatures and from the aerodynamic roughness length or roughness height of heat transfer, to derive latent heat flux (Li et.al, 2009). However, van den Hurk (2001) highlighted that the SEBI roughness height is poorly computed for estimating total evaporation; hence the SEBI model needs further testing and verification against ground-based estimates under various bio-physical and climatic regions. Menent et.al, (2003) has demonstrated the applicability of the SEBI model in France, Spain, Italy, China and the United States of America. Their results agreed well with estimates derived from the ground-based scintillometer (Menenti et.al, 2003). Roerinket et.al, (2000) highlighted that total evaporation can be accurately estimated in wet or humid areas (*e.g.* England) and in extremely dry areas, such as the Sahara Desert, using the SEBI model, where the S-SEBI is inapplicable.

2.3.2.2 Simplified Surface Energy Balance Index

The S-SEBI model estimates instantaneous evaporation, using surface temperature, albedo and NDVI derived from remote sensing (Roerink et.al, 2000). The major strength of S-SEBI is, simple, does not need additional meteorological data, which is ideal in inaccessible areas, nor does it need the vegetation height for heat transfer, like SEBS. The model computes total evaporation and the evaporative fraction, by assuming a constant atmospheric forcing (i.e. constant global radiation and air temperature). Under constant atmospheric forcing, surface temperature is correlated with surface reflectance.

To date, a number of international studies have estimated total evaporation, using the S-SEBI method (Boronina and Ramillien, 2008; Roerink et.al, 2000; Sobrino et.al, 2007). In the Alpilles Province of France, Gómez et.al, (2005) estimated the total evaporation from agricultural fields (i.e. corn, maize, wheat and alfalfa) and the results were validated, using ground-based Bowen ratio estimates. Their results show that the derived S-SEBI total evaporation estimates were in agreement with the crop development stages in the fields and also close to ground-based Bowen ratio estimates. In addition, Sobrino et.al, (2007) estimated the total evaporation in the Iberian Peninsula, using S-SEBI (derived from AVHRR images) for different land cover types, namely, rice fields, olive trees, vineyard, forests and non-irrigated agricultural area. From the results, estimated total evaporation coincided well with surface characteristics, where high estimates of total evaporation were obtained from vegetated areas. The effect of incoming radiation and seasonal variations on total evaporation was also indicated, where higher estimates were obtained during summer and spring, while low estimates were obtained during the winter and autumn seasons. Boronina and Ramillien (2008), using AVHRR-derived S-SEBI, observed similar seasonal patterns of total evaporation estimates over the Lake Chad Basin.

The major limitations of S-SEBI include its assumption of constant atmospheric forcing and its requirement of extreme surface temperature values, which are not always available on every remote sensing image (Roerink et.al, 2000; Sobrino et.al, 2007). Global radiation and air temperature are not always constant, especially in mountainous areas. Moreover, unlike SEBI, this model performs poorly in humid areas, as it prefers dry pixels, as well as in extremely dry conditions, such as the Sahara Desert, and over larger continental areas, where atmospheric conditions are not constant (Roerink et.al, 2000). S-SEBI yields low estimates, when using coarse resolution images, due to mixed land cover spectral features in a single pixel. Further, the selection of extreme temperatures, representing the dry and wet conditions of the area, are derived by means of the image feature space (relationship between reflectance and surface temperature), without the use of location specific conditions. This introduces errors and uncertainties in the estimation of total evaporation.

2.3.2.3 Surface Energy Balance System for Land

SEBAL is a model, which was developed by Bastiaanssen et.al, (1998) for computing turbulent fluxes or energy exchanges between land and the atmosphere using remote sensing data and meteorological data. Remote sensing inputs include vegetation indices, albedo and surface temperature, whereas meteorological inputs include temperature, wind speed, humidity and solar radiation. A detailed explanation of how all the energy balance components are derived to compute evaporation, using SEBAL is provided by Bastiaanssen et.al, (1998). In brief, SEBAL uses the aerodynamic roughness length or roughness height of heat transfer (Li et.al, 2009) in estimating latent heat flux. SEBAL has been widely-used internationally under varying climatic conditions in agriculture and natural forests.

In Africa, Mutiga et.al, (2010) used SEBAL to estimate total evaporation for a catchment in Kenya and their results showed that the model is effective in estimating the spatial variation of total evaporation for water resources management. In South Africa, Kongo and Jewitt (2006) used SEBAL-derived total evaporation estimates to examine the hydrological effects of rain water harvesting within a catchment. Their results indicated that SEBAL underestimated sensible heat flux, when compared with measurements from eddy covariance. Hellegers et.al, (2009) used SEBAL to estimate total evaporation for the Inkomati Catchment and their results showed the variation of total evaporation between different vegetation types. They concluded that SEBAL, when combined with biomass production and rainfall data, shows the spatial distribution of water availability, consumption and surplus, based on different land cover types. Furthermore, Jarmain et.al, (2009) also used SEBAL in estimating total evaporation from Landsat images over different climatic regions and with varying land cover types, in the KwaZulu-Natal and Eastern Cape provinces. They concluded that the SEBAL model agrees well with ground-based measurements, especially with regard to net radiation. They further highlighted that SEBAL agrees well with the other energy balance models (SEBS, METRIC and VITT), which were used.

The algorithm has also been adopted for different total evaporation estimation from different water bodies (lakes) around the world. Ahmed and Bastiaanssen (2000) adopted the SEBAL technology in combination with remote sensing data to estimate evaporation for Lake Naivasha, Kenya; they compared daily evaporation rate based on evaporative fraction method and the surface energy balance approach with pan data based average evaporation estimation, for the period of thirty years. Comparison between the two approaches to estimate evaporation showed reasonable results. Mohamed Hassan (2013) also adopted the SEBAL technology in combination with remote sensing data to estimate evaporation for Lake Nasser, Egypt. The study compared daily evaporation rate based on evaporative fraction method and the surface energy balance approach with different conventional evaporation estimation approaches. In the above studies, daily estimation of evaporation was estimated using Landsat Thematic Mapper (TM) spectral data. The Landsat TM based estimation was compared with the other methods estimated average evaporation on the same date.

Even though SEBAL has been successfully applied, a further understanding of the model and the impact of surface heterogeneity on heat fluxes at watershed or regional scales is required (Long et.al, 2011). Despite its usefulness in understanding the spatial variations of total evaporation, SEBAL has some drawbacks. Gibson et.al, (2013) state that the SEBAL model is protected by intellectual property. SEBAL is also difficult to apply at large spatial scales (van den Hurk, 2001). In addition, if the SEBAL model is applied, its surface roughness parameter is poorly defined and its use of fixed temperature values for the dry and wet conditions of evaporation is problematic (Li et.al, 2009).

2.3.2.4 Mapping Evapotranspiration at High Resolution with Internalized Calibration

The METRIC model (Allen et.al, 2007) was developed based on the SEBAL model and it computes the spatial variations of total evaporation, based on remotely sensed data and reference evaporation (Li et.al, 2009). The model also requires solar radiation, air temperature dew point temperature and wind speed (Hankerson et.al, 2012). METRIC computes and shows the estimated total evaporation as a fraction of the reference evaporation (Hankerson et.al, 2012) independent of vegetation type. METRIC differs from SEBAL in its use of meteorological-based reference evaporation and it also incorporates the soil moisture balance from meteorological-based data, to determine wet and dry limits for estimating evaporative fraction. The METRIC model has been widely-used in United States under varying climatic and land cover types for various applications (Allen et.al, 2007). The model-based results also agreed well with ground-based (lysimeter) measurements.

The METRIC model was also used in South Africa (Jarmain et.al, 2009) to estimate total evaporation for different sites under varying climatic conditions. The results showed that METRIC agreed well with other energy balance models, as well as with ground-based measurements, especially with regard to the estimation of net radiation.

Although METRIC has been used extensively, much of its utility has been shown in the United States (where the model was developed), with Landsat images, or images with similar spatial resolution. Allen et.al, (2011) also highlighted that the disadvantage of the METRIC model is that it requires trained experts or specialized personnel, high quality weather data and it relies highly on the ability of the operator to select the appropriate cold and hot pixels for the accurate estimation of total evaporation.

2.3.2.5 Surface Energy Balance System

The SEBS model, which was developed by, Su (2002), estimates heat fluxes, using remotely sensed data (*i.e.* land surface temperature, albedo, emissivity, fractional vegetation cover, leaf area index, NDVI) and meteorological data (*i.e.* temperature, humidity, wind speed and pressure) at a reference height. SEBS also requires solar radiation, which can be directly measured on the ground or it can be modeled from remote sensing data (Su, 2002).

SEBS uses the Monin-Obukhov Similarity Theory (MOST) to estimate the sensible heat (H) and latent heat (λE) fluxes. MOST relates surface fluxes to surface variables and variables in the Atmospheric Surface Layer (ASL), a detailed explanation of which is given by Su (2002). Unlike other energy balance models, SEBS computes the aerodynamic resistance of heat transfer more explicitly, instead of using fixed values, like SEBI and SEBAL (Li et.al, 2009). Aerodynamic resistance varies with environmental conditions for different surface types, hence it has an effect on the estimation of heat fluxes, and subsequently, on total evaporation (Sugita and Kishii, 2002). Liu et.al, (2006) highlight the importance of aerodynamic resistance when estimating total evaporation, using remotely sensed-based methods. SEBS is part of the open source freeware Integrated Land and Water Information System (ILWIS) package available free of charge (http://www.52north.org), unlike SEBAL, which is protected by intellectual property (Gibson et.al, 2013).

SEBS has been used internationally to estimate total evaporation for different land cover types, using different remote sensing sensors and yields reliable estimates. Su et.al, (2007) evaluated the accuracy of total evaporation estimates from SEBS, using MODIS data, against ground-based measurements in the grasslands of Netherlands and Germany, the croplands of the United States, the rainforests of Brazil and the Canadian forests. Their results showed a close agreement between SEBS-based estimates and ground-based measurements, as well as the feasibility of using SEBS to estimate heat fluxes over inaccessible areas, where in-situ data are not readily available. However, there were uncertainties, due to satellite spatial resolution in capturing the spatial heterogeneity of the land cover types; hence, they recommended the use of medium resolution Landsat imagery. This is also supported by Vinukollu et.al, (2011), who noted a disparity between total evaporation estimates derived using remote sensing data and ground-based measurements using eddy covariance system. They highlighted that the coarse spatial resolution MODIS data did not capture the heterogeneity of the surface (Vinukollu et.al, 2011).

In the African context, Elhag et.al, (2011) used SEBS to estimate total evaporation for the Nile Delta agricultural production zone of Egypt from Advanced Along-Track Scanning Radiometer

(AATSR) images. SEBS showed a very high correlation, with ground-based measurements and its applicability in estimating daily total evaporation over agricultural areas was demonstrated. Rwasoka et.al, (2011) used SEBS to estimate the spatial variation of total evaporation of a catchment in Zimbabwe, using MODIS data. The results showed that SEBS is a valuable model for determining the spatial variations of total evaporation and for managing water resources. However, Rwasoka et.al, (2011) concluded that there is also a need for further research to determine the best approach for arid and semi-arid areas characterized by various land cover types. Gibson et.al, (2013) highlight the applicability of SEBS in estimating total evaporation in the heterogeneous catchment of the Piketberg region, in South Africa, based on MODIS data. Their results show that SEBS is very sensitive to temperature gradient. Recently, Gibson et.al, (2013) reviewed the estimation of total evaporation using SEBS and they concluded that the model did not yield accurate daily evaporation results at the MODIS spatial resolution. They recommended that any further research, using the SEBS model in South Africa, should be limited to fully vegetated areas or agricultural areas, and should also consider the potential of high resolution images. The SEBS model was also applied by Mengistu et.al, (2014) to provide accurate estimates of total evaporation from agricultural fields in KwaZulu-Natal, South Africa. These estimates were based on images from MODIS, Landsat 7 ETM+ and Landsat 8 satellites. The results showed that Landsat provided better total evaporation estimates, when compared to MODIS, possibly because of their spatial resolution (30 m, compared to 1000 m).

There are also a number of applications of SEBS algorithm over open water evaporation estimation. Ahmed et.al (2016) has adopted SEBS algorithm to estimate evaporation from saline and fresh water bodies (AquaSEBS). The study compares the AquaSEBS estimates with the in-situ measurements and found a good agreement. Mohamed (2013) investigates the use of remotely sensed imagery data MODIS L1B within Surface Energy Balance System (SEBS) to estimate daily evaporation rates from Nasser Lake. The study compares the SEBS algorithm with other seven conventional methods, and approves good correlation except with water budget and Papadakis method. On Lake Mutirikwi, Zimbabwe, Chenyepe (2010) also makes use of MODIS L1B within SEBS algorithm. The study, after comparing the SEBS results with the locally available Pan Evaporation data, concludes that SEBS is an applicable method of estimating spatial distribution of evaporation over open water bodies.

In Ethiopia application of remote sensing for estimation of evaporation, is limited or only small number of studies have been carried out regarding the issue. Fortunately, the country's rift valley is may be the most studied basin as far as evaporation is concerned. Ayenew, (2003) has studied evapotranspiration from the Ethiopian rift and from adjacent highlands, applying satellite image. Assefa et.al (2009) has also makes use of remote sensing data while comparing different models for estimating evapotranspiration from three rift valley lakes. Yibeltal and Binyam (2015), make use of this algorithm to estimate evaporation loss from Lake Hawassa, Ethiopia. Daily estimation of evaporation was estimated using Moderate Resolution Imaging Spectro-radiometer (MODIS) spectral data. They have stated that evaporation rate is highly coupled with sedimentation.

Abreham (2009) has carried out satellite based estimation of evaporation estimation on Lake Tana, and he makes use of MODIS instrument. The study makes use of remote sensing as a tool to show that the effect of spatial and temporal variability on monthly evaporation estimate. Duan, (2014), assessed twenty two lakes of the world (Lake Tana was among these Lakes) using remote sensing products. The study uses the new hysteresis model of its own to estimate main surface energy balance equation component, and compares the estimated values with the measured ones. Even though the first stage (i.e. acquiring the satellite image and preprocessing to some extent) is the same for all remote sensing applications, there is slight to huge difference in their interpretation or in their method of analysis (i.e. input parameters and assumptions).

2.4 Moderate Resolution Imaging Spectro-radiometer (MODIS)

The Moderate Resolution Imaging Spectro-radiometer (MODIS) is one of the research facility instruments designed as part of NASA's Earth Observing System (EOS) to provide long-term global surveillance of the Earth's land, ocean, and atmospheric properties (Asrar and Dokken, 1993). MODIS was built upon the occurrence of Advanced Very High Resolution Radiometer (AVHRR) and the Landsat Thematic Mapper (TM). It was designed not only for providing continual (high temporal resolution) global observations, but also as a new generation of sensor with an increased combination of spectral, spatial, radiometric, and temporal resolutions. In addition to improvement in sensor instrument, the MODIS mission also emphasized the development of operational data processing algorithms to generate global remote sensing spectral datasets and a variety of value added products spanning both the optical and biophysical domains. The motivation was to provide MODIS standard products to the general scientific community to support both theoretical and applied applications.

Two MODIS instruments were initially scheduled for launch on the EOS-AM (EOS-Terra) and EOS-PM (EOS-Aqua) Plat forms in June 1998 and December 2000, respectively (Running et.al, 1994). The actual launch dates were December 18, 1999 (EOS-Terra) and May 4, 2002 (EOS-Aqua). Terra MODIS data have been available since February 2000. Both EOS-Terra and EOS-Aqua are polar orbiting sun-synchronous platforms. The orbit height of EOS platforms are 705 km at the Equator. Terra's equatorial crossing time (descending) is at 10:30am local time; approximately 30 minutes later than the Landsat 7 satellite. Aqua crosses (ascending) the equator at approximately 1:30 pm. Each MODIS instrument has a two-sided scan mirror that operates perpendicular to the spacecraft track. The mirror scanning extends 55° at either side of nadir, providing a nominal swath of 2330 km (whisk-broom). The wide swath allows the nearly global coverage to be obtained by each instrument every 1–2 days. A total of 36 spectral bands were carefully positioned across the 0.412–14.235 μm spectral region. Among the 36 spectral bands, the first two bands are located in the red (0.648 μm) and near-infrared (0.858 μm) with a spatial resolution of 250 m. There are five additional bands (bands 3–7: 0.470 μm, 0.555 μm, 1.240 μm, 1.640 μm, and 2.13 μm) with a spatial resolution of 500 m located in the visible to short-wave infrared (SWIR) spectral regions. The remaining 29 spectral bands (bands 8–36) have 1000 m spatial resolution, and are located in the middle and long-wave thermal infrared regions (TIR). The MODIS instrument also has a 12-bit radiometric resolution with advanced onboard calibration subsystem that ensures high calibration accuracy (Guenther et.al, 1998; Justice et.al, 1998). Table 2.5 provides the technical specifications of MODIS data set which have been employed in this study; including primary use, band numbers, band widths, spectral radiance, and spatial resolutions.

Muira, et.al, (2008) carried out comparative accuracy assessment between of ASTER and MODIS standard products; and from the results it has been suggested that the performance of the ASTER atmospheric correction algorithm was not as good as that of MODIS. MODIS data sets have also been employed and evaluated for different hydrological (specifically evaporation) applications and have showed a good performance (Yibeltal and Binyam, 2015; Mohamed, 2013; Chenyepe, 2010; Aberham, 2009; Su, 2002).

Table 2.4: MODIS Technical Specifications

Band Number	Primary Use	Band Width (µm)	Spectral Region	Spectral Radiance (W/m^2-µm)	Spatial Resolution at Nadir (m)
1	Land/Cloud Boundaries	0.620-0.670	Red	21.8	250
2		0.841-0.876	NIR	24.7	
3	Land/Cloud Properties	0.459-0.479	Blue	35.3	500
4		0.545-0.565	Green	29	
5		1.230-1.250	NIR	5.4	
6		1.628-1.652	SWIR	7.3	
7		2.105-2.155	SWIR	1	
17	Atmospheric Water Vapor	0.89-0.920	NIR	10	1000
18		0.931-0.941	NIR	3.6	
19		0.915-0.965	NIR	15	
31	Surface/Cloud Temperature	10.78-11.28	LWIR	9.55	
32		11.770-12.27	LWIR	8.94	

2.5 Evaporation on Lake Hawassa

Evaporation is typically computed as the residual loss from storage or estimated through the use of a surrogate such as evaporation pan (Evans, 2009). And many studies which have been carried out on Lake Hawassa prove the above statement. Gebreegziabher, (2004), while assessing water balance of the lake, he estimated Evaporation as component using Penman (combination approach) and Pan Evaporation. In the study, the values obtained using both methods were presented in comparative manner and, it has been observed that, the two values gives almost the same monthly value. But annual values for Penman (combination approach) and Pan Evaporation were, 1375 mm year^{-1}(132 Mm^3) and 1567 mm year^{-1}(150.432 Mm^3) respectively. For the penman method he carried out sensitivity analysis and it has been found out that, evaporation from the lake was more sensitive to shortwave radiation. It has been also stated by the author that, 1% increase or decrease in evaporation could lead to 5cm increase or decrease in lake level. Brook and Deganovsky, (2008), have assessed water balance and level regime of Ethiopian lakes. And on their water balance result, long term average annual evaporation from Lake Hawassa was found to be, 1440 mm (138.24 Mm^3). Which is exactly the same as the long term average annual inflow value, and it was computed from the result that, evaporation accounts for almost 33 percent of the total water balance. Ayenew, (2004), makes use of ground water models to determine water balance components and found out that, evaporation is the major water balance component of the lake with the long term annual value of 132Mm^3. From the study result it has been computed that, evaporation accounts for about 35 percent of total water budget. Lemlem, (2007), has also estimated the mean annual potential evapotranspiration of the lake catchment (i.e. not the water body itself) using pan evaporation data from the metrology, and the result was found to be 1581mm (151.776 Mm^3). Shewangizaw, (2010), determined the lake evaporation as 178.93 Mm^3 per annum, which was greatest among other water balance components.

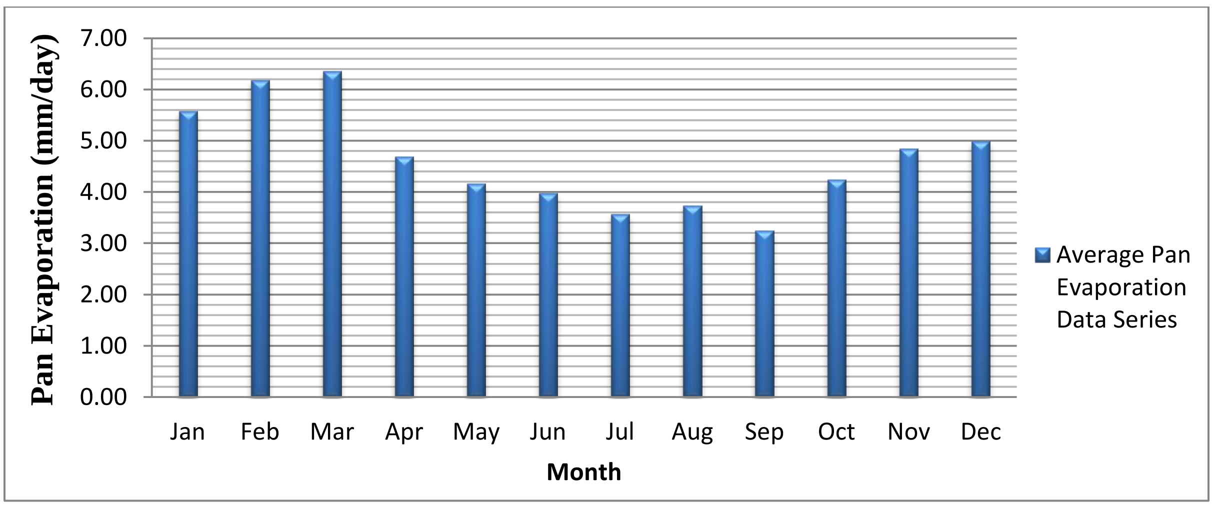

Figure 2.1:Monthly Average Pan Evaporation (2013-2017)

From figure 2.1 it can be observed that, March followed by April, January and February, experiences the highest evaporation rate through the year. There is increasing evaporation trend from January to March, and decreasing pattern from March to September, again the increasing pattern continues from October to December. The lowest pan evaporation rate is observed at the month of September.

3 Materials and Methods

3.1 Description of the Study Area

3.1.1 Location and Topography

Lake Hawassa watershed is located in the Central Main Ethiopia Rift valley (MER) and lies between latitude 6˚48’45”-7˚14’49”N, and longitude 38˚16’34”-38˚43’26”E and the Lake Hawassa lies between 6˚59’0”-7˚7’45”N, and longitude 38˚24’0”-38˚28’40”. The lake watershed falls in two administrative regions, Oromia and Southern Nations Nationalities and Peoples Region (SNNPR) and has a total area of 1407.23 Km^2 of which 112.78 Km^2 (around 8.1% of the total area) is the Lake surface. Elevation of the area generally ranges from 1680m.a.s.l. to 2940m.a.s.l. comprising escarpments, ridges, plateau, undulating to rolling and dissected plains, depressions, and swamps.

Lake Hawassa is a Closed-watershed Lake with no surface water outflow. It is located at about 275Km from the capital city Addis Ababa in SNNPR bordering the capital of the region Hawassa in the west. It stretches 16 km NE-SW (the longest axis) and 6 km NW-SE (the shortest axis) with a maximum depth of 21 meter at its NE part and decrease in depth to the shores (Gebreegziabher, 2004). The lake is fed both by few ephemeral streams on the north-west and western side of the catchment and by the Tikur Wuha River, which is the only perennial river, enters Lake Hawassa draining the Cheleleka swamp on the northeast side. Cheleleka swamp receives surface runoff from the headwaters of the eastern rift escarpment and from groundwater upstream. Lake Hawassa Watershed is a result of volcano-tectonic depression (caldera) as a result its drainage pattern is radial, where rivers flow in all directions away from a raised feature, which is volcano. Surface and sub-surface fracture intensities, rock and soil formation, topography and climate are the governing factors for the drainage density and pattern.

The lake watershed mainly is characterized by a flat-lying topography with scattered small hills. Elevation of the rift escarpments and ridges in the east and west of the watershed range from 2000 to the maximum of 2940 m.a.s.l. It is known that the uplands on either side of the flat lowlands are deforested and denudated. The steeply sloping and deforested uplands are likely to produce high runoff to the lowlands shortly after individual storms. The continuous erosion process on the eastern highlands have resulted on filling Chelelaka Lake with sediment load and transformed it to a swamp (Gebreegziabher, 2004).

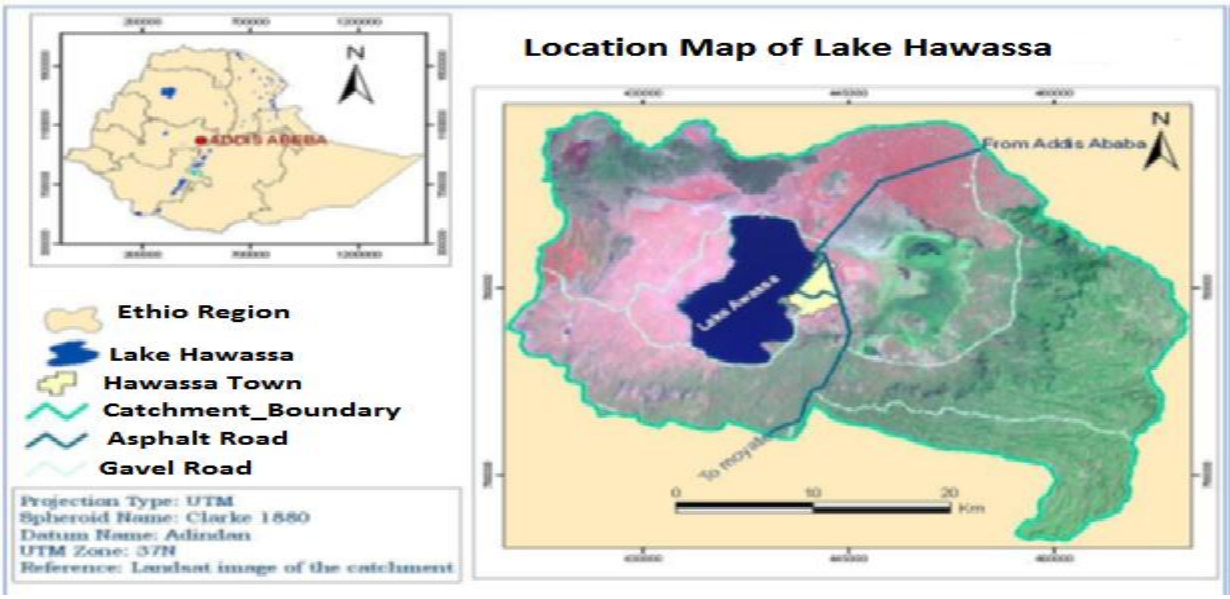

Figure 3.1: Lake Hawassa Watershed Location Map. Source: (Orkodjo, 2014)

3.1.2 Climate

The watershed is characterized by three main seasons (Kiremt, Bega and Belg). The long rainy season in the summer from June-September is known locally as Kiremt and is primarily controlled by the seasonal migration of the inter-tropical convergence zone (ITCZ), which lies to the north of Ethiopia at this period Legesse et.al, (2003). The wet period (locally named as Kiremt) represents 50% of the mean annual total rainfall. The dry period (locally named as Bega) extends between October and February when the ITCZ lies to the south of Ethiopia (Legesse et.al, 2004), this season contributes only 20% of the mean annual total rainfall. During between March and May, season (locally named as Belg) about 30% of the annual rainfall falls.

The climate in the area varies from dry to sub-humid according to the Thornthwaite’s system of defining climate or moisture regions (Dessie, 1995). The mean annual rainfall on basis of 30 years of record of rainfall station which situated 1km from the lake contribute to the catchment is estimated to be 954mm. The wettest months are, May July and August, presented in the following chart.

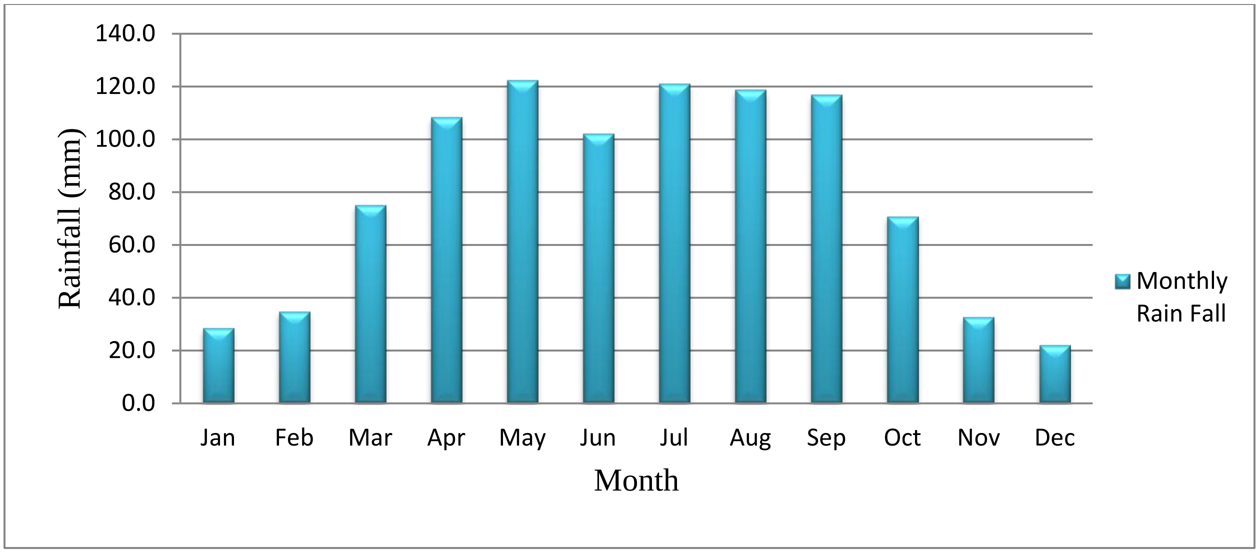

Figure 3.2**:** Long-term mean monthly rainfall (1987-2016)

From the long-term (i.e. 30 years) temperature data, the mean annual air temperature in the area is 20.3 ^{0}C. The hottest months are, March, February, and January, with highest values of maximum air temperature of 29.98 ^{0}C, 29.96 ^{0}C, and 28.96 ^{0}C respectively. The coldest months are November and December, with lowest values of minimum air temperature of 10.6 ^{0}C and 10.4 ^{0}C respectively. The long term mean monthly air temperature values are presented in the following figure.

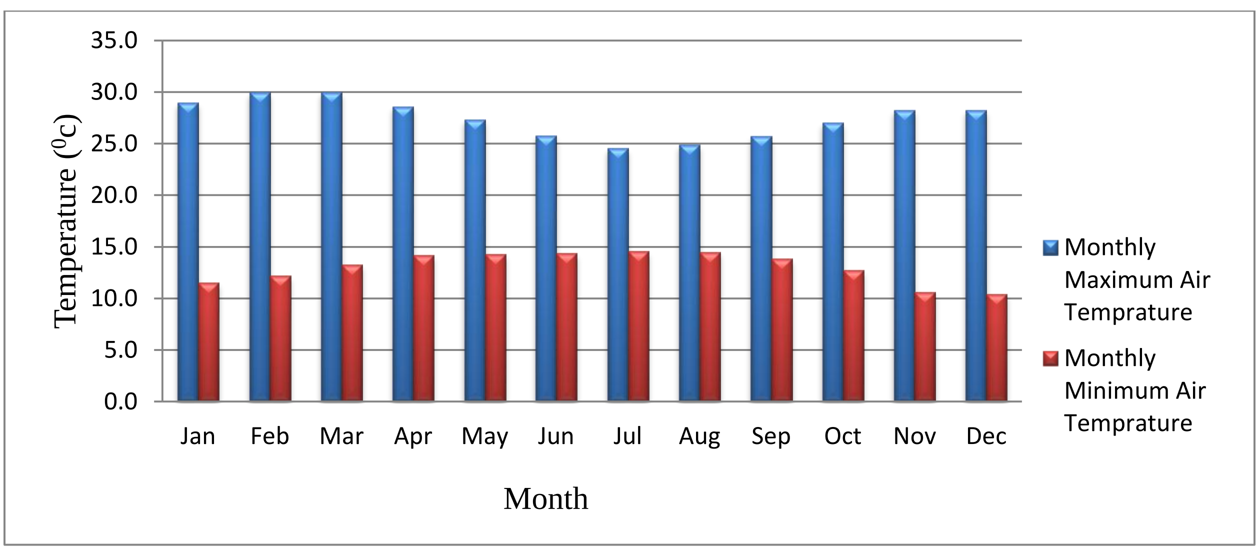

Figure 3.3: Long-term mean monthly air temperature (1987-2016)

At a station in Hawassa town relative humidity has been measured three times (at 6:00 AM, 6:00 PM and 12 PM) in 24 hrs, since 1972. The Relative humidity records show the mean minimum monthly of 50% in February and reaches maximum 73% in September.

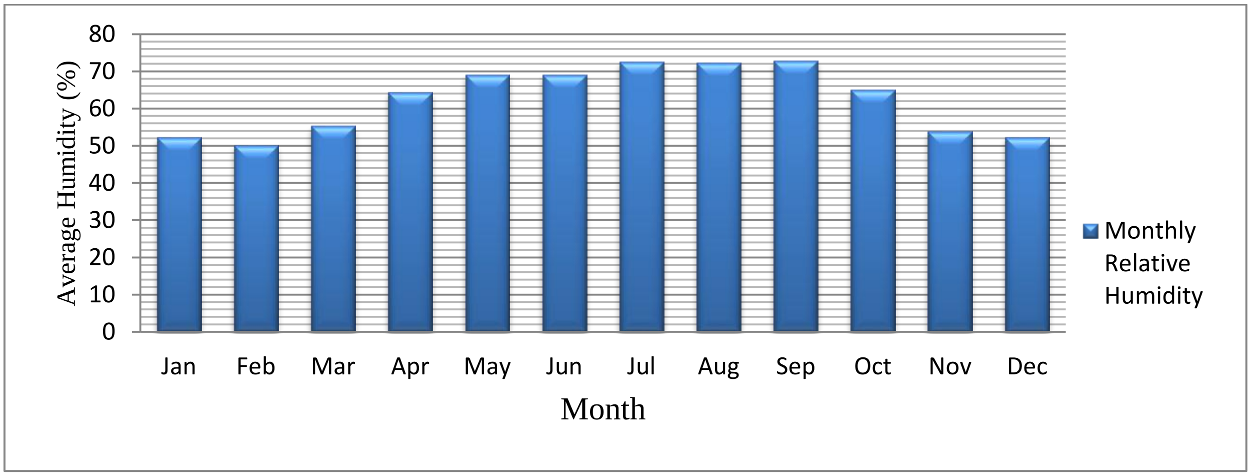

Figure 3.4: Long-term mean monthly Relative Humidity (1987-2016)

Through the recording period of 1989 up to 2016, the highest long term mean monthly wind speed in June about 0.995m/s and the lowest long term mean monthly wind speed in October about 0.566m/s.

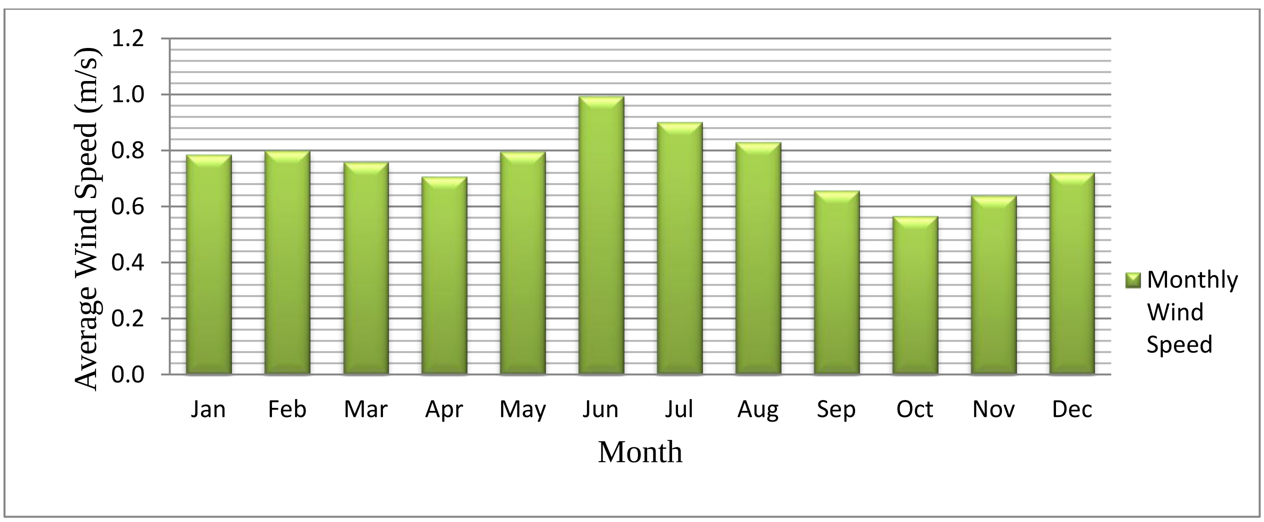

Figure 3.5: Long-term mean monthly Wind Speed (1989-2016)

From the records of Hawassa Station, it has been observed that, the value of wind speed is decreasing with time. Wind speed record of 28 years shows that, a decrease of average annual wind speed from 1.011 m/s in 1989 to 0.557 m/s in 2016 with some fluctuations in between. The decreasing trend is mainly due to deforestation and building of construction around the lake (Gebreegziabher, 2004).

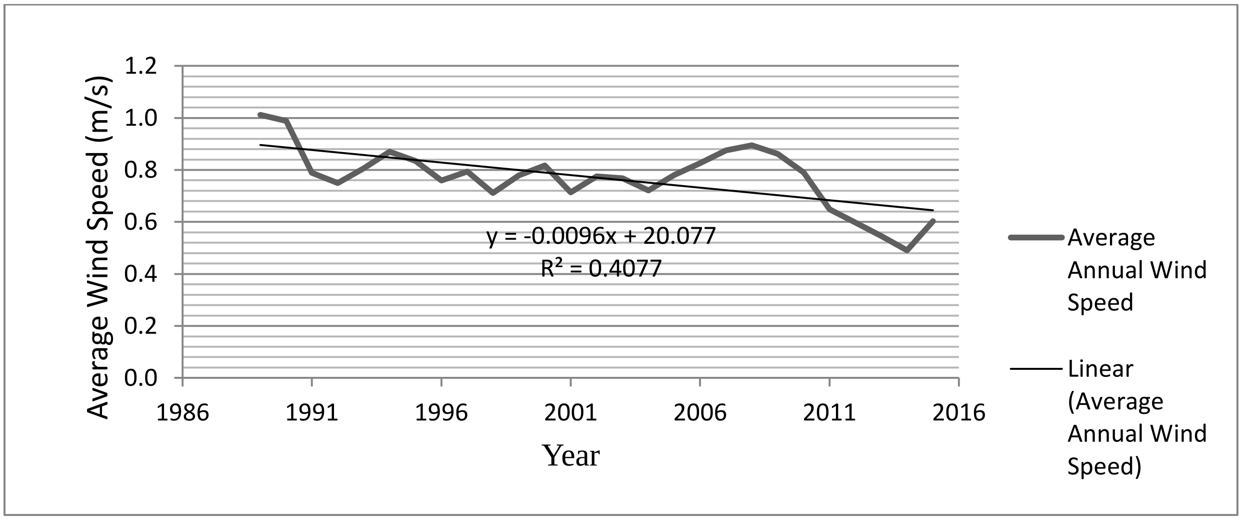

Figure 3.6: Long-term Average Annual Wind Speed (1989-2016)

The sunshine hours vary from minimum of 4.84 hrs in July to a maximum value of about 9.31 hrs in December through the period of 1987 up to 2016.

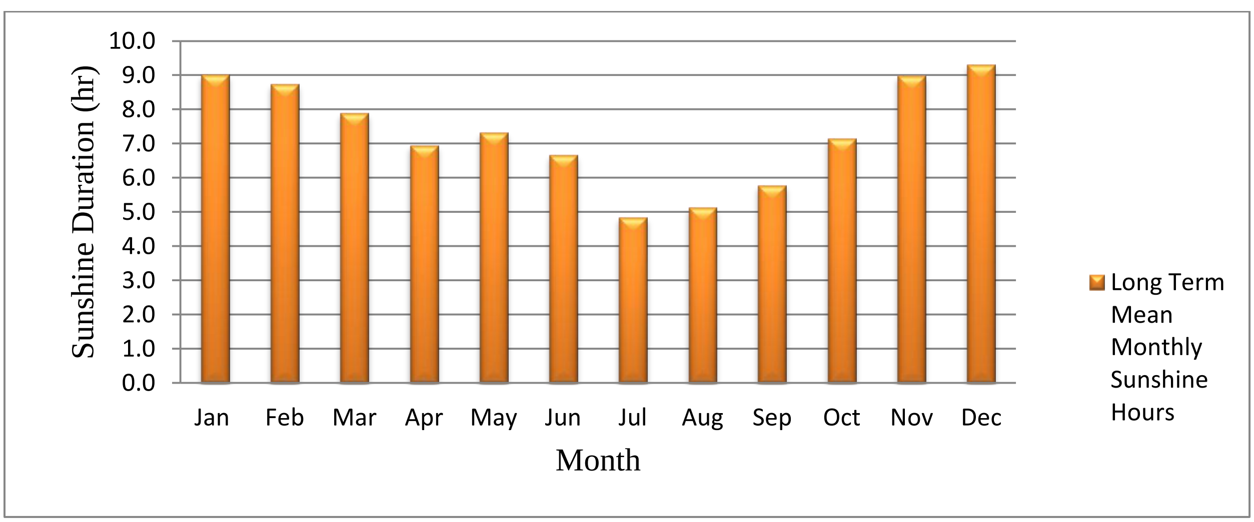

Figure 3.7: Long-term Mean Monthly Sunshine Duration (1989-2016)

3.1.3 Land use and land cover

The land cover changes in the Hawassa Lake Watershed take place as a result of changes in the purpose of land utilization. Human factors play dominant roles in influencing the changes that take place over a period of time. Due to increase in population and demand for fire wood and construction materials, dense woodland and bushy woodland have been changed to open bush land, open grass land and cultivated land by about 70% as compared to the situation of the lake watershed in 30 years of period (WWDSE, 2001).The main land cover of the catchment is dominated by the intensive smallholder cultivation. It covers an area of 88,021ha which is 61.27% of the watershed and 65.53% of the watershed's land area. Water covers an area of 9324ha which is 6.49% of the. Bare eroded land with scattered vegetation covers an area of 7913 ha which is 5.51% of the watershed and 5.89% of the watershed's land area. Open shrub land, shrub land, wood land, grass land, forests, marsh land and bare rock cover the remaining watershed's area (MoWR, 2010).

3.1.4 Hydrology and Morphology

Telford, (1998) developed a steady state water balance for Lake Hawassa, and he found out that direct precipitation and runoff accounted for 56% and 44% of the total input to the lake respectively. The main source of the runoff water is Tikurwuha River sub-catchment which is about 52% of the Hawassa Lake watershed. Tikurwuha River, a channel connecting L. Cheleleka and L. Hawassa, is gauged at Tikurwuha and Datovillages. Following the rainfall trend, the runoff is higher in between August and December the runoff is maximum during this period and minimum runoff amount is recorded between February and May. All gauged rivers are perennial even if they have low discharge in dry period.

Evaporation dominates water losses from the lake (93%), and the rest percent of water loss is accounted by some ground water seepage (7%), which supposed to flow to other low lying lakes. Groundwater outflow is considered as the main responsible factor for the fresh nature of the closed Lake Hawassa Telford (1998), Lamb et.al, (2002). When we compare the elevation of Lake Hawassa (1680 m) with Lake Ziway (1636 m), Langano (1585 m), Abiyata (1578 m), Shalla (1550 m) and Abaya and Chamo (~1180m) (Geberegiziabher, 2004), it is possible for ground water to flow from Lake Hawassa to low lying lakes when hydro-geological condition permits.

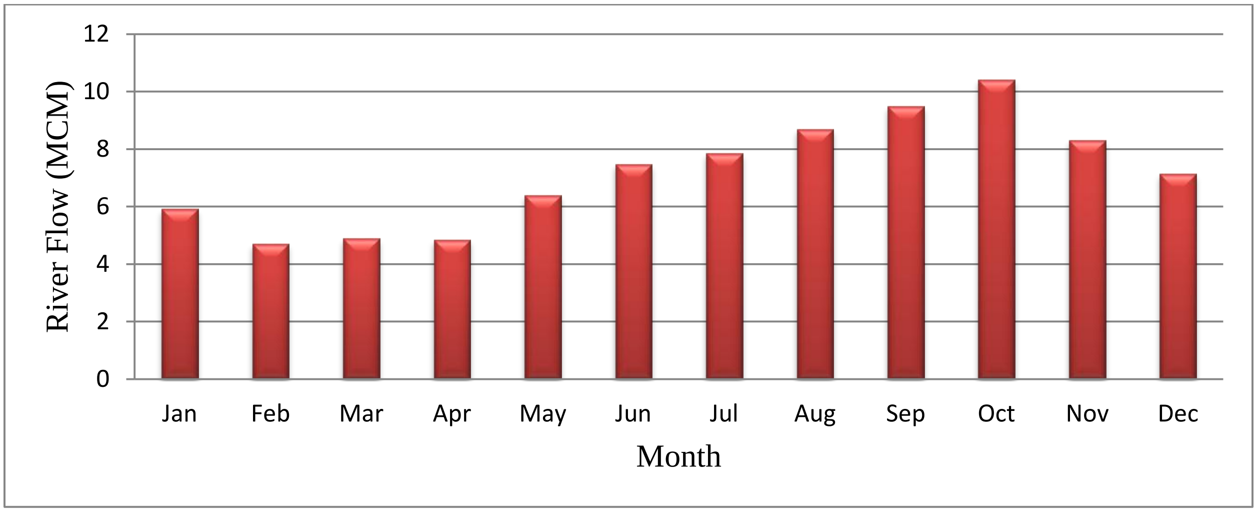

Figure 3.8: Long-term Mean Monthly Flow at Gauge near Dato Village (1980-2015)

As it can be observed from the chart, the highest long term mean monthly flow to the lake is in October. The inflow increasing trend starts from May up to October; whereas, the decreasing trend starts from November to April. The overall trend follows the climatic condition of the catchment.

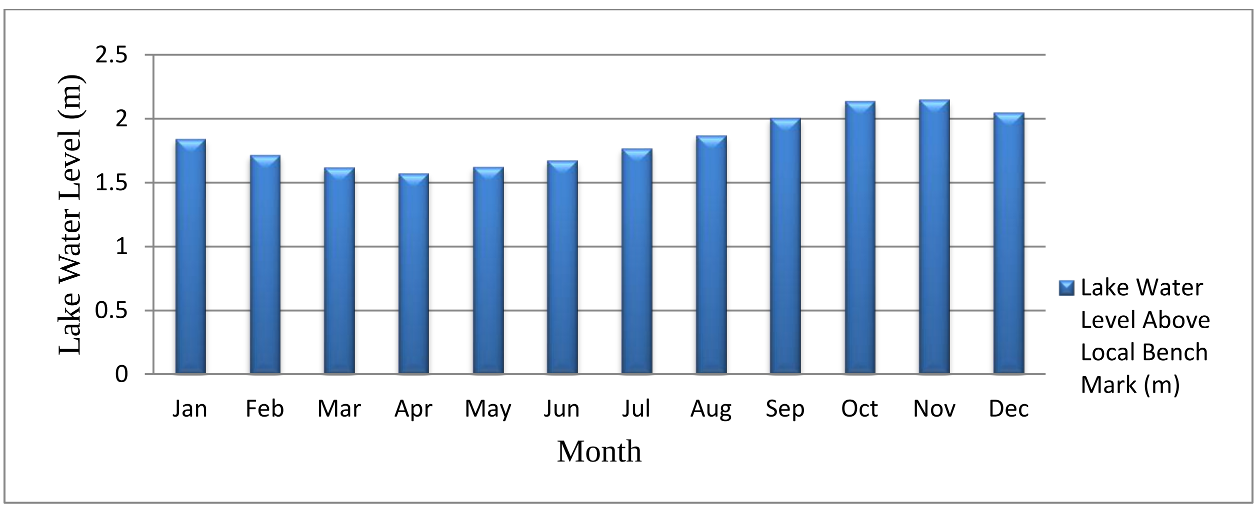

Figure 3.9: Long-term Mean Monthly Lake Water Level above Local Benchmark (1980-2015)

According to Belete (2013), the maximum depth of the lake is 23.4 m and an average depth of 13.3 m. As extracted from satellite imagery, the length of north-to-south axis is 16 km and the east-west axis is 8 km with lake surface area of 96 km^2. The water storage capacity of the lake is 1.36 km3 (Ayenew et.al, 2007). The Hawassa Lake level has been monitored since 1969 by the Ministry of Water Resources, department of hydrology. The lake level shows a general increasing trend. During the period of lake level observation starting from 1981, the level was fluctuating at an average of 1.3m until 1988 since then the lake level was never been below its base period average 1.94m with the exception of the years 1991, 1992 and 1995 with a 1.6m, 1.4m and 1.8m record, respectively (MoWR, 2010).

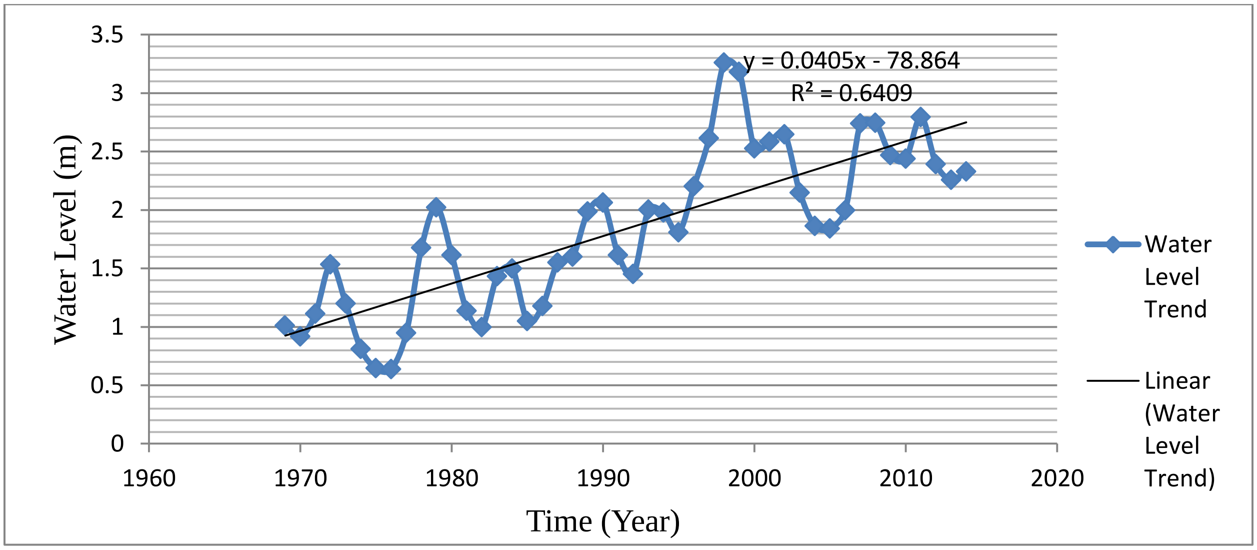

Figure 3.10: Mean Annual Lake Water Level Trend above Local Benchmark (1980-2015)

3.2 Lake Evaporation Estimation

Lake evaporation and energy balance components (lake heat fluxes) estimation involves meteorological and remote sensing approach. Based on previous literatures, meteorological methods (Penman and Debruine-Keijman methods) with good performance were selected for estimation and comparison with the remote sensing approach The Bowen Ratio Energy Balance (BREB) method was also made use to estimate evaporation from Lake Hawassa. The BREB method has been widely evaluated and indicated to be very accurate in most cases and is often considered as a standard method particularly where other methods are validated or calibrated (Winter et.al, 1995; Lenters et.al, 2005; Rosenberry et.al, 2007; Finch and Calver 2008). Based on availability and previous studies results the SEBS algorithm in ILWIS was employed as a remote sensing approach. Pan evaporation method was used as a reference to compare conventional methods with remote sensing approach; because it is the only available direct evaporation measurement on Lake Hawassa. Figure 3.11 presents the overall estimation process in the form of flow chart.

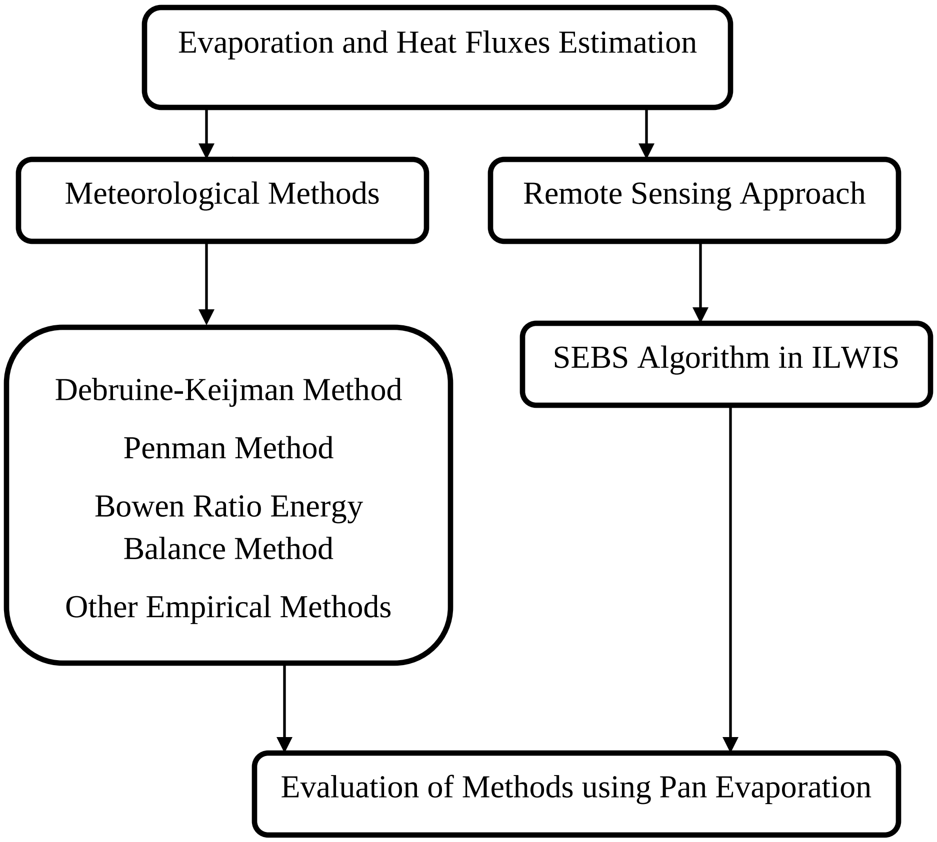

Figure 3.11: Overall Evaporation and Energy Balance Components Estimation Process

3.2.1 Data available

The available data used to compute the evaporation estimate using the meteorological and micro meteorological methods is taken based on the available satellite data, for the sake of the comparative assessment. For instance, there was meteorological and micro meteorological data representing the month of June, July, and August, but the satellite data couldn’t be retrieved due to data quality. Therefore, the meteorological and micro meteorological data considered unavailable for the months. Utilized available data are presented in table 3.1.

Table 3.1: Available Data (Utilized Data)

Recording Date	Satellite Overpass Time	Julian day Number	Pan Evaporation (mm/day)	Solar Radiation (w/m^2)	RH (%)	Air Temp (^{0}C)	Sunshine Duration (Hr)	Wind Speed (m/s)
6-Jan-17	1:30:00 AM	6	5.10	267.30	30	15.20	9.90	0.79
3-Feb-17	1:55:00 AM	34	6.10	251.50	41	24.50	9.70	0.74
11-Mar-17	1:30:00 AM	70	5.93	290.60	34	22.10	9.00	0.72
1-Apr-17	1:50:00 AM	91	5.90	269.50	39	22.10	7.00	0.55
10-May-17	1:55:00 AM	130	3.00	260.10	44	22.50	10.20	0.60
1-Sep-17	1:45:00 AM	244	1.20	159.60	71	22.30	3.60	0.72
3-Oct-17	1:55:00 AM	274	2.80	257.90	68	19.30	2.00	0.47
9-Nov-17	1:00:00 AM	313	5.40	265.60	64	19.90	10.30	0.67
1-Dec-17	1:25:00 AM	335	4.30	239.20	44	19.00	10.80	0.62

3.3 Pan Evaporation

The daily evaporation was estimated using the pan evaporation method. The nearly present pan was found 1km away from the lake. The pan was class A pan; covered with the wire mesh to keep away interference of birds and other animals and it was placed in short green cropped area (annex 1). The pan station is characterized by light wind speed and medium relative humidity. The nearest fence to the pan is about 15 to 20 meters; Table 3.2 presents coefficients for class A pan for different pan sitting and environment, and different levels of mean relative humidity and wind speed.

A pan-coefficient of 0.75 was used based on FAO irrigation and drainage paper 24, and as recommended by Ayenew and Gebreegziagher (2006), Legesse et.al, (2003), and Ayenew (2002). The daily evaporation measured from the pan multiplied by the pan coefficient gives the daily pan evaporation of the lake. The daily evaporation calculation was computed for the days, which coincide with the date the MODIS satellite image is obtained.

Table 3.2: Coefficients for class A pan (FAO Irrigation and Drainage Paper No. 241)

Class A Pan	Case A: Pan Placed in short green cropped				Case B: Pan Placed in dry fallow area			
RH (%) ⟶		Low <40	Medium 40-70	High >70		Low <40	Medium 40-70	High >70
Wind Speed (m/S)	Windward side distance of green crop (m)				Windward side distance of green crop (m)			
Light <2	1	0.55	0.65	0.75	1	0.70	0.80	0.85
	10	0.65	0.75	0.85	10	0.60	0.70	0.80
	100	0.70	0.80	0.85	100	0.55	0.65	0.75
	1000	0.75	0.85	0.85	1000	0.50	0.60	0.70
Moderate 2-5	1	0.50	0.60	0.65	1	0.65	0.75	0.80
	10	0.60	0.70	0.75	10	0.55	0.65	0.70
	100	0.65	0.75	0.80	100	0.50	0.60	0.65
	1000	0.70	0.80	0.80	1000	0.45	0.55	0.60
Strong 5-8	1	0.45	0.50	0.60	1	0.60	0.65	0.70
	10	0.55	0.60	0.65	10	0.50	0.55	0.65
	100	0.60	0.65	0.70	100	0.45	0.50	0.60
	1000	0.65	0.70	0.75	1000	0.40	0.45	0.55
Very Strong >8	1	0.40	0.45	0.60	1	0.50	0.60	0.65
	10	0.45	0.55	0.60	10	0.45	0.50	0.55
	100	0.50	0.60	0.65	100	0.40	0.45	0.50
	1000	0.55	0.60	0.65	1000	0.35	0.40	0.45

3.4 Meteorological Data Based Methods

Bowen Ratio Energy Budget method (BERB), generally considered being among the most robust and most accurate method for determining open water evaporation (Sturrock et.al, 1992; Lenters et.al, 2005), BREB-determined evaporation estimates are assumed to be within 10% of true values when averaged over a season and within 15% when averaged over a month. The energy budget method after direct measurement of evaporation is considered to be the most accurate method to determine the open water evaporation (Lenters et.al, 2005). And many previous studies have used the method to evaluate other evaporation estimation methods (Winter et.al, 1995; Rasmussen et.al, 1995; Rosenberry et.al, 2007).

The surface energy balance at the land-air interface can be written as Equation (1) as follows and the net radiation is considered as a residual of the soil heat flux, the sensible heat flux, and the latent heat flux.

$R_n = \lambda E + H + G_{lake}$ (Eqn. 3.1)

In the above equation, all parameters of energy are (W/m^2), λE is latent energy used by evaporation of lake water. And λ is the latent heat of vaporization (J/Kg). E is the evaporation (mm), R_{net} is net radiation (W/m^2), H is sensible heat transfer from lake surface to atmosphere (W/m^2), and G_{lake} is the change of heat stored in the lake (W/m^2) (due to temperature changes) during the period.

The sensible heat term can be expressed as $H = B \cdot \lambda E$, where B is the mean Bowen ratio for the period. Equation (1) is rewritten as

$E = \frac{R_n - G_{lake}}{\lambda(1+B)}$ (Eqn. 3.2)

$B = \frac{\gamma}{n}\sum_i^n \frac{T_s - T_a}{e_s - e_a}$ (Eqn. 3.3)

Where; γ is psychometric constant (-), n is the number of days in a period, i is any day within a period, T_s and T_a are daily mean temperature (°C) of lake surface and air above the lake respectively, e_s and e_a are saturated vapor pressure (Pa) at the lake surface and air temperatures. $(e_s - e_a)$ is deficit of saturated vapor pressure as following.

$(e_{s-} e_a) = [\exp\left(\frac{16.78T - 116.9}{T + 273.3}\right)](1 - \frac{R_h}{100})$ (Eqn. 3.4)

Where; T and R_h are daily mean temperature (°C) and relative humidity (%)

The biggest problem of this method is that it requires measurement of surface temperature, which is costly and not available for the Lake Hawassa. Therefore, using regression coefficients determined from different twenty two lakes around the world including Lake Tana has been employed (Duan, and Bastiaanssen, 2015); the lake surface temperature has been computed as:

$T_s = 0.83T_a + 4.27^0c$ (Eqn. 3.5)

Various methods for estimating evaporation from lakes have been tested before by for instance (Winter et.al, 1995; and Rosenberry et.al, 2007). Based on their comprehensive comparisons, Priestley-Taylor (PT) (Priestley and Taylor, 1972), Penman (Penman, 1948), and the De Bruin-Keijman (DK) (De Bruin and Keijman, 1979) models were generally found to generate reasonable and relatively accurate evaporation values. The DK model is actually a modification of the PT model based on net radiation and air temperature. Duan, and Bastiaanssen, (2015) have proved that, DK method performed better than PT model tested on different five lakes around the world. Therefore, Penman (Penman, 1948), and the DeBruin-Keijman (DK) (De Bruin and Keijman, 1979) methods were selected among other meteorological methods to estimate evaporation from Lake Hawassa.

$$\lambda E_{penman} = \frac{\Delta\,(Rn-Glake)}{\Delta+\gamma} + \frac{C_p\rho_a(es-ea)}{ra(\Delta+\gamma)} \qquad \text{(Eqn. 3.6)}$$

$$ra = \frac{4.72\ln(\frac{Z_m}{Z_0})}{(1+0.536UZ_m)} \qquad \text{(Eqn. 3.7)}$$

$$\lambda E_{DK} = \frac{\Delta(Rn-Glake)}{(0.85\Delta+0.63\gamma)} \qquad \text{(Eqn. 3.8)}$$

Where; λE is the latent heat flux, Rn is the net all wave radiation, and G_{lake} is the heat storage changes of the lake, all three terms are in the unit of W m-2; Δ is the slope of the saturated vapor pressure-temperature curve at air temperature (kPa $°C^{-1}$); γ is the psychrometric constant (kPa $°C^{-1}$) that varies with the atmospheric pressure (P, kPa) that is a function of altitude (m), r_a is aerodynamic resistance to heat transport between the surface and the reference level; ρa is the density of air (kg m-3) cp is the specific heat of air (1.00035kJ $kg^{-1}°C^{-1}$). es is the saturated vapor pressure at the air temperature (kPa); ea is the vapor pressure at the air temperature (kPa).Uz is the wind speed U at z meter above the water surface, Ta is air temperature, Z_0 is the roughness length (m), taken in this study as 0.00137 m (Duan, and Bastiaanssen, 2015), Zm is the height of wind speed measurements. Uzm is the wind speed at zm above the water surface (m/s).

3.4.1 Net all wave radiation (Rn):

Net radiation Rn is a sum of net short wave radiation and net long wave radiation. Net radiation is a key term in the energy balance equation because it stands for the energy that must be balanced by the thermodynamic equilibrium of the other terms. In this study the net radiation value was computed using the slob's equation as;

$R_n = (1 - \alpha)R_s - 110\frac{R_s}{R_a}$ (Eqn. 3.9)

$R_s = (0.24 + 0.59\frac{n}{N}).R_a$ (Eqn. 3.10)

Where; R_n is net daily radiation [W.m-2], R_s is incoming short wave solar radiation [W.m-2], R_a is Daily Extra-terrestrial short wave solar radiation [W.m-2], α is albedo of the lake surface is 0.05 (Duan ,2014), N is Maximum possible sunshine hours, n is Sunshine hours.

3.4.2 Water heat flux density (Glake)

The heat balance at water surfaces works very differently than at land surfaces. Generally, albedo values for clear water are very small (less than .05) when the sun angle is more than 10^{o} above the horizon. Shortwave radiation penetrates into a water body according to the transparency of the water and is absorbed at a range of depths below the surface where it is converted into heat (G). For oceans and rivers, a large amount of energy is transferred horizontally with the currents, and the vertical heat balance equation is no longer consistent. Hence, the equation for G/R_n for a water surface is difficult to define. The function for G/R_n that is most suited for a specific water surface must be evaluated. Jensen et.al, (2005) estimated G_{lake} for three lakes with average depth of 8m to 40m, based on, net short wave and long wave radiation.

$G_{lake} = 0.5(1 - \alpha)R_s - 0.8110\frac{R_s}{R_a}$, for Day of year <180 and (Eqn. 3.11)

$G_{lake} = 0.5(1 - \alpha)R_s - 1.3110\frac{R_s}{R_a}$, for Day of year >180 (Eqn. 3.12)

3.4.3 Sensible heat Flux (H)

Sensible heat is heat energy transferred between the surface and air when there is difference in temperature between them (Su, 2002). The surface temperature is usually much higher than the air temperature during the day. Therefore the sensible heat flux is normally directed upwards during the day. During the night the situation may be reversed Sensible heat transport takes place mostly by diffusive processes near the surface, but after a distance, surface turbulent transport becomes more vital. The formula for sensible heat (Su, 2002) is given below.

$$H = \frac{R_{n-G_{lake}} - \left(\frac{\rho_a C_p}{r_a}\right)\left(\frac{es-ea}{\gamma}\right)}{1+\frac{\Delta}{\gamma}} \qquad \text{(Eqn. 3.13)}$$

Where; Δ=Slope of saturated vapor pressure curve (-)

3.5 Remote Sensing Approach

The surface energy balance system (SEBS) is developed for the estimation of atmospheric turbulent fluxes evaporative fractions, instant and daily evaporation rate. The SEBS model requires three sets of information or data. The first set of data consists of land surface albedo, emissivity, temperature, Normalized Difference Vegetation Index (NDVI) fractional vegetation coverage (FVC) leaf area index (LAI), and the height of the vegetation. If vegetation information is not available, the NDVI is used as a surrogate. These input data can be derived from remote sensing data in conjunction with other information about the surface of interest. The second set includes meteorological data, such as air pressure, temperature, humidity, and wind speed at a reference height. These meteorological variables can be estimated by large scale meteorological models. The third set includes downward solar radiation, which can either be measured or estimated as model output or parameterization (Su, 2002). The overall remote sensing approach estimation process is provided in figure 3.12 in a flow chart form.

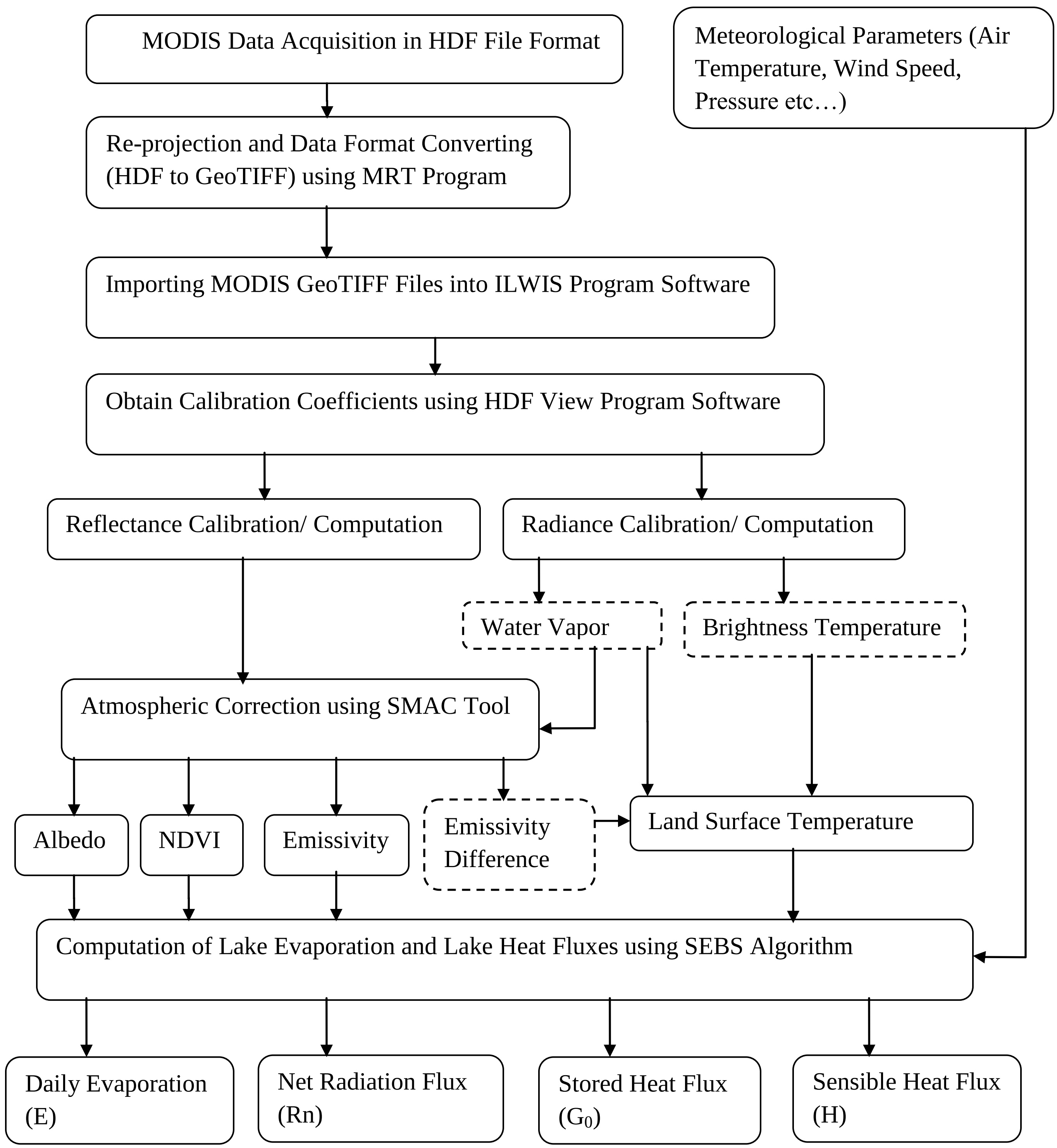

Figure 3.12: Remote Sensing Approach (SEBS Algoritm) Overall Process

3.5.1 Meteorological and Solar Radiation Data Inputs

Meteorological data used in the SEBS model included daily mean temperature, wind speed, humidity, pressure (calculated), sunshine duration and solar radiation (2014-2017). These data sets were recorded from meteorological station, which is about 1km away from the east side of the lake. The data from this station were acquired from National Meteorological Agency, SNNPR Meteorological Service Center, Hawassa. The data presented are only for the selected few days in which the SEBS model was run for the corresponding MODIS images.

3.5.2 Remote Sensing Data Inputs

3.5.2.1 Surface Albedo

Surface albedo represents cumulative reflectivity of a certain surface. And it will be computed from the MODIS reflectance bands (band1-7, except band 6), which are atmospherically corrected in SMAC tool. The process was executed in the Compute Land surface Albedo dialog box. The formula for albedo computation used is;

$$\mathrm{Albedo} = 0.160r1 + 0.291r2 + 0.243r3 + 0.116r4 + 0.112r5 + 0.01r7 - 0.0015 \qquad \text{(Eqn. 3.14)}$$

Where; r1, r2, r3, r4, r5, r7 are the MODIS surface reflectance bands.

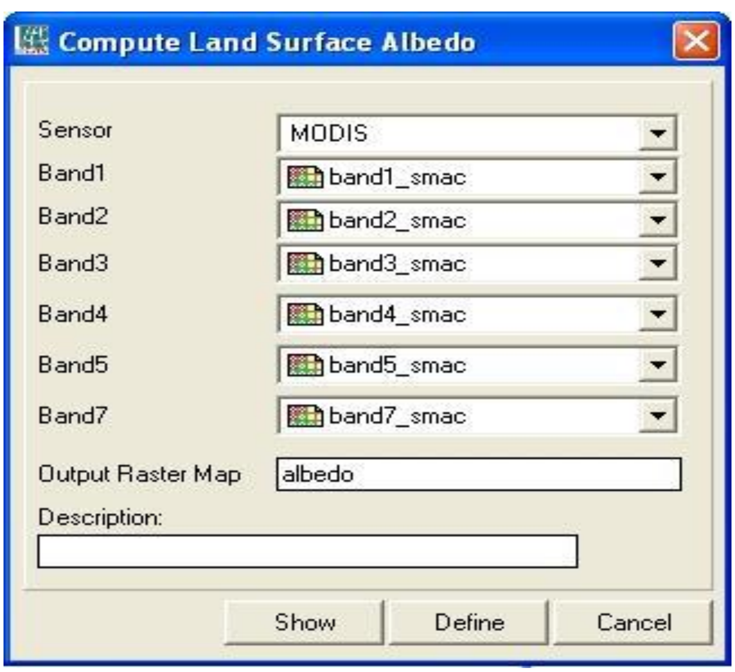

Figure 3.13: Surface Albedo Computation Dialog Box in ILWIS

3.5.2.2 Surface Emissivity and NDVI

The process uses atmospherically corrected surface reflectance in the red and NIR bands (Sobrino et.al, 2003). The emissivity for water pixels has been assigned a value of 0.995. Here assume that an albedo value < 0.035. The NDVI values will be calculated with the equation based on the atmospherically corrected surface reflectance as shown below:

NDVI= (Bnir-Bred)/ (Bred+Bnir) (Eqn. 3.15)

Using atmospherically corrected Band 1, Band 2, and Albedo map as an input, Emissivity map will be generated and optionally, NDVI, Emissivity difference map, and Vegetation map can be generated. The process is carried out in the Compute Surface Emissivity dialog box.

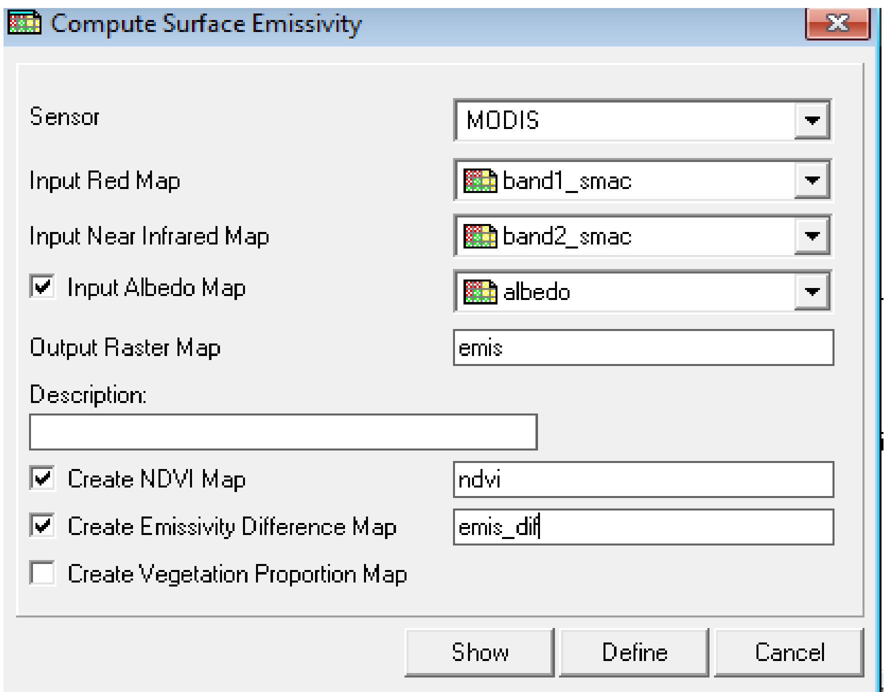

Figure 3.14: Surface Emissivity Computation Dialog Box in ILWIS

3.5.2.3 Surface Temperature

This operation computes the surface temperature using a Split Window Technique (SWT). The advantage of the SWT is the cancellation of the effect of the atmospheric components, with exception of the atmospheric water column. The equation is given below:

$$ST = btm2 + (1.97 + 0.2\ W)(btm2 - btm1) - (0.26 - 0.08\ W)\ sqrt(btm2 - btm1) + (0.02 - 0.67\ W) + (64.5 - 7.35\ W)(1 - e) - (119 - 20.4\ W)\ de \qquad \text{(Eqn. 3.16)}$$

Where; ST= Surface temperature, btm31=brightness temperature obtained from MODIS band 31 using brightness temperature computation, btm32=brightness temperature obtained from MODIS band 32 using brightness temperature computation, W= water vapor content, e = Surface emissivity, and de= surface emissivity difference. The computation process is carried out in Compute Land Surface Temperature dialog box.

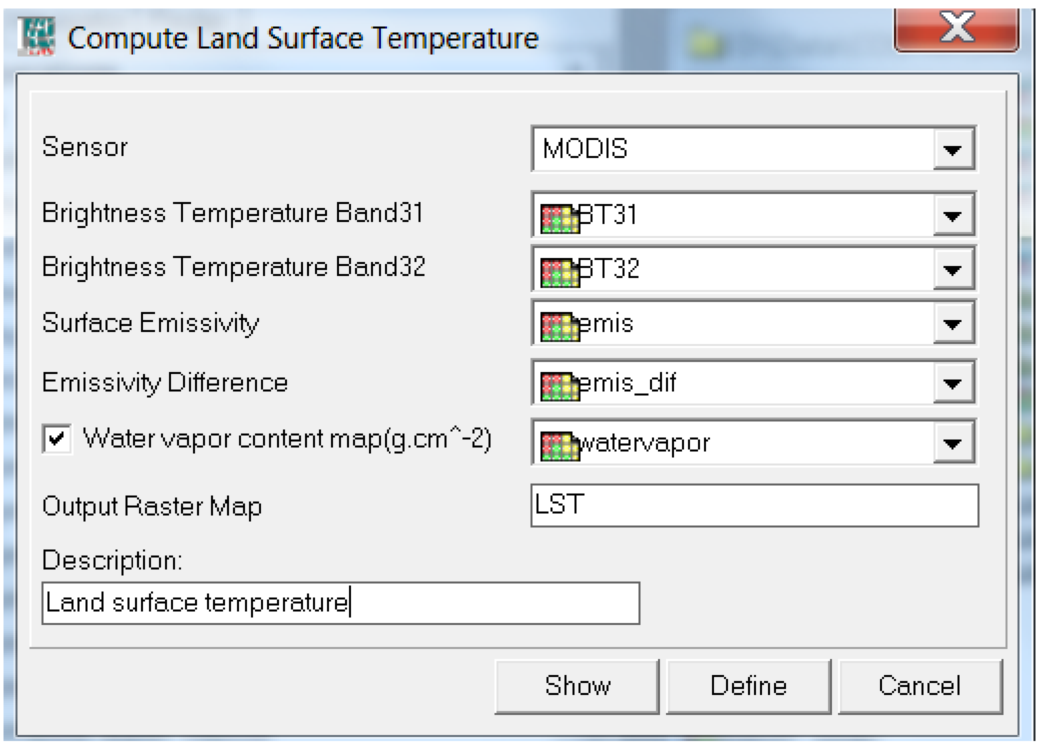

Figure 3.15: Surface Temperature Computation Dialog Box in ILWIS

3.5.3 MODIS Satellite Image Preprocessing

Preprocessing MODIS satellite data involves; re-projecting the row data, importing to the GIS environment, calibration, water vapor content estimation brightness temperature computation, and atmospheric correction. The whole process made use of three different program softwaresIntegrated Land and Water Information System (ILWIS), Hierarchical Data Format Viewer (HDF View), and MODIS Re-projection Tool (MRT).

3.5.3.1 Remote Sensing Data Acquisition:

The satellite images were downloaded from NASA`s Level 1 and Atmospheric Archive and Distribution System (LAADS) website. In selecting the images the following coordinates were entered in the LAADS web window of MODIS Terra, 1km spatial resolution images 7°.12N, 7S, 38.40W and 38.50E. Clear daily images were selected and ordered after checking for cloud cover. The data acquisition process is presented in the form of flow chart (see figure 3.14). For the one year period, based on its quality one MODIS image per month was obtained.

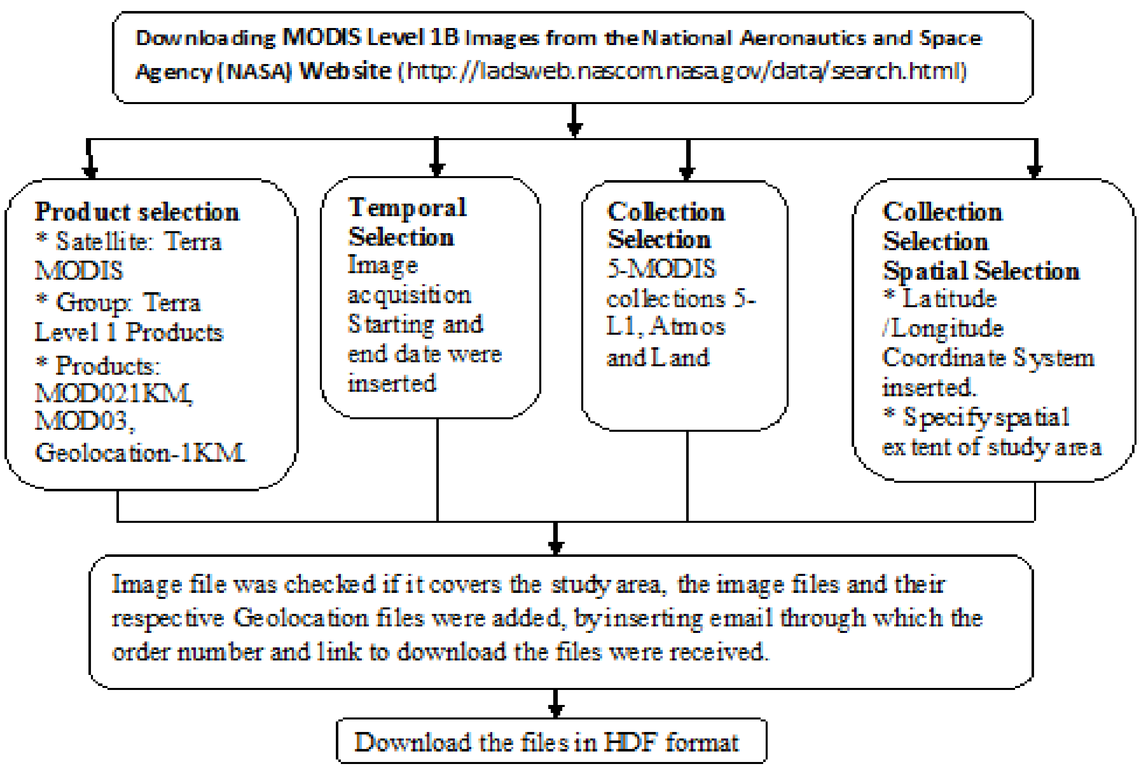

Figure 3.16: Remote Sensing Data Acquisition Overall Process

3.5.3.2 Re-projecting MODIS Level-1B Data:

The extracted MODIS L1B data are in swath (orbit based) format, therefore in this part, the data will be re-projected to a standard projection and format compatible with GIS software. The MODIS Re-projection Swath Tool, downloaded from,http://gcmd.nasa.gov/records/MRT/.html allows the user to transform MODIS L1B data from swath format to other widely supported projections and formats for GIS applications. Both the MODIS Level-1B and Geo-location products were re-projected and converted to TIFF/GeoTIFF format, and re-projected to the Geographic projection ready for importing into ILWIS. Other than format conversion, image spatial subset was specified; resampling was executed using Nearest Neighbor. In addition geographic coordinates were assigned and the output pixel size was fixed to 0.01 in degrees.

3.5.3.3 Importing GEOTIFF Files into ILWIS:

After the image is re-projected, the next step is importing the GEOTIFF files into ILWIS raster via Geospatial Data Abstraction Library (GDAL). To obtain the desired ILWIS raster file the output file name was specified. Final step in importing the data was verifying that if all images have been correctly imported (checking the coordinate system and geo-reference, if they are affected in the import process).

3.5.3.4 Calibration:

SEBS4ILWIS provides the tools to convert the imported MODIS channels from raw digital number (DN) into radiances or reflectance. This will be done by obtaining and applying the proper calibration coefficients. The calibration coefficients consist of a radiance scale, reflectance scale, and offset are provided in the HDF header file of the original MODIS image. They will be obtained using http://www.hdfgroup.org/hdf-java-html/hdfview/software.Each raw data/ band/channel will be calibrated. This will involve feeding the calibration coefficients into the Raw to radiance/reflectance (MODIS) dialog box, and the output fill will be raster file. Certain bands will use radiance scale and offset value and some will use reflectance scale and offset coefficients. Band-2 will use both reflectance and radiance scale and offset coefficients, for further analysis. The Geo-location products will also be calibrated using map calculation dialog box. The value range for the solar zenith and satellite/sensor azimuth angles were set as minimum 0 and maximum 90. And the value range for the solar azimuth and satellite/sensor zenith angles were set as minimum 0 and maximum 360. Precision value for all Geo-location calibration was set as 0.01.

3.5.3.5 Water vapor content estimation:

Water vapor content is estimated using the radiance values of MODIS bands 2, 17, 18, and 19. These input bands are radiance bands. The output raster data name was defined, for the use of atmospheric correction. This task was executed in the Compute Atmospheric Water Vapor Dialog Box.

3.5.3.6 Brightness temperature computation:

This procedure is about converting the bands 31 and 32 of MODIS from radiance to blackbody temperatures. The conversion is done in the Compute Brightness Temperature dialog box, by applying the well-known Planck equation;

$$T_c = \frac{C_2}{\lambda_c \log[\frac{C_1}{\lambda_c^5 \pi L_s} + 1]} \qquad \text{(Eqn. 3.14)}$$

Where; T_c= brightness temperature, λ_c= the sensor's central wave length, C_1 and C_2 are black body constants.

Radiance bands of 31 and 32 were used as input, and the proper name for the output file was specified. The output file will be used for land surface temperature calculation.

3.5.3.7 Atmospheric Correction (SMAC)

The calibrated raster images are atmospherically corrected using the SMAC. SMAC is a tool for the atmospheric effect correction of the visible and near visible bands of different sensors MODIS is among them. The tool can't be applied for solar zenith angles greater than 60 degrees and/or satellite zenith angles greater than 50 degrees. The set of input for SMAC tool are; Aerosol Optical Thickness (AOT), water vapor content map, Ozone Content, Surface pressure, and sun/satellite angle data. AOT (evaluated at 550 nm wavelengths): The value ranges from 0.05 to 0.8. Aerosol in the atmosphere has an extreme dynamic behavior. To evaluate a reasonable value of aerosols in case that a station is located close to the area of interest, use could be made of the aero-net service http://aeronet.gsfc.nasa.gov/ Ozone content can be also measured in DU (Dobson Units. 1000 DU = 1 g.atm.cm). Ozone content is less dynamic than the AOT component (changes during days or weeks). Ozone is monitored quite intensively from satellites and other ground resources. A good source of ozone content on the internet is http://mascuv.gsfc.nasa.govfrom Earth-Probe sensor. SMAC model has in-built standard coefficients for different sensors and two atmospheres (desert and continental). SMAC for ILWIS allows the user to select from this list. The procedure of atmospheric correction was repeated seven times (one for each visible channel).

3.5.4 Main SEBS Output Data

As part of the process of estimating total evaporation the SEBS model also produces estimates of the other energy balance components or energy fluxes, which include net radiation flux (Rn), heat storage flux (G_0), sensible heat flux (H) and latent heat flux (LE).

3.5.4.1 Net Radiation Flux (Rn)

Net radiation Rn is a sum of net short wave radiation and net long wave radiation. Net radiation is a key term in the energy balance equation because it stands for the energy that must be balanced by the thermodynamic equilibrium of the other terms. SEBS calculates net radiation as;

$$Rn = Rs \downarrow - Rs \uparrow + Rl \downarrow - Rl \downarrow \qquad \text{(Eqn. 3.17)}$$

The net short-wave radiation (W/m^2) can be written as follows:

$$\sum RS = (1 - \alpha)\, RS \downarrow = (1 - \alpha)\,(Sc \cos\theta dr \tau a) \qquad \text{(Eqn. 3.18)}$$

Where; α is the surface albedo, Sc is the solar constant (W-m2), θ is the solar incident angle, dr is the relative Earth-Sun distance, and τa is the atmospheric transmissivity.

The incoming long-wave radiation is the downward thermal radiation flux from the atmosphere. The air emissivity can be estimated by a function of the vapor, pressure, and temperature in the cloudless atmosphere:

$$Rl \downarrow = \varepsilon_{sky}\sigma T_a^4 \qquad \text{(Eqn. 3.19)}$$

$$Rl \uparrow = \varepsilon_0\sigma T_a^4 \qquad \text{(Eqn. 3.20)}$$

Where; ε_0 is the surface emissivity and Ts is the surface temperature (K) ε_{sky} is the air emissivity, σ is the Stefan-Boltzmann equation.

3.5.4.2 Stored Heat Flux (G_0)

G_0 represents the energy used to heat the ground. Over land, G_0 is calculated as a function of the surface properties. In many SEBS applications, ground and water cover is not differentiated.

$$G0 = \Gamma_c + (1 - f_c)(\Gamma_s - \Gamma_c) \qquad \text{(Eqn. 3.21)}$$

in which it is assumed that the ratio of soil heat flux to net radiation Γ_c = 0.05 for full vegetation canopy and Γs = 0.315 for bare soil An interpolation is then performed between these limiting cases using the fractional canopy coverage, f_c.

3.5.4.3 Sensible Heat Flux (H)

The sensible heat flux is the exchange of heat between the atmosphere and the surface through air molecules, resulting from the vertical temperature gradient between the water surface and the atmosphere. The friction velocity, the sensible heat flux and the Obukhov stability length are obtained by solving the system of non-linear Equations of the Monin-Obukhov Similarity (MOS). Derivation of the sensible heat flux using Equations requires only the wind speed and temperature at the reference height as well as the surface temperature and is independent of other surface energy balance terms.

$$U = \frac{U*}{K}[\ln(\frac{Z-d_0}{Z_{0m}}) - \Psi_m\left(\frac{Z-d_0}{L}\right) + \Psi_m(\frac{Z_{0m}}{L})] \qquad \text{(Eqn. 3.22)}$$

$$\theta_0 - \theta_a = \frac{H}{KU_*\rho C_p}[\ln(\frac{Z-d_0}{Z_{0h}}) - \Psi_h\left(\frac{Z-d_0}{L}\right) + \Psi_h(\frac{Z_{0h}}{L})] \qquad \text{(Eqn. 3.23)}$$

$$L = \frac{\rho C_p U_*^2 \theta_v}{kgH} \qquad \text{(Eqn. 3.24)}$$

Where; u is the velocity of air (m. s^{-1}); u_* is the friction velocity (m. s^{-1}); k is the von Karman's constant (k = 0.4 (-);` z is the reference height above the water surface (m); d_0 is the zero plane displacement (m); Z_{0m} is the surface roughness length for momentum transfer (m); L is the Monin-Obukhov length (m); θ_0 is the potential temperature of the water surface (K); $\theta_a$is the potential temperature of air at reference height z (K); Z_{0h} is the surface roughness length for heat transfer (m); Ψm and Ψh are the stability correction functions for momentum and sensible heat transfer, respectively; ρ is the air density (kg.m^{-3}); cp is the specific heat of air at constant pressure (J. kg^{-1}.K^{-1}); and is the gravitational acceleration g = 9.81 (m.s^{-2}).

3.5.4.4 Latent Heat Flux (λE)

The latent heat is the energy needed for evaporation. SEBS calculates the latent heat using the evaporative fraction term (Λ) and the actual sensible heat Su (2002). Evaporative fraction is the ratio between the latent heat and the available energy at the water surface.

The actual sensible heat flux value is constrained between the dry (minimum latent heat flux) and wet (minimum sensible heat) conditions. The terms are coming from land application, where the sensible heat in dry conditions is equal to the difference between the net radiation and the ground heat flux, i.e., there is no water available for evaporation, and the soil moisture is at wilting point. In wet conditions, when there is no water limitation, the sensible heat flux reaches its minimum; and evaporation will occur at the potential (maximum) rate. SEBS estimates the total energy used for evaporation in a day-based evaporative fraction term (Λ).

$$\lambda E_{daily} = 8.64 \text{ X } 10^7 \Lambda \, (R_n + G_0) \qquad \text{(Eqn. 3.25)}$$

Finally, this total daily energy is converted into daily evaporation estimates by considering the latent heat of vaporization (λ):

$$E_{\ daily} = \frac{\lambda E_{daily}}{\lambda \rho_w} \qquad \text{(Eqn. 3.26)}$$

Where; E_{daily} is the daily evaporation (mm.day^{-1}); ρ_w is the water density (kg.m^{-3}).

3.6 Statistical Analysis

To assess the performances of selected methods, dimensionless statistic Nash-Sutcliffe efficiency coefficient (E) (Nash and Sutcliffe, 1970) is used. (E) is computed as shown in equation (3.27).

$$E = 1 - \frac{\sum_1^n (o_i - p_i)^2}{\sum_1^n (o_i - \bar{o_i})^2} \qquad \text{(Eqn. 3.27)}$$

Where; Oi is the observed Ep at time t = i; P_i is simulated Ep at time i; O_i mean observed Ep and n is the number of observations. Values of (E) between 0.0 and 1.0 are generally viewed as acceptable levels of performance, whereas values less than 0.0 indicate unacceptable performance. (E) is recommended for two major reasons: (i) it is recommended by (Legates and McCabe, 1999), and (ii) it provides extensive information on reported values.

The refined Willmott's index (willmott, et.al, 2012) method is applied to quantify the degree to which observed values of evaporation are captured by the selected methods? The refined Willmott's index (dr) is expressed as shown in equation (3.28).

$$dr = 1 - \frac{\sum_1^n (o_i - p_i)^2}{\sum_1^n (o_i - \bar{o_i})^2} \text{ , when } \sum_1^n |o_i - p_i| \leq 2\sum_1^n |o_i - \bar{o_i}|$$

$$dr = \frac{\sum_1^n (o_i - p_i)^2}{\sum_1^n (o_i - \bar{o_i})^2} - 1 \text{ , when } \sum_1^n |o_i - p_i| > 2\sum_1^n |o_i - \bar{o_i}| \qquad \text{(Eqn. 3.28)}$$

The range of (dr) is from -1.0 to 1.0. A (dr) of 1.0 indicates perfect agreement between model and observation, and a (dr) of -1.0 indicates either lack of agreement between the model and observation or insufficient variation in observations to adequately test the model.

Here it should be noted that the Pan Evaporation method is used as an observed value. The performance of other selected methods (BREB, Penman, DK, and Remote Sensing) estimates are evaluated as per the above two methods.

Root Mean Square Deviation and relative Root Mean Square Deviation are applied to compare the remote sensing based energy balance fluxes with meteorologically determined energy balance components.

$$RMSD = \sqrt{\frac{\sum_{i=1}^{n}(X_{1,i} - X_{2,i})^2}{n}} \qquad \text{(Eqn. 3.29)}$$

Where; $X_{1,t}$ and $X_{2,t}$ are the two data series, and n is sample size.

$$rRMSD = \frac{RMSD}{X_{1,max} - X_{1,\min}} \qquad \text{(Eqn. 3.30)}$$

Where; $X_{1,max}$ and $X_{1,min}$ are the reference estimates.

4 Results and Discussions

4.1 Evaporation Estimation

The remote sensing and meteorological based daily evaporation estimates were compared and evaluated using Pan Evaporation method as a bench mark. The graphical and tabular representation of the result uses average and correlation coefficient as additional statistical measurements of comparison.

Table 4.1: Daily Evaporation Comparison using E_Pan as a Benchmark

	E_pan	E_BREB	E_DK	E_PM	E_SEBS
6-Jan-17	3.83	5.23	4.20	3.29	4.33
3-Feb-17	4.58	4.25	4.08	3.27	5.20
11-Mar-17	4.45	3.00	2.79	2.23	5.13
1-Apr-17	4.43	2.06	1.91	1.53	4.30
10-May-17	2.25	1.71	1.59	1.28	4.04
1-Sep-17	0.90	1.36	1.24	1.00	1.16
3-Oct-17	1.88	3.28	2.94	2.34	3.76
9-Nov-17	4.05	4.71	4.09	3.24	4.34
1-Dec-17	3.23	5.36	4.66	3.68	4.19
Aerage	3.29	3.44	3.06	2.43	4.05
Correlation Coefficient		0.48	0.52	0.53	0.86
Nash-Sutcliffe efficiency coefficient (E)		-0.23	0.35	-0.55	0.48
Willmott's index (dr)		-0.23	0.35	-0.55	0.48
Rank		3	2	4	1

Using E_Pan as benchmark the E_SEBS (Remote Sensing approach) estimates show the highest correlation coefficient followed by E_PM (Penman) and E_DK (DeBruin-Keijman) estimates, the E_BREB estimates show the worst correlation. The Nash-Sutcliffe efficiency coefficient (E) of the E_SEBS (Remote Sensing approach) and E_DK (DeBruin-Keijman) estimates show a performance, which are in the acceptable range of efficiency. According to this statistical measurement E_PM (Penman) method performed unacceptable efficiency. The Willmott's index (dr) checks the other estimates agreement with the E_Pan. In all the above time series data the criteria follow $\sum_1^n |o_i - p_i| \leq 2\sum_1^n |o_i - \overline{o_i}|$, which is almost the same as Nash-Sutcliffe efficiency coefficient (E) estimates. As it can be observed in the table the E_SEBS method agrees well with the benchmark followed by E_DK. The E_PM (Penman) estimates show unacceptable agreement with the benchmark estimates. The E_BREB method estimates also show a poor agreement with the pan E_Pan estimates. Generally as per statistical measurements and using E_Pan as a reference tool, E_SEBS estimates ranked first amongst other conventional methods. Except the Debruene-Keijman method meteorological methods were failed to give a good estimates of evaporation on Lake Hawassa.

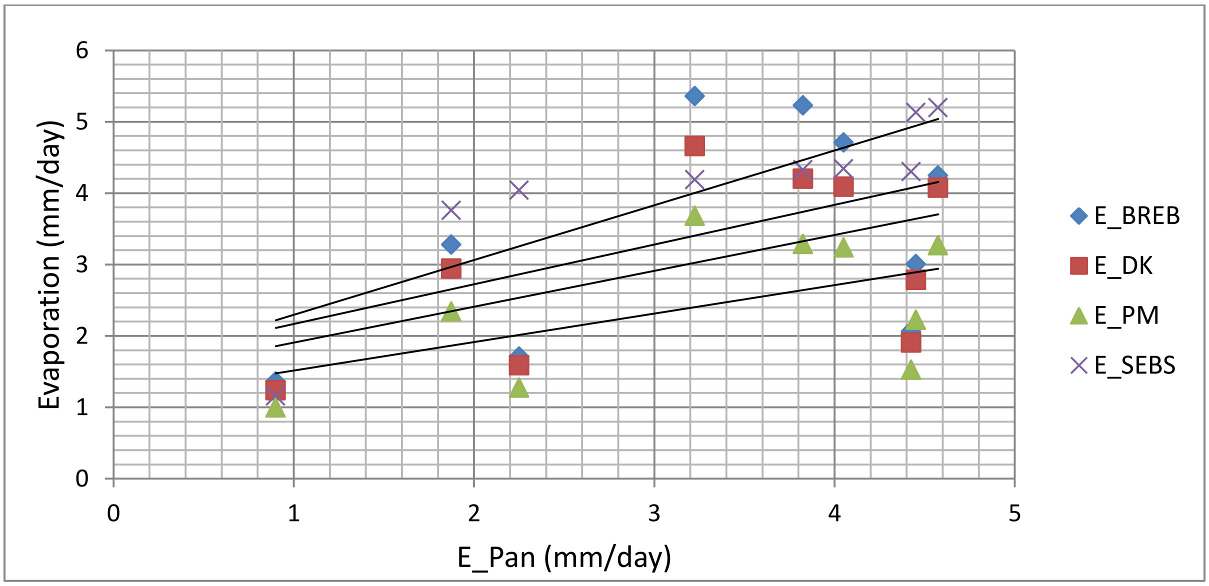

Figure 4.1: Scatter plots of E_Pan against other methods

As it can be seen from figure 4.1, the remote sensing approach estimate points are distributed far well ahead of the other two meteorological based estimates. And except for the month of September all the SEBS estimates are lay above the conventional estimates, also its trend line is above all the other trend lines. The lowest trend line is E_PM trend line laying below all the other.

Figure 4.2 presents spatial distribution of daily evaporation rates in the middle of Lake Hawassa on different days of the year.

2017, January 6

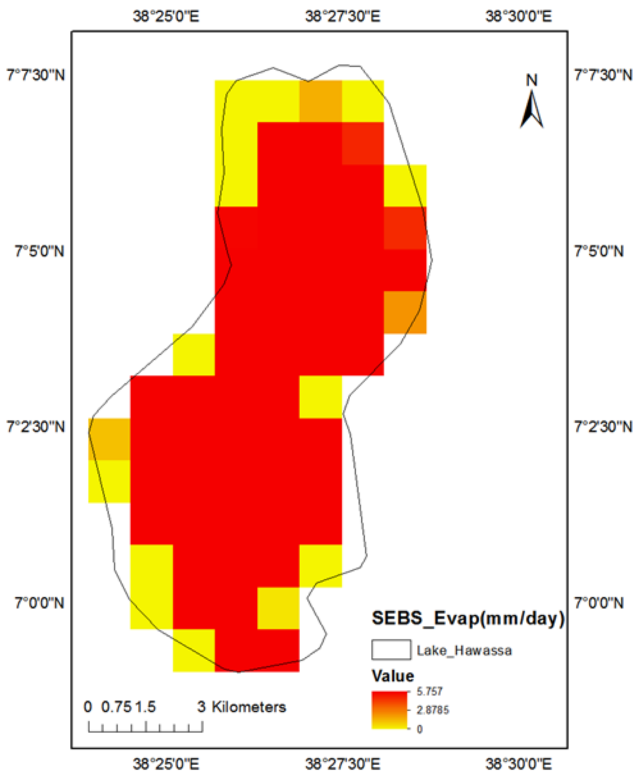

2017, February 3

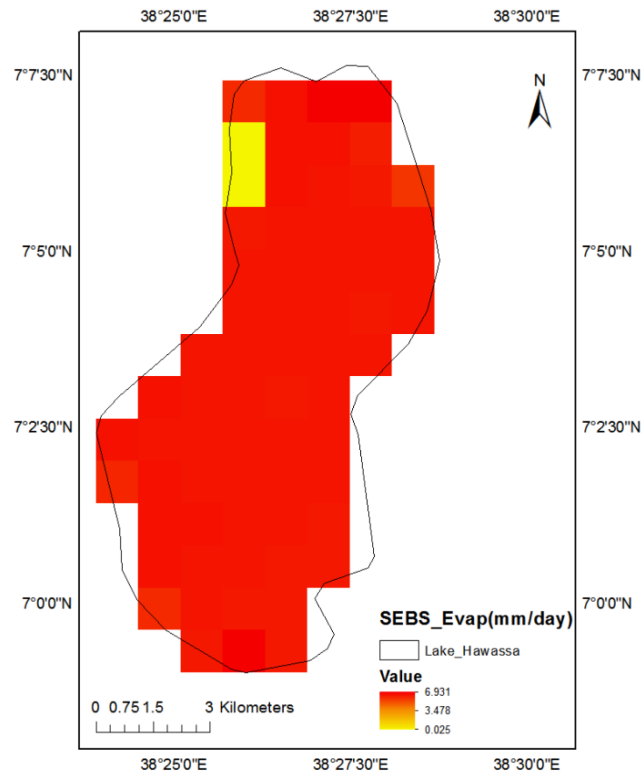

2017, March 11

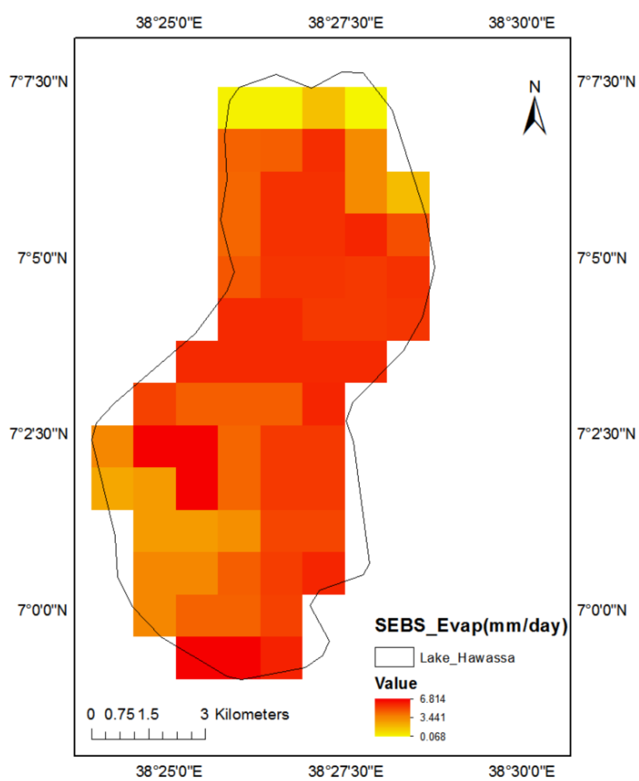

2017, April 1

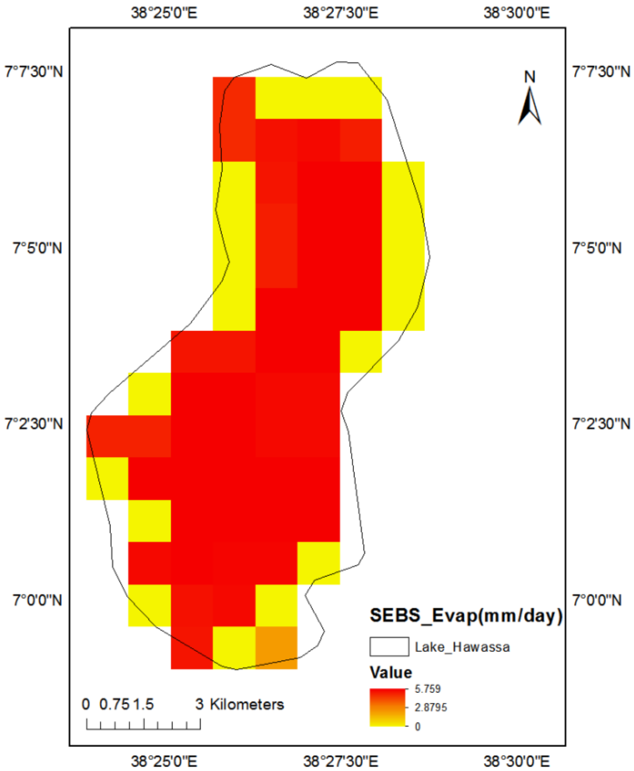

2017, May 10

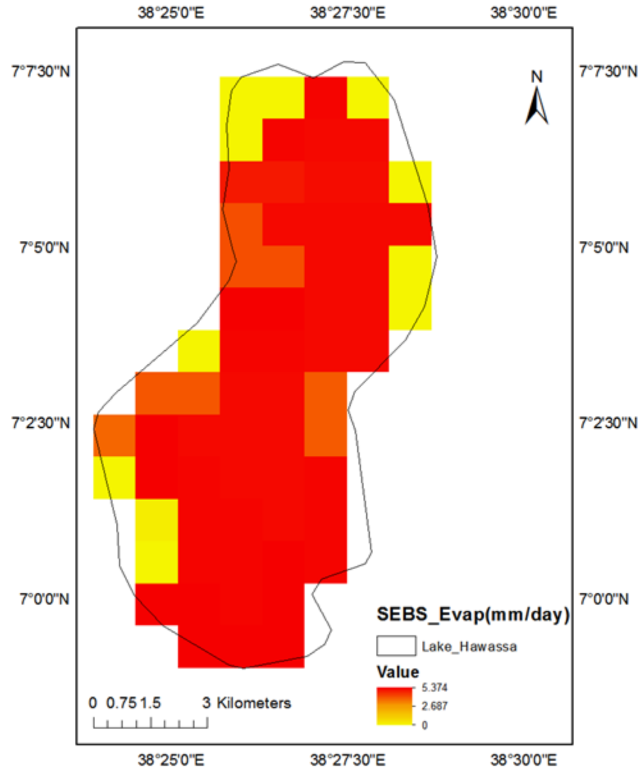

2017, September 1

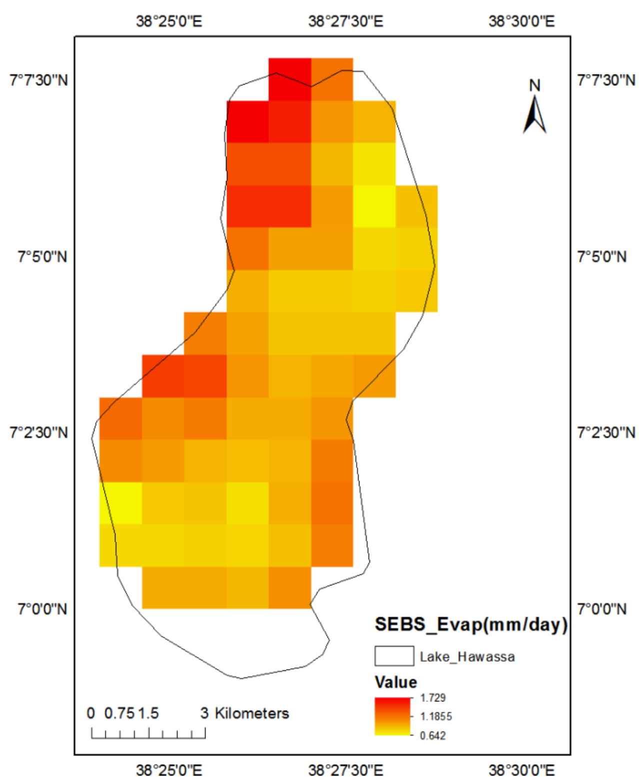

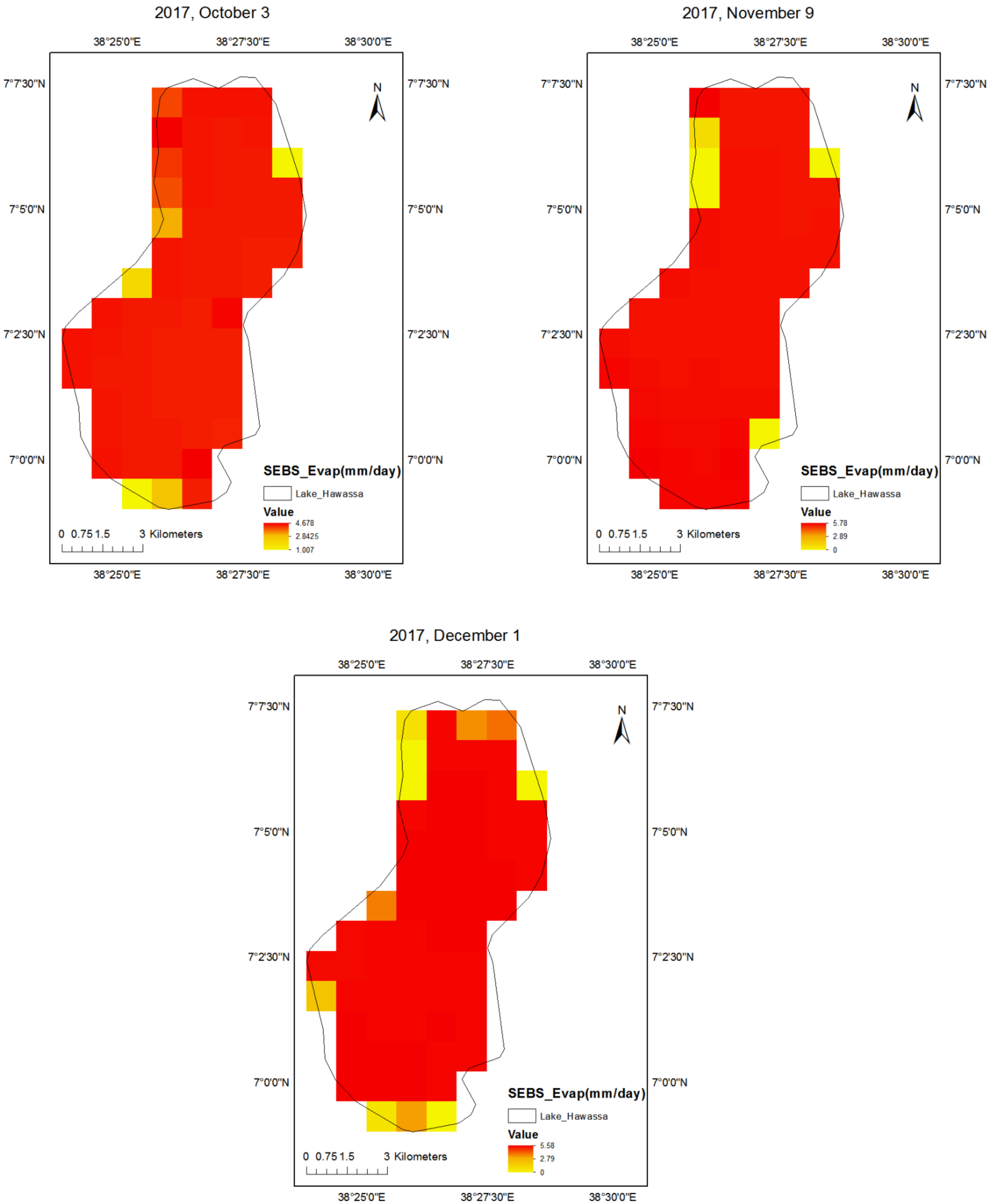

Figure 4.2**:** Evaporation Spatio-Temporal Distribution on Lake Hawassa

The evaporation maps showed that there is high evaporation loses going to the middle of the lake than the shore line. This is due to the fact that, there is high surface area in the main lake exposed to the direct sun energy compared with the vegetated lake edges. Furthermore, low evaporation along the Lake shore might be due to high turbidity and salinity resulted from relatively high sediment loads. Some parts of the lake shore show no evaporation at all that part of the lake shore is considered as a rock, that it can't hold any moisture in it.

Generally, according to Pan Evaporation measurement the remote sensing approach is the best among penman and De Bruin and Keijman methods. The average of the remote sensing estimates is a little exaggerated than all the other methods estimates.

Evaporation estimates of almost all the previous studies on Lake Hawassa were presented in the annual basis. When dividing the annual values for the number of days of the year, the values range from 3.7 mm/day to 5.1 mm/day on average (Brook and Deganovsky, (2008); Ayenew (2004); Lemlem, (2007); Shewangizaw, (2010)). Most of the methods utilized were Water Balance, Penman, and Pan Evaporation methods. In this study the mean value ranges from 2.427 mm/day to 4.05 mm/day. The minimum value of the average daily lake evaporation is under estimated; and it was the result from the worst performing method (Penman). According to Gebregziabher, (2004) the lowest evaporation estimate was in September month (excluding June, July, and August). Lake evaporation estimate shows decreasing trend from March to September and an increasing trend from September to December, as in the case of this study. Evaporation is mainly affected by shortwave radiation followed by relative humidity and it is least sensitive to wind speed. In this study also, lowest estimate of evaporation was observed in September month using all methods; this is due to the fact that, low air temperature, high relative humidity small sunshine duration, and most of all solar radiation. However for the other months, the factors which affect evaporation may not be as severe as the month of September. The highest pan evaporation estimate (4.58 mm/day) was recorded on February which corresponds to the highest air (297.6 k) and surface temperature (297.71K).

4.2 Comparison of RS-estimated G_0 with Meteorological estimated G_{lake}

The maps which show the spatio-temporal distributions of heat storage estimates are presented in annex4. The maximum estimate is at 11-March-2017 which is 68.077 W/m^{2}and the minimum estimate at 1-Sept-2017 which is 20.742 W/m^2.

Table 4.2: Heat Storage Flux Estimates Comparison

	SEBS G (W/m2)	Meteorological G (W/m^2)
6-Jan-17	54.71	43.72
3-Feb-17	48.83	30.92
11-Mar-17	68.08	40.65
1-Apr-17	48.07	38.41
10-May-17	35.58	33.62
1-Sep-17	20.74	21.89
3-Oct-17	49.15	37.28
9-Nov-17	48.14	34.08
1-Dec-17	53.44	45.80
Max	68.08	45.80
Min	20.74	21.89
Average	47.42	36.26
Correlation Coefficient	0.81	
Correlation Slope	1.46	
RMSD	13.70	
rRMSD	29%	

The remote sensing heat storage flux estimates were compared with meteorological heat storage flux estimates using different statistical measurements. There is a considerable difference between the two averages (i.e. 47.416W/m^{2}for the SEBS estimates and 36.263W/m^2 for the meteorological estimates) for the provided sample size. The correlation coefficient and correlation slope were 0.806 and 1.461 (i.e. that was within the acceptable range). Therefore the two samples were correlated well. The root mean square deviation and the relative mean square deviation were 13.701 W/m^2 and 29% respectively.

Therefore for the given sample size, the performance of the SEBS heat storage flux estimates was moderate when compared with the meteorological heat flux estimates. As per the graph, except for the minimum and the maximum values, all the points are scattered near by the trend line. This indicates that, the two samples are in good agreement.

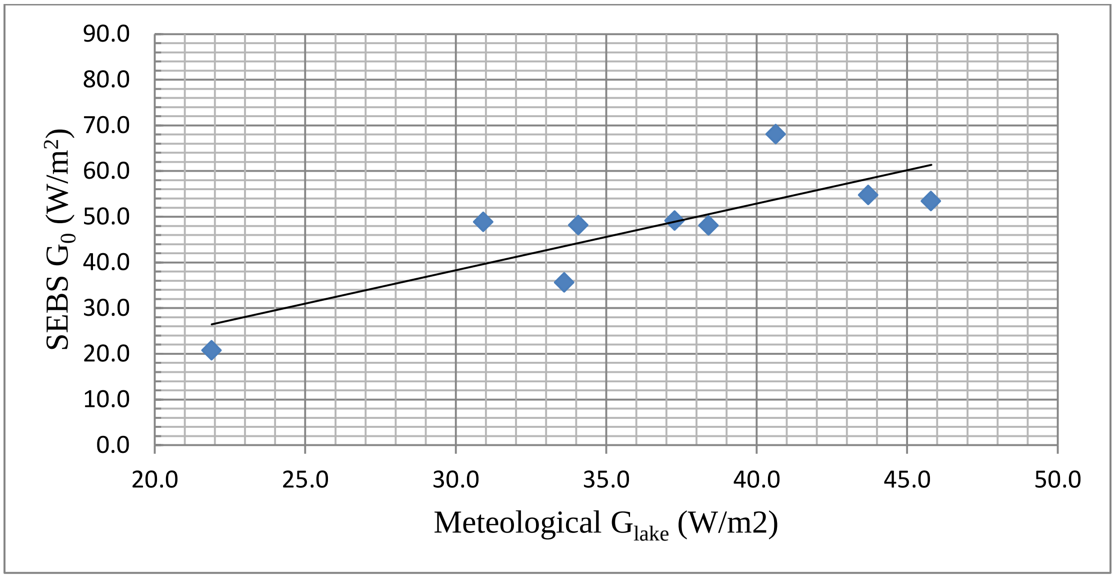

Figure 4.3: Scatter Plot of Heat Storage Flux Estimates

Lake Stored heat flux is mainly affected by the lake water depth (Finch and Calver, 2008). Since for shallow water bodies the stored heat flux is not considered, the values at the lake offshore should be ignored. The Lake Hawassa water depth long term data series shows increasing trend from September to December, and a decreasing trend from January to April (see figure 3.9). The temporal trend of Lake Hawassa water depth and stored heat flux shows opposite direction.

The maximum and minimum values of stored heat flux (G) do not always coincide with the maximum and minimum values of net radiation (Rn) due to the fact that, the water body has a thermal inertia and phase shifts induce a hysteresis effect. But the maximum and minimum values of stored heat flux (G) depend mainly on the time rate of change of lake surface temperature (Duan, and Bastiaanssen, 2015). But in this study, the stored heat flux estimates graph follows the same trend as that of the net radiation flux (Rn). Figure 4.5 presents the relationship between the stored heat flux and net radiation.

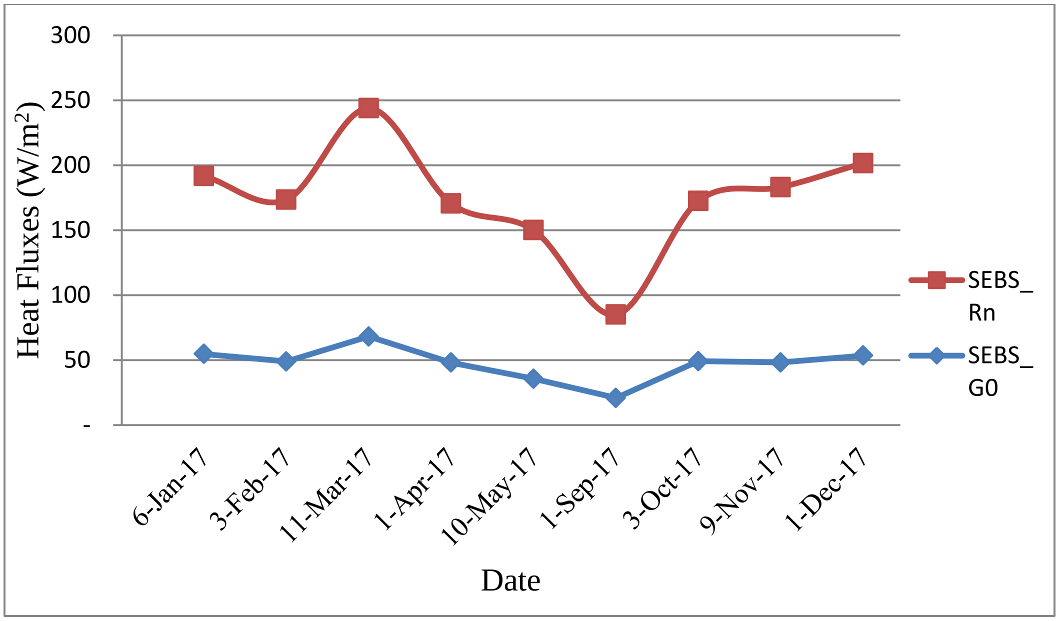

Figure 4.4: Stored Heat Flux Relation with Net Radiation

For large water bodies like Lake Hawassa the stored heat flux can be a significant component of the energy balance. Duan, and Bastiaanssen (2017) conducted a study which investigates the effect of stored heat on evaporation estimation, and the study showed that ignoring such component leads to a poor evaporation estimation performance. The RMSD of estimated stored heat flux from measured stored heat flux for different five lakes were, 9.3 W/m2 to 17.2 W/m2 on monthly time scale. In the case of this study, the SEBS remote sensing algorithm in ILWIS automatically considers or accounts for stored heat flux of the lake.

4.3 Comparison of RS-based R_n with Slob's estimated R_n

Table 4.3: Net Radiation Flux Estimates Comparison

	SEBS R_n (W/m2)	Slob's R_n (W/m2)
Jan6	191.79	181.60
Feb3	173.49	149.55
Mar11	243.92	237.86
Apr1	170.45	186.00
May10	150.00	163.62
Sep1	84.96	97.36
Oct3	172.52	165.48
Nov9	183.13	159.59
Dec1	201.73	190.42
Min	84.96	97.36
Max	243.92	237.86
Average	174.67	170.16
Correlation Coefficient	0.94	
Correlation Slope	1.06	
RMSD	15.01	
rRMSD	9%	

The remote sensing net radiation flux estimates were compared with the meteorological net radiation flux estimates using different statistical measurements. There is a considerable agreement between the two averages (i.e. 174.67 $W/m^2$for the SEBS estimates and 170.16W/m^2 for the meteorological estimates) for the provided sample size. The correlation coefficient and correlation slope were 0.94 and 1.06 (i.e. that is within the acceptable range). Therefore the two samples were correlated well. The root mean square deviation and the relative mean square deviation were 15 W/m^2 and 9% respectively. Therefore for the given sample size, the performance of the SEBS net radiation estimates was very good using meteorological net radiation estimates as a bench mark. As shown on the graph, the points are scattered near by the trend line. This indicates that, the two samples are in good agreement.

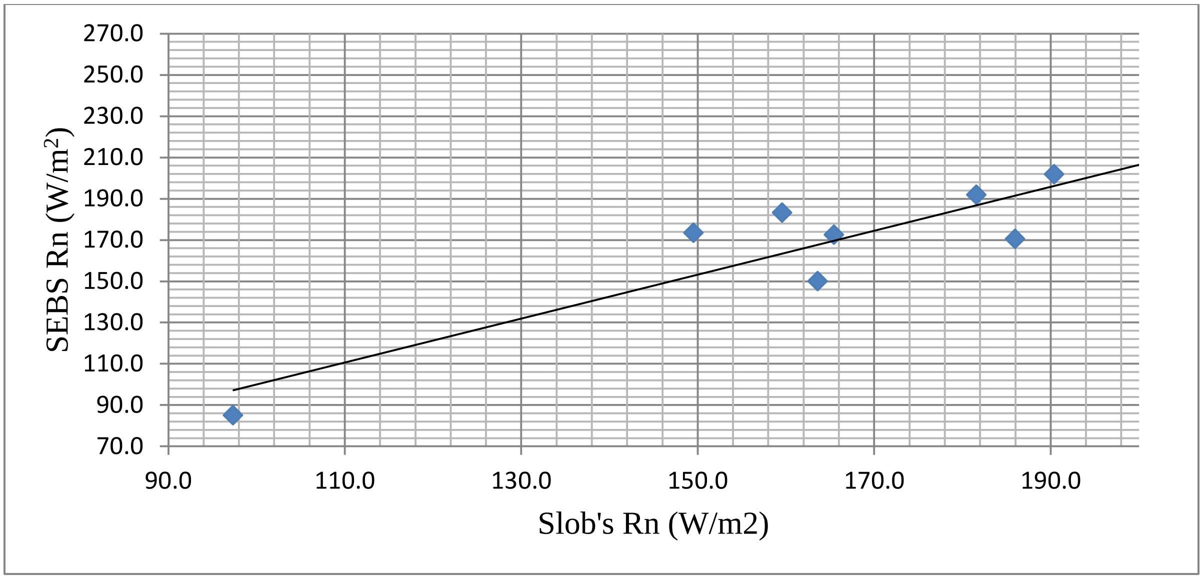

Figure 4.5: Scatter Plot of Net Radiation Flux Estimates

Radiation emitted from the surface is a function of the water surface temperature, and incident atmospheric radiation was determined primarily from the air temperature and solar radiation (humidity was least important) (Jan, 1976).In the case of Lake Hawassa the net radiation estimates from remote sensing trend mainly follows the trend of solar radiation data from meteorological observation; as it can be observed from figure 4.6 the two graphs are identical.

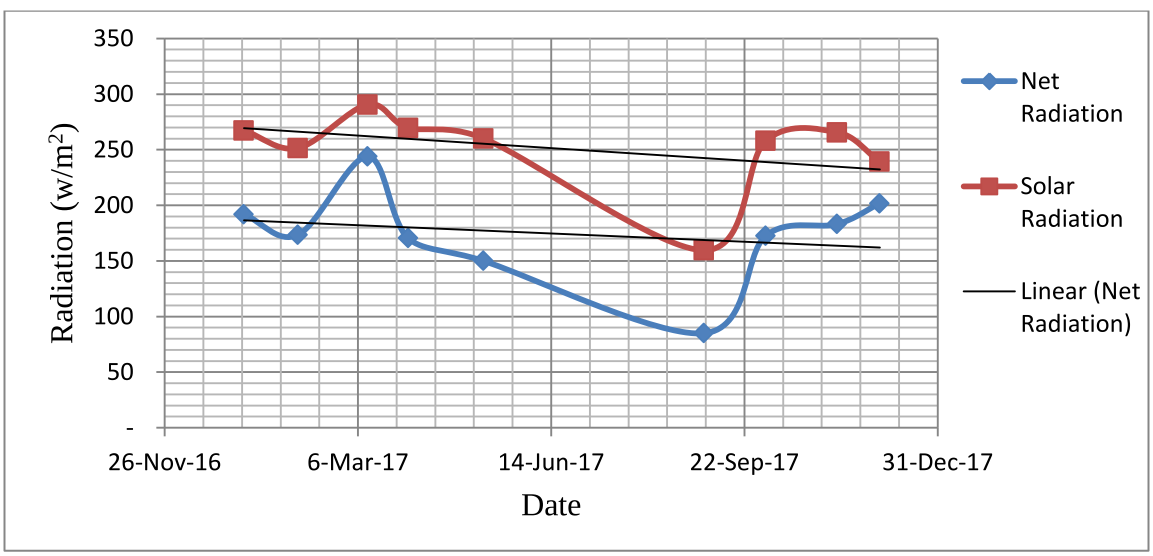

Figure 4.6: Net Radiation Flux Relation with Solar Radiation

Duan, and Bastiaanssen (2015), made use of Slob's equation(using satellite derived short wave radiation) to estimate the net radiation (Rn); and compare it with in-situ measurements found a good agreement (with R^2above 0.9 and RMSD of below 25 W/m^2).

4.4 Comparison of RS-based H with Meteorological based H

Table 4.4: Sensible Heat Flux Estimate Comparison

	SEBS H (W/m2)	Meteorological H(W/m2)
6-Jan-17	35.831	37.954
3-Feb-17	37.757	45.453
11-Mar-17	56.697	27.546
1-Apr-17	29.316	21.205
10-May-17	22.449	14.604
1-Sep-17	14.466	11.958
3-Oct-17	31.312	25.938
9-Nov-17	19.587	11.441
1-Dec-17	42.154	34.659
Min	14.466	45.453
Max	56.697	11.441
Average	32.794	26.15
Correlation Coefficient	0.673	
Correlation Slope	0.719	
RMSD	11.54	
rRMSD	27%	

The remote sensing sensible heat flux estimates were compared with the meteorological sensible heat flux estimates using different statistical measurements. There is a considerable disagreement between the two averages (i.e. 32.794 W/$m^2$for the SEBS estimates and 26.150 W/m^2 for the meteorological estimates) for the provided sample size. The correlation coefficient and correlation slope were 0.673 and 0.719 (i.e. that was within the acceptable range). Therefore the two samples were correlated well. The root mean square deviation and the relative mean square deviation were 11.54w/m^2 and 27% respectively. Therefore for the given sample size, the performance of the SEBS sensible heat flux estimates was well using meteorological sensible heat flux estimates as a bench mark. The biggest deviation was found at Mar-11-2017, SEBS estimate of 56.697W/m^2 and meteorological estimate of 27.546W/m^2.

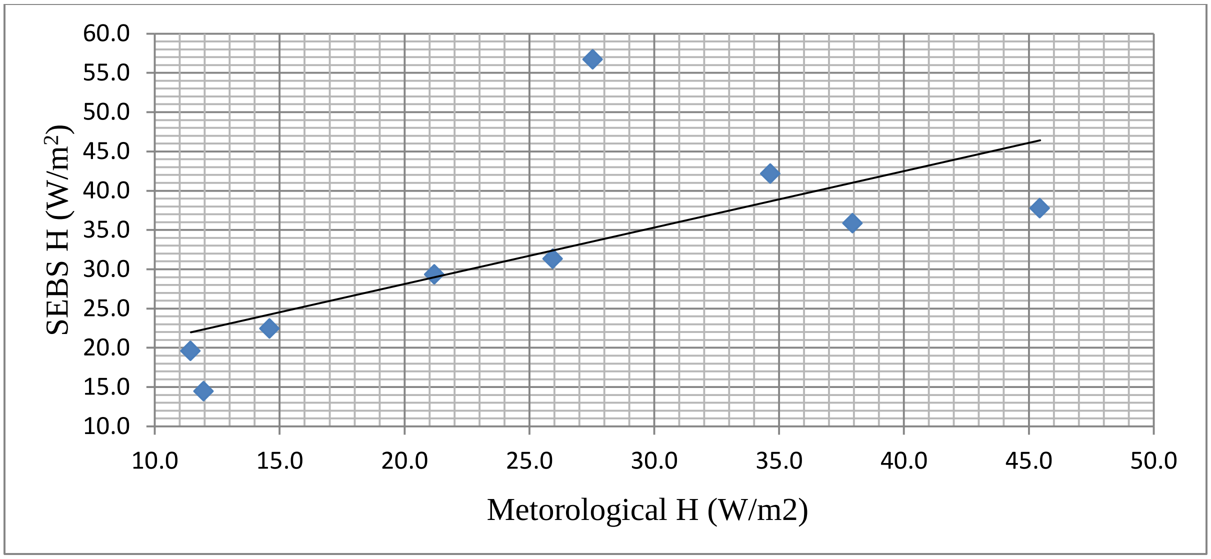

Figure 4.7: Scatter Plot of Sensible Flux Estimates

The sensible heat flux estimate and evaporation rate is mainly controlled by Bowen ratio. Water vapor deficit or humidity and temperature also alter the result of sensible heat estimation (McJannet, et.al, 2011). Nadeau et al., 2009, stated that sensible heat flux is also sensitive to surface conditions from which energy is being released. Evaporation is also affected primarily by variations in meteorological conditions. This is also supported by the findings of Zhang et.al, (2007) and Xu et.al, (2006), who demonstrated that the spatial variations in climatic variables influence the temporal spatial trends of reference evaporation.

Annexes 3 through Annex 5, spatio-temporal distribution of the three energy balance components are provided. For all energy balance components, the evaporation estimate spatial distribution increases to the middle of the lake. And going to the offshore the decreasing trend is observed. MODIS Level 1B products show the same spatial distribution of energy fluxes as Landsat 8 images at uMgeni catchment, South Africa (Shoko, 2014).

5 Conclusions and Recommendations

5.1 Conclusions

The Surface Energy Balance System (SEBS) to estimate daily lake evaporation rate was applied for a Lake Hawassa in Southern Ethiopia. Latent heat flux, the main driving force for evaporation, is estimated as a residual in net radiation flux Rn, sensible heat flux H, change in stored heat flux G_0. The algorithm is applied to MODIS spectral data for the lake. Daily evaporation rates are estimated on nine different dates, representing the whole months through the year (except June, July, and August). Daily evaporation values of three conventional methods (with good performance in the literatures) were compared with the SEBS values at the Hawassa weather meteorological station. For the comparison the Pan Evaporation data were used as a reference or as a benchmark. While using Pan Evaporation data as a comparison tool, the remote sensing approach SEBS, performs better than any other conventional meteorological based methods. As per statistical measurements only Debruine-Keijman method was able to perform well in estimating evaporation rate from Lake Hawassa, among other empirical methods.

The remote sensing application SEBS also utilized to estimate the energy balance terms, (i.e.net radiation flux Rn, sensible heat flux H, change in stored heat flux G_0). The results were compared with meteorological based estimates, and have shown a good relation. Maps showing spatial and temporal variations of evaporation and other energy balance components were generated successfully.

Generally application of the remote sensing algorithm SEBS for Lake Hawassa evaporation and lake heat fluxes was feasible.

5.2 Recommendations

- For future there have to be flux measurements over the lake, from which other estimating methods are evaluated.
- The pan evaporation by itself is about 1km away from the lake, which hardly represent the real time condition of the lake; if floating pan is provided for the lake it would be better.
- Also surface temperature measurement and temperature profile measurement is helpful in estimating a reliable heat storage flux and sensible heat flux.
- For future, there is a possibility of application of high spatial and temporal resolution remote sensing data, for the better quality of estimates.
- Implementing remote sensing data in to the deBruin-Keijman meteorological model should also be foresighted in the future studies for the better accuracy of estimates.

References

Abdelrady, A., Timmermans, J., Vekerdy Z., and Mhd, Salma, S. 2016. Surface Energy Balanceof Fresh and SalineWaters: AquaSEBS. Remote Sens, 8,583.

Abreham, A. 2009. Open Water Evaporation Using Ground Measurements and Satellite Remote Sensing: A case study of Lake Tana, Ethiopia. ITC Library.

Allen, R, Irmak, A, Trezza, R, Hendrickx, JM, Bastiaanssen, W, Kjaersgaard, J. 2011.Satellite-based ET estimation in agriculture using SEBAL and METRIC. Hydrological Processes.

Allen, R, Tasumi, M, Trezza, R., 2007. Satellite-Based Energy Balance for Mapping Evapotranspiration with Internalized Calibration (METRIC)-Model. Journal of Irrigation and Drainage Engineering.

Anderson, E.R., 1954. Energy-Budget Studies, Water Loss Investigations: Lake Hefner Studies, Professional Paper 269, Geological Survey, U.S. Department of Interior, Washington, D.C.

Asrar, G., and Dokken, D.J., 1993. EOS Reference Handbook (Greenbelt; MD: NASA). Sensing, edited by G. Asrar (New York: Wiley).

Assefa, M., Wossenu, A. and Tibebe, D., 2009.Evaporation Estimation of Rift Valley Lakes, Comparison of Models: Department of Earth and Environment, Florida International University, 11200 SW 8th Street, Miami, FL 33199, USA.

Ayenew, T., and Gebreegziabher, Y., 2006.Application of a spreadsheet hydrological model for computing the long-term water balance of Lake Awassa, Ethiopia, Hydrological Sciences Journal, 51 (3).

Ayenew, T., 2004. Environmental implications of changes in the levels of lakes in the Ethiopian Rift since 1970: Regional environmental changes.

Ayenew, T., 2003. Environmental isotope-based integrated hydro-geological study of some Ethiopian rift lakes: Journal of radio-analytical and nuclear chemistry.

Ayenew, T., 2002. Recent changes in the level of Lake Abiyata, central main Ethiopian Rift. Hydrological Sciences Journal. 47(3):

Bastiaanssen, WGM., 2000. SEBAL based sensible and latent heat fluxes in the irrigated Gediz Basin, Turkey. Journal of Hydrology.

Bastiaanssen, WGM, Menentia, M, Feddesb, RA, Holtslagc, AAM., 1998. A remote sensing surface energy balance algorithm for land (SEBAL) 1 Formulation. Journal of Hydrology

Bedient, Philip B. and Huber, Wayne C., 1992.Hydrology and Floodplain Analysis. New York: Addison-Wesley Publishing Company.

Belete, M.D., 2013. The Impact of Sedimentation and Climate Variability on the Hydrological Status of Lake Hawassa: Dissertation, Bonn University, Germany.

Blanken, P. D., Spence, C., Hedstrom, N., and Lenters, J.D., 2011. Evaporation from Lake Superior: 1. Physical controls and processes. Journal of Great Lakes Research

Boronina, A, Ramillien, G., 2008.Application of AVHRR imagery and GRACE measurements for calculation of actual evapotranspiration over the Quaternary aquifer (Lake Chad basin) and validation of groundwater models. Journal of Hydrology

Bras, Rafael L., 1990.Hydrology. New York, New York: Addison-Wesley Publishing Company.

Brook, A.G. and Deganovsky, A.M., 2008. Water Balance and Level Regime of Ethiopian Lakes as Integral Indicators of Climate Change: Faculty of Hydrology, Russian State Hydrometeorology University, Saint Petersburg, Russia,

Brutsaert, W., 2013.Use of pan evaporation to estimate terrestrial evaporation trends: The case of the Tibetan Plateau. Water Resources Research.

Brutsaert, W., 1982.Evaporation into the Atmosphere. D.Reidel Publishing Co. Dordrecht, Holland.

Carpenter, L.G., 1898.The loss of water from reservoirs by seepage and evaporation. Agr. Exp. Stn.Bull. No.

Chen, D, Gao, G, Xu, C, Guo, J, Ren, G. 2005. Comparison of the Thornthwaite method and pan data with the standard Penman-Monteith estimates of reference evapotranspiration in China. Climate Research.

Chenyepe A., 2010.Satellite Remote Sensing of Surface Water Evaporation Over Lake Muirikwi, Zimbabwe MSc Thesis, University of Zimbabwe.

Chow, V.T., and Maidment, D.R., Mays, L.W., 1988. Applied Hydrology. McGraw-Hill, New York.

Churchill, J.H., and Kerfoot, W.C., 2007. The impact of surface heat flux andwind on thermal stratification in Portage Lake, Michigan. Journal of Great Lakes Research.

Cogley, J.G. 1979.“The albedo of water as a function of latitude.”Monthly Weather Rev.

Croley, T.E. II. 1989. “Verifiable evaporation modeling on Laurentian Great Lakes. WaterResourcesRes., 25(5).

Crow, S.F. and Hottman S.D., 1973.Network density of temperature profile stations and its influence on the accuracy of lake evaporation calculations. Water Resource. Res.

Cummings, N.W., and Richardson, B., 1927.“Evaporation from lakes.”Physical Review.

De Bruin, H. A.R., 1982. Temperature and energy-balance of a water reservoir determined from standard weather data of a land station. Journal of Hydrology.

De Bruin, H.A.R., and Keijman, J.Q., 1979.Priestley-Taylor Evaporation Model Applied to a Large, Shallow Lake in the Netherlands: Journal of Applied Meteorology.

Delclaux, F., Coudrain, A., and Condom, T., 2007.Evaporation estimation on Lake Titicaca: A synthesis review and modeling. Hydrological Processes.

Demelash, A.S., 2008. Assessment of Non-Point Source Pollution in Lake Awassa Watershed Using the Annualized Agricultural Non-Point Source (AnnAgNPS) Model: MSc thesis, Addis Ababa University, Ethiopia.

Dessie, N., 1995 Hydro-geological investigation of Lake Hawassa catchment: MSc thesis, Addis Ababa University, Ethiopia

Duan, Z., 2014. Estimating Water Balance Components of Lakes and Reservoirs Using Various Open Access Satellite Databases: Dissertation, Amsterdam, Netherlands.

Duan, Z., and Bastiaanssen, W.G.M., 2015.Estimating water volume variations in lakes and reservoirs from four operational satellite altimetry databases and satellite imagery data: Remote Sensing of Environment.

Duan, Z., and Bastiaanssen W.G.M., 2017.Evaluation of three energy balance-based evaporation models for estimating monthly evaporation for five lakes using derived heat storage changes from a hysteresis model. Environ. Res. Lett. 12 (2017) 024005.

Dutton, J. A., and Bryson, R. A., 1962.Heat flux in Lake Mendota. Limnology and Oceanography.

Elhag, M, Psilovikos, A, Manakos, I, Perakis, K., 2011.Application of the SEBS Water Balance Model in Estimating Daily Evapotranspiration and Evaporative Fraction from Remote Sensing Data Over the Nile Delta. Water Resources Management

Elsawwaf, M., Willems, P., 2012.Analysis of the climate variability on Lake Nasser evaporation based on the Bowen ratio energy budget method. Journal of Environmental Biology.

ETCOLD (Ethiopian Committee on Large Dams), 2014.Ethiopian Dam Safety Guidelines.

Evans, R. S. Evans, R., Sharon, H., Murrihy, E., Bastiaanssen, W., Robert M., and Miltenburg, R., 2009. Using Satellite Imagery to Measure Evaporation from Storages: Richard; 1SKM, WaterWatch, Delft University of Technology.

Ficke, J. F., 1972. Comparison of evaporation computation methods, Pretty Lake, Lagrange County, northeastern Indiana. Geological Survey Professional Paper 686-A.

Finch, J., and Calver, A., 2008.Methods for the quantification of evaporation from lakes: Available at: http://nora.nerc.ac.uk/14359/1/wmoevap_271008.pdf

Finch, J. W. and Hall R. L., 2001.Estimation of Open Water Evaporation, a Review of Methods Rand D Technical Report W6-043/TR: Environment Agency, Rio House, Waterside Drive, Aztec West, Almondsbury, Bristol, BS32 4UD, United Kingdom.

Fooladmand, HR., 2011. Evaluation of Blaney-Criddle equation for estimating evapotranspiration in south of Iran. African Journal of Agricultural Research.

Gebreegziabher, Y., 2004. Assessment of the Water Balance of Lake Awassa Catchment, Ethiopia. M.Sc Thesis, International Institute for Geo-information Science and Earth Observation http://www.itc.nl/library/papers_2005/msc/wrem/yemane.pdf

Gianniou, S. K., and Antonopoulos, V. Z., 2007. Evaporation and energy budget in Lake Vegoritis, Greece. Journal of Hydrology.

Gibson, LA, C Jarmain, C, Su, Z, Eckardt, FE., 2013. Estimating evapotranspiration using remote sensing and the Surface Energy Balance System (SEBS) – A South African perspective.Water SA 39(4).

Gómez, M, Olioso, A, Sobrino, JA, Jacob, F., 2005.Retrieval of evapotranspiration over the Alpilles/ReSeDA experimental site using airborne POLDER sensor and a thermal camera. Remote Sensing of Environment.

Guenther, B., Godden, G.D., Xiong, X.X., Knight, E.J., Qiu, S.Y., Montgomery, H., Hopkins, M.M., Khayat, M.G., and Hao, Z.D., 1998. Prelaunch algorithm and data format for the Level 1 calibration products for the EOS-AM1 Moderate Resolution Imaging Spectro-radiometer (MODIS). Itc Transactions on Geo-science and Remote Sensing.

Hankerson, B, Kjaersgaard, J, Hay, C., 2012. Estimation of Evapotranspiration from fields with and without cover crops using remote sensing and in situ methods. Remote Sensing.

Harbeck, George E., 1962.A Practical Field Technique for Measuring Reservoir Evaporation Utilizing Mass-Transfer Theory. U.S. Geologic Survey Professional Paper 272.

Hassan M., 2013. Evaporation Estimation for Lake Nasser Based on Remote Sensing Technology (SEBAL). Ain Shams Engineering Journal.

Hellegers, PJGJ, Soppe, R, Perry, CJ, Bastiaanssen, W.G.M., 2009. Combining remote sensing and economic analysis to support decisions that affect water productivity. Irrigation Science

Hemakumara, HM, Chandrapala, L, Moene, AF., 2003. Evaporation fluxes over mixed vegetation areas measured from large aperture scintillometer. Agricultural Water Management.

Hicks, B.B., and Hess, G.D., 1977.Bowen Ratio and Surface-Temperature at Sea. Journal of Physical Oceanography.

Hoedjes, JCB, Chehbouni, A, Ezzah, J, Escadafal, R, de Bruin, HAR., 2007. Comparison of Large Aperture Scintillometer and Eddy Covariance Measurements: Can Thermal Infrared Data Be Used to Capture Footprint-Induced Differences. Journal of Hydrometeorology.

Hostetler, S.W., and Bartlein, P.J., 1990. Simulation of lake evaporation with application to modeling lake level variations of Harney-Malheur Lake, Oregon. Water Resources Res.

Iqbal, M., 1983.An Introduction to solar Radiation. New York, New York: Academic Press.

Jan, A. D., 1976. Lake Erie Terrestrial Radiation. National Oceanic and Atmospheric Administration, Great Lakes Environmental Research Laboratory. Ann Arbor, Michigan 48104.

Jarmain, C, Everson, C, Savage, M, Mengistu, M, Clulow, A, Walker, S, Gush, M., 2009. Refining tools for evaporation monitoring in support of water resources management. Report No. 1567/1/08 Water Research Commission, Pretoria, South Africa.

Jensen, M., Dotan, A., and Sanford, R., 2005. Penman-Monteith estimates of reservoir evaporation: Impacts of Global Climate Change

Johnson, M., Saito, L., Anderson, M.A., Weiss, P., Andre, M., and Fontaine, D.G., 2004., Effects of climate and reservoir and dam operations on reservoir thermal structure. Water Resources Planning and Management.

Justice, C.O., Vermote, E., Townshend, J.R.G., Defries, R., Roy, D.P., Hall, D.K., Salomonson, V.V., Privette, J.L., Riggs, G., Strahler, A., Lucht, W., Myneni, R.B., Knyazikhin, Y., Running, S.W., Nemani, R.R., Wan, Z.M., Huete, A.R., van Leeuwen, W., Wolfe, R.E., Giglio, L., Muller, J.P., Lewis, P., and Barnsley, M.J., 1998. The Moderate Resolution Imaging Spectro-radiometer

(MODIS): Land remote sensing for global change research. Ieee Transactions on Geo-science and Remote Sensing.

Keijman, J.Q., 1974. The estimation of the energy balance of a lake from simple weather data. Boundary-Layer Meteorology.

Keskin, M. E., and Terzi, O., 2006.Evaporation estimation models for Lake Egirdir, Turkey. Hydrological Processes.

Kettle, H., Thompson, N. J., and Livingstone, D. M., 2004.Empirical Modeling of Lake Surface Temperatures. Limnology and Oceanography.

Koberg, G.E., 1958. Energy budget studies, Geological Survey Professional Paper 298, U.S. Department of the Interior, Washington, D.C.

Kongo, VM, Jewitt, GPW., 2006. Preliminary investigation of catchment hydrology in response to agricultural water use innovations: A case study of the Potshini catchment – South Africa. Physics and Chemistry of the Earth

Lee, TS, Najim, MMM, Aminul, MH., 2004. Estimating evapotranspiration of irrigated rice at the West Coast of the Peninsular of Malaysia. Journal of Applied Irrigation Science.

Legates ,D. R., and McCabe G. J., 1999. Evaluating the use of goodness of fit measures in hydrologic and hydro climatic model validation, Water Resources Res.

Legesse D,Vallet-Coulomb C, and Gasse F., 2004.Analysis of the hydrological response of a tropical terminal lake, Lake Abiyata (Main Ethiopian Rift Valley) to changes in climate and human activities. Hydrological Process.

Legesse D,Vallet-Coulomb C, and Gasse F., 2003.Hydrological response of a catchment to climate and land use changes in Tropical Africa: case study South Central Ethiopia, J. Hydrology.

Lemlem, A., 2007. Assessing the Impact of Land Use and Land Cover Change on Groundwater Recharge Using RS and GIS; a Case of Awassa Catchment. MSc thesis, Addis Ababa University, Ethiopia.

Lenters, J.D.,Kratz, T. K., and Bowser, C. J., 2005.Effects of climate variability on lake evaporation: Results from a long-term energy budget study of Sparkling Lake, northern Wisconsin (USA). Journal of Hydrology.

Liu, S, Mao, D, Lu, L., 2006. Measurement and estimation of the aerodynamic resistance. Hydrology and Earth System Sciences Discussions

Li, Z, Tang, R, Wan, Z, Bi, Y, Zhou, C, Tang, B, Yan, G, Zhang, X., 2009. A review of current methodologies for regional evapotranspiration estimation from remotely sensed data.Sensors 9.

Long, D, Singh, VP, Li, Z-L., 2011. How sensitive is SEBAL to changes in input variables, domain size and satellite sensor. Journal of Geophysical Research.

Lott, RB, Hunt, RJ. (2001). Estimating evapotranspiration in natural and constructed wetlands. Wetlands 21(4).

Lu, J, Sun, G, McNulty, SG, Amatya, DM., 2005. A comparison of six potential evapotranspiration methods for regional use in the South Eastern United States. Journal of American Water Resources Association.

Maeda, EE, Wiberg, DA, Pellikka, PKE., 2011. Estimating reference evapotranspiration using remote sensing and empirical models in a region with limited ground data availability in Kenya. Applied Geography 31.

McCuen, Richard H., 1989.Hydrologic Analysis and Design. Englewood Cliffs, New Jersey: Prentice-Hall, Inc.

McCormick, M. J., Meadows, G. A., 1988. An inter-comparison of four mixed layer models in a shallow inland sea. Journal of Geophysical Research.

McJannet, D. L., Cook,F. J.,McGloin, R. P., McGowan,H. A., and Burn,S., 2011. Estimation of evaporation and sensible heat flux from open water using a large aperture scintillometer, Water Resour. Res., 47, W05545, doi: 10.1029/2010WR010155.

McMahon, TA, Peel, MC, Lowe, L, Srikanthan, R, McVicar, T. R., 2012. Estimating actual, potential, reference crop and pan evaporation using standard meteorological data: a pragmatic synthesis. Hydrology and Earth System Sciences Discussions.

Mengistu, M.G., Everson, C.S., Moyo, N.C., Savage, M.J., 2014.the Validation of the Variables (Evaporation and Soil Moisture) in Hydro-meteorological Models.2066/1/13 Pretoria, South Africa.

Mengistu M.G., Savage M.J., 2010. Open water evaporation for a small shallow dam in winter using surface renewal and eddy covariance methods. Journal of Hydrology.

Menenti, M, Jia, L, Su, H., 2003. On SEBI-SEBS validation in France, Italy, Spain, USA and China. Proceedings of the workshop on use of remote sensing of crop evapotranspiration for large regions. International Commission on Irrigation and Drainage (ICID).Montpellier, France.

Meijninger, W. M. L., and de Bruin, H. A. R., 2000. The sensible heat fluxes over irrigated areas in western Turkey determined with a large aperture scintillometer, J. Hydrology., 229(1–2), doi: 10.1016/S0022-1694(99)00197-3.

Miura, T. Yoshioka, H., Fujiwara k. and Yamamoto, H., 2008. Inter-Comparison of ASTER and MODIS Surface Reflectance and Vegetation Index Products for Synergistic Applications to Natural Resource Monitoring. ISSN 1424-8220 MDPI www.mdpi.org/sensors.

MoWR (The Federal Democratic Republic of Ethiopia-Ministry of Water Resources), 2010. Rift Valley Lakes Basin Integrated Resources Development Master Plan Study Project. Phase 3 Report: Lake Hawassa Sub-basin Integrated Watershed Management Feasibility Study. Part 1 and 2: Halcrow Group Limited and Generation Integrated Rural Development (GIRD) Consultants. Addis Ababa.

Mutiga, JK, Su, Z, Woldai, T., 2010.Using satellite remote sensing to assess evapotranspiration: Case study of the upper EwasoNg'iro North Basin, Kenya. International Journal of Applied Earth Observation and Geoinformation12, Supplement 1(0)

Nadeau, DF, Brutsaert, W, Parlange, M, Bou-Zeid, E, Barrenetxea, G, Couach, O, Boldi, M-O, Selker, J, Vetterli, M., 2009. Estimation of urban sensible heat flux using a dense wireless network of observations. Environmental fluid mechanics 9(6).

Nash, J. E., and Sutcliffe J. V., 1970. River flow forecasting through conceptual models: Part 1. A discussion of principles, J. Hydrology 10(3).

Parkinson, C.L., 2003. Aqua: An Earth-Observing Satellite Mission to Examine Water and Other Climate Variables: IEEE Transactions on Geo science and Remote Sensing, VOL. 41, NO. 2.

Penman, H.L., 1948."Natural evaporation from open water, bare soil and grass."Proc. Roy. Soc. London, A193.

Pereira, A.R., Pruitt, W.O., 2004. Adaptation of the Thornthwaite scheme for estimating daily reference evapotranspiration. Agricultural Water Management66(3).

Rana, G, Katerji, N., 2000. Measurement and estimation of actual evapotranspiration in the field under Mediterranean climate: a review. European Journal of Agronomy.

Rasmussen, A.H., Hondzo, M., Stefan, H.G., 1995.A test of several evaporation equations for water temperature simulations in lakes. Water Resources.

Richter, D., 1988. Methods for the determination of the albedo and of the long wave outgoing radiation from a free-water surface and of the long wave incoming radiation of the atmosphere: Zeitschrift fur Meteorologie.

Rimmer, A., Samuels, R., and Lechinsky, Y., 2009.A comprehensive study across methods and time scales to estimate surface fluxes from Lake Kinneret, Israel.Journal of Hydrology.

Rodriguez-Rodriguez, M., Moreno-Ostos, E., De Vicente, I., 2004.Thermal structure and energy budget in a small high mountain lake: La Caldera, Sierra Nevada, Spain. New Zealand Journal of Marine and Freshwater Research.

Roerink, GR, Su, Z, Menenti, M., 2000. S-SEBI: A Simple Remote Sensing Algorithm to Estimate the Surface Energy Balance. Physics and Chemistry of the Earth.

Rosenberry, D. O.,Winter, T. C., Buso, D. C., and Likens, G. E., 2007. Comparison of 15 evaporation methods applied to a small mountain lake in the northeastern USA. Journal of Hydrology.

Rohwer, C., 1931. Evaporation from Free Water Surfaces. USDA Tech. Bull. 271.

Ruhoff, A.L, Paz, A.R., Collischonn, W., Aragao, LEOC, Rocha, H.R., Malhi, Y.S., 2012. A MODIS-based energy balance to estimate evapotranspiration for clear-sky days in Brazilian Tropical Savannas. Remote Sensing.

Running, S.W., Justice, C.O., Salomonson, V., Hall, D., Barker, J., Kaufmann, Y.J., Strahler, A.H., Huete, A.R., Muller, J.P., Vanderbilt, V., Wan, Z.M., Teillet, P., and Carneggie, D., 1994. Terrestrial Remote-Sensing Science and Algorithms Planned For Eos MODIS. International Journal of Remote Sensing, 15, 3587-3620

Rwasoka, DT, Gumindoga, W, Gwenzi, J., 2011. Estimation of actual evapotranspiration using the Surface Energy Balance System (SEBS) algorithm in the Upper Manyame catchment in Zimbabwe.Physics and Chemistry of the Earth

Sacks, L. A., Lee, T. M., and Radell, M. J., 1994.Comparison of energy-budget evaporation losses from two morpho-metrically different Florida seepage lakes. Journal of Hydrology.

Safavi H., 2009 Hydrology Engineering Book: ArkanDanesh.

Savenije, HHG., 2004. the importance of interception and why we should delete the term evapotranspiration from our vocabulary. Hydrological Processes

Shewangizaw, D., 2010Assessing the effect of land use changes on the hydraulic regime of Lake Hawassa: M.sc thesis, Addis Ababa University, Ethiopia [http://www.nilebasin-journal.com/download_link.asp?id=168

Shoko, C., 2014. The Effect of Spatial Resolution in Remote Sensing Estimates of Total Evaporation in the Umngeni Catchment. MSc thesis, University of KwaZulu-Natal, Pietermaritzburg.

Singh, Vijay P., 1992.Elementary Hydrology. Englewood Cliffs, New Jersey: Prentice Hall, Inc.

Singh, V. P., and Xu, C. Y., 1997.Evaluation and generalization of 13 mass-transfer equations for determining free water evaporation. Hydrological Processes.

Sobrino, JA, Gómez, M, Jiménez-Muñoz, JC, Olioso, A., 2007.Application of a simple algorithm to estimate daily evapotranspiration from NOAA–AVHRR images for the Iberian Peninsula. Remote Sensing of Environment.

Spano, D, Snyder, RL, Ducec, P, U.K.T., P., 2000. Estimating sensible and latent heat flux densities from grapevine canopies using surface renewal. Agricultural and Forest Meteorology.

Stauffer, R.E., 1991. Testing lake energy budget models under varying atmospheric stability conditions. Journal of Hydrology.

Sturrock, A.M., Winter, T.C., and Rosenbery, D.O., 1992. Energy budget evaporation from Williams Lake: A closed lake in north central Minnesota. Water Resources Res.

Sugita, F, Kishii, T. 2002.Effect of roughness distribution on evaporation processes over non-homogeneous sand surfaces: a wind tunnel investigation. Hydrological Processes

Sumner, DM, Jacobs, JM., 2005. Utility of Penman–Monteith, Priestley–Taylor, reference evapotranspiration, and pan evaporation methods to estimate pasture evapotranspiration. Journal of Hydrology

Su, H, Wood, EF, Mccabe, M, F,, Su, Z., 2007. Evaluation of remotely sensed Evapotranspiration over the CEOP EOP-1 Reference Sites. Journal of the Meteorological Society of Japan.

SU, Z., 2002. The Surface Energy Balance System (SEBS) for estimation of turbulent heat fluxes: Hydrology and Earth System Sciences.

Telford, R.J., 1998. The pala eoenvironmental record of Holocene environmental change in the Ethiopian Rift Valley. Unpublished Ph.D. Thesis, University of Wales.

Vallet-Coulomb, C., Legesse, D., Gasse, F., Travi, Y., and Chernet, T., 2001.Lake evaporation estimates in tropical Africa (Lake Ziway, Ethiopia). Journal of Hydrology.

Van den Hurk, B., 2001. Energy balance based surface flux estimation from satellite data and its application for surface moisture assimilation. Meteorology and Atmospheric Physics.

Vinukollu, R.K, Wood, EF, Ferguson, RC, Fisher, JB., 2011. Global estimates of evapotranspiration for climate studies using multi-sensor remote sensing data: Evaluation of three process-based approaches. Remote Sensing of Environment

Vuglinsky, V.S., 2002. Hydrological Cycle –Vol.II- Evaporation from Open Water Surface and Ground Water. Encyclopedia of Life Support System.

Wartena, L., 1959. The climate and the evaporation from a lake in central Iraq. Available at: http://edepot.wur.nl/182877

Willmott, C.J., Robeson S.M. and Matsuura, K., 2012.A refined index of model performance, Int. J. Climatology.

Winter, T.C., Rosenberry, D.O., Sturrock, A.M., 1995.Evaluation of 11 equations for determining evaporation for a small lake in the north central United States .Water Resource.

World Meteorological Organization, 1966."Measurement and estimation of evaporation and evapotranspiration Tech. Note No. 83, Working Group on Evaporation Measurement, WMO, Geneva, Switzerland.

WWDSE (Water Works Design and Supervision Enterprise), 2001.The study of Lake Awassa Level Rise: Southern Nations Nationalities and Peoples Regional State. Water, Mines and Energy Resources Development Bureau. Addis Ababa, Ethiopia.

Xu, Chong-yu, Gong, L, Jiang, T, Chen, D, Singh, V.P., 2006.Analysis of spatial distribution and temporal trend of reference evapotranspiration and pan evaporation in Chang Jiang (Yangtze River) catchment. Journal of Hydrology.

Yamamoto, G., and Kondo, J., 1968.Evaporation from Lake Nojiri. Journal of the Meteorological Society of Japan.

Yibeltal G. and Biniam T., 2015.Modeling Soil Erosion and Lake Evaporation Using Remote Sensing and GIS in Lake Hawassa Catchment. Proceedings of Annual Research Review Workshop, College of Social Sciences and Humanities: Hawassa University.

Young, A.A., 1947. Evaporation from Water Surfaces in California. Department of Public Works, Division of Water Resources and U.S. Department of Agriculture and Soil Conservation Service. Bull No. 54.

Zhang, Y, Liu, C, Tang, Y, Yang, Y., 2007. Trends in pan evaporation and reference and actual evapotranspiration across the Tibetan Plateau. Journal of Geophysical Research: Atmospheres 112(D12): n/a-n/a.

Appendices

Annex 1: Pan Evaporation Condition at Hawassa Meteorological Station

Annex 2: Standard Micro-Meteorological Expressions for Evaporation Calculations

$$e_s = 6.11\exp\frac{17.27\,(Ta - 273)}{(Ta-273)+237.3}$$

Where; T= Air temperature at observation height [K]

e_s= Saturated vapor pressure [mbar]

$e_a = e_s X\ RH$

Where; e_a is actual vapor pressure [mbar]

RH is Relative Humidity [-]

$$D = e_s - e_a$$

Where; D= vapor pressure deficit

$$\Delta = 4098\,\frac{e_s}{[(Ta-273)+237.3]^2}$$

Where; Δ=Slope of saturated vapor pressure curve

$$\rho_v = \frac{e_s}{T_a X 4.61}$$

Where; ρ_v= actual vapor density [Kg.m-3]

$$\rho_d = \frac{P-e_a}{T_a\ X\ 2.87}$$

Where; ρ_d = dry air density [Kg.m-3], P = total pressure [mbar]

$$\rho_a = \rho_v + \rho_d$$

Where; ρ_a = Moist air density [Kg. m-3]

$$P = 1004 \frac{(293 - 0.0065Z)^{5.26}}{T_a \text{ X } 2.87}$$

Where; P = total pressure [mbar] , Z= Elevation [m]

$$\lambda = [2.501 - 0.002361(T - 273)] \text{ X } 10^6$$

Where; λ = Latent heat of vaporization [J. Kg^{-1}], T = average of surface and air temperature [K]

$$\gamma = 1630 \frac{P}{\lambda}$$

Where; γ= Psychrometric Constant [mbar. K^{-1}]

$$\delta = 0.409 \sin(0.0172 \, J - 1.39)$$

Where; δ = Solar declination [rad], J = day number of the year [-], sin = sine function which should be in radian mod

$$d_s = 1 + 0.0167 \sin \left[\frac{2\pi(J - 93.5)}{365} \right]$$

$$E_0 = 1 + 0.033 \cos(0.0172J)$$

Where; d_s = relative distance between earth and sun [AU], Eo= Eccentricity correction factor of the earth orbit [-], cos = cosine function which should be in radian mode

$$\mathbf{w} = \cos^{-1}(-\tan(lat) \tan \delta)$$

Where; **w**= Solar hour angle representing the 24 hour solar radiation [rad]

$$R_a = 435.2 \text{ X} E_0 \text{X } (w \sin(lat) \sin \delta + \cos(lat) \cos \delta \sin w$$

Where; R_a= Daily Extra-terrestrial short wave solar radiation [W.m^{-2}]

N = 7.64 **w**

Where; N = Maximum possible sunshine hours

R_s= (0.24 + 0.59 n/N).R_a

Where; R_s = incoming short wave solar radiation [W.m-2]

$R_n = (1 - \alpha)R_s - 110\frac{R_s}{R_a}$

Where; α = albedo of the surface, R_n = net daily radiation

Annex 3: Heat Storage Flux Spatio-Temporal Distribution

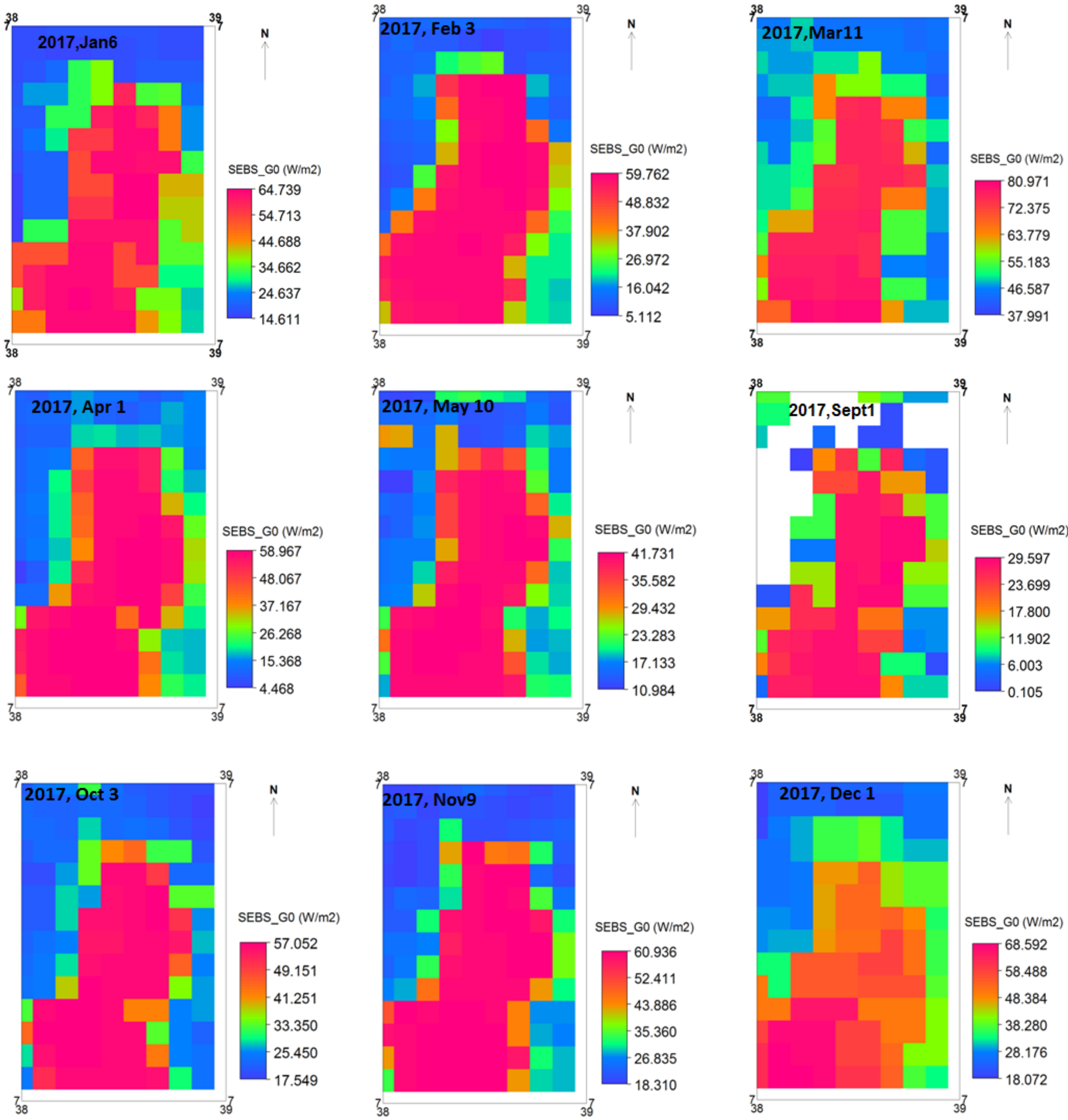

Annex 4: Net Radiation Flux Spatio-Temporal Distribution

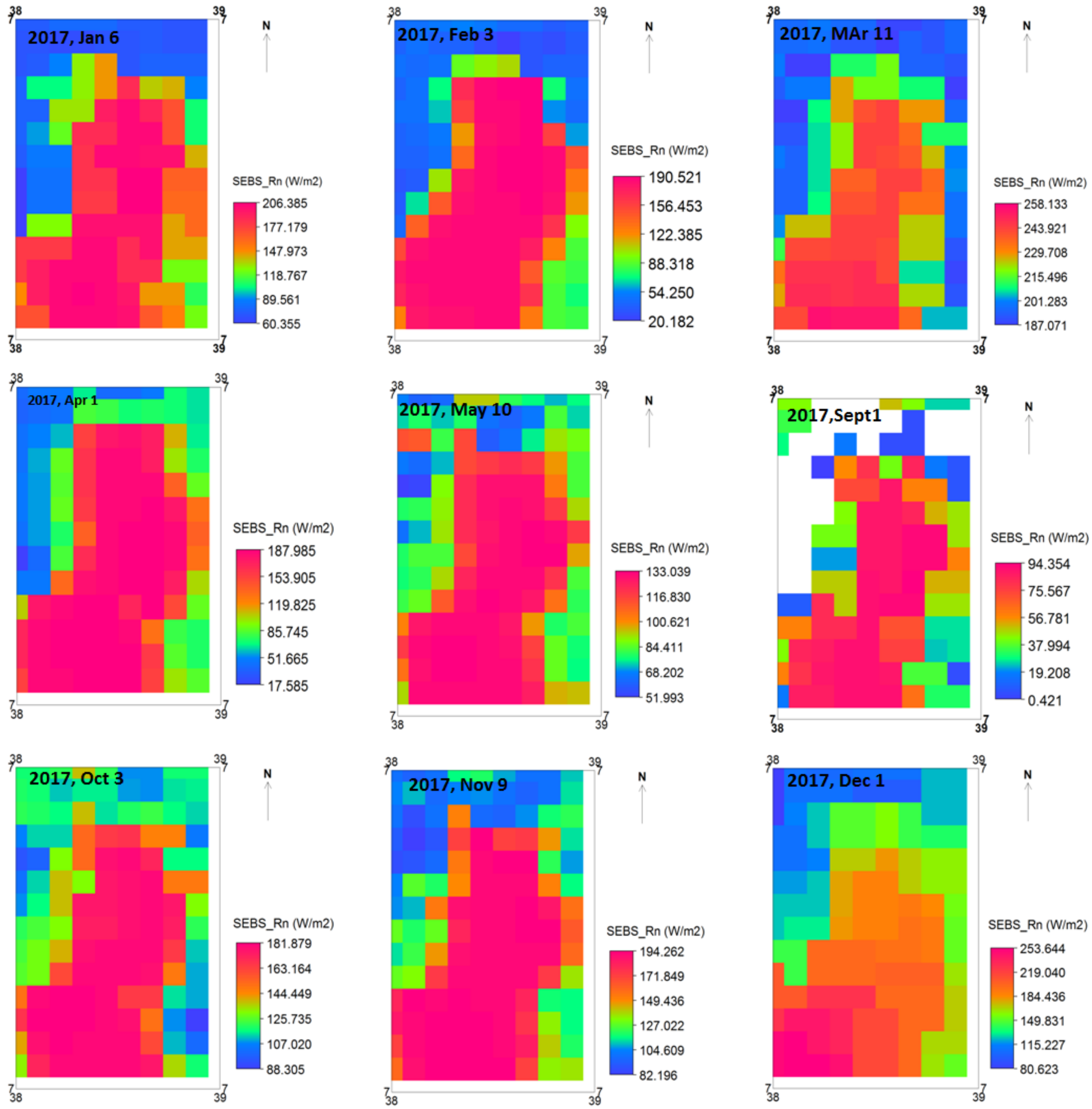

Annex 5: Sensible Heat Flux Spatio-Temporal Distribution

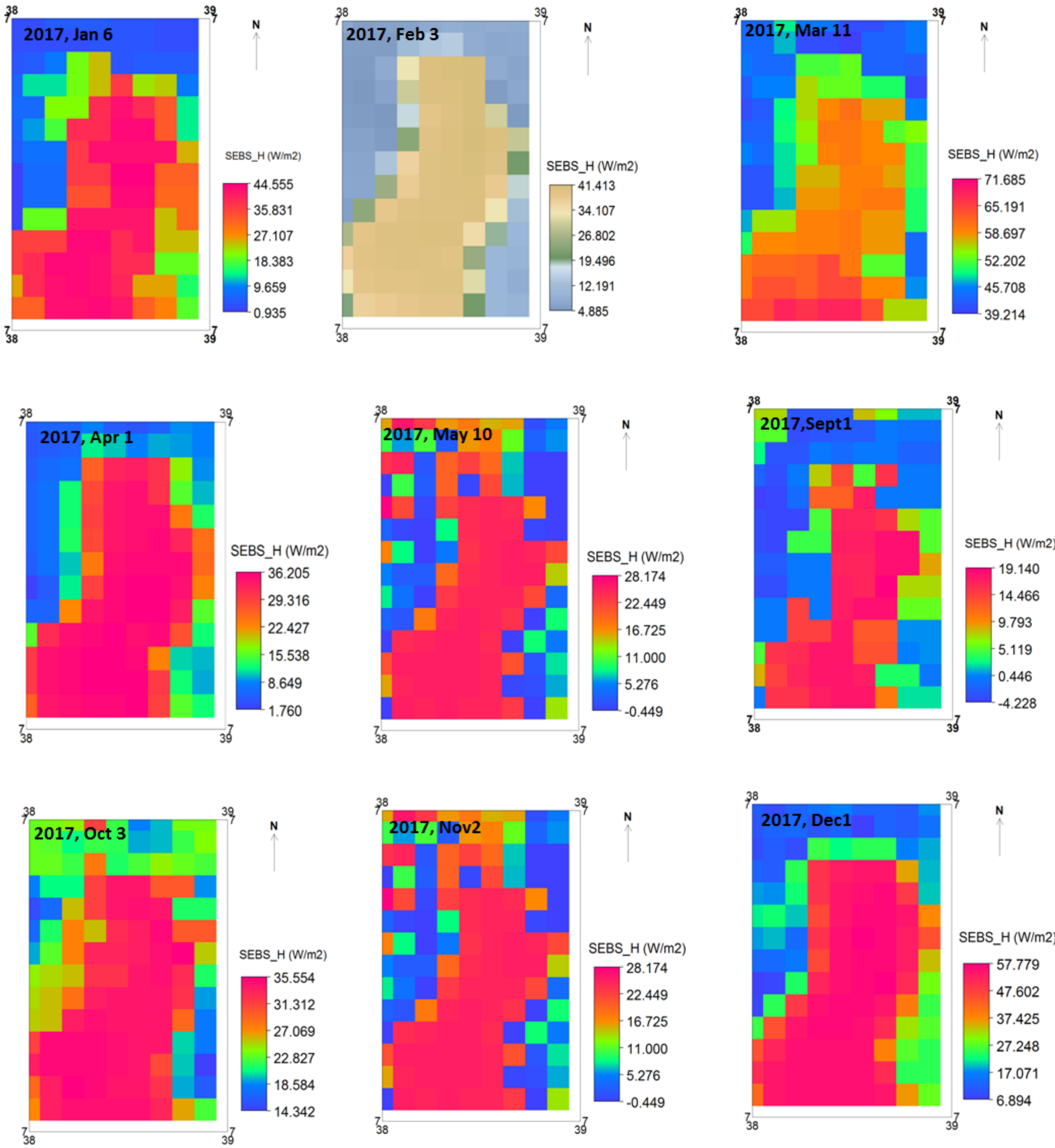

Annex 6: SEBS Input Maps